



Experience the commitment®



The sky is the limit, the lower limit!

Final Report

Mitigating the loss of solar visibility on GOME-2 reflectance data quality after the end of Metop-A orbit inclination maintenance

Contract number: EUM/CO/15/4600001614/RL

Document Reference: GOME2-SOL-FR-001

Issue: Rev1





Mitigating the loss of solar visibility on GOME-2 reflectance data quality after the end of Metop-A orbit inclination maintenance
GOME2-SOL-FR-001
Rev1

Approval Table:

Action	Name	Function	Signature	Date
Prepared by:	Matthijs Krijger	Author		
	Natalie Raettig	Author		
	Huan Yu	Author		
	Barry Latter	Author		
Approved by:	Ruediger Lang	EUMETSAT Study Manager		

Authors and Contributors:

Name	Contact	Description	Date
Matthijs Krijger	krijger@earthspace.nl	Author	20/09/2016
Natalie Raettig	natalie.raettig@cgi.com	Author	20/09/2016
Huan Yu	huan.yu@aeronomie.be	Author	20/09/2016
Barry Latter	barry.latter@stfc.ac.uk	Author	20/09/2016

Document Change Log:

Issue	Date	Description
Rev0A	19/09/2016	Initial Draft
Rev0B	20/09/2016	Updated
Rev0C	25/10/2016	Updated
Rev0D	27/10/2016	Updated
Rev0E	28/10/2016	Updated
Rev1	04/11/2016	Issued

Table of contents

1	Purpose of this document	11
1.1	REFERENCE DOCUMENTS	11
2	Objective of the study	12
3	Model	13
3.1	FITTING PARAMETERS	14
3.2	SOLAR VARIATION	18
3.2.1	MGII INDEX	19
3.2.2	DIFFERENT SCENARIOS FOR MODELLING SOLAR ACTIVITY	19
3.2.3	TIME DEPENDANCE OF SOLAR INDICES	25
3.3	DEGRADATION	30
3.4	SOLAR AZIMUTH VARIATION	30
3.5	MODEL RESULTS	34
3.5.1	FIT VALUES	34
3.5.2	FIT CONTRIBUTIONS	39
3.5.3	ACCURACY	40
3.6	INSTRUMENT ANOMALIES AND STEP FUNCTION	45
3.7	WAVELENGTH-SHIFTED VS. NOT SHIFTED DATASET	46
3.8	SUMMARY ATBD LIKE DOCUMENT	48
4	Reference Period	50
4.1	SOLAR LOSS PERIODS	50
5	Results: Quality impact in time based on region	51
5.1	SAHARA & PRISTINE EQUATORIAL PACIFIC	51
6	Results: Global quality impact based on shorter periods	56
7	Results: Sensitivity of L2 NO₂ products	58
7.1	SINGLE ORBIT ANALYSIS	58
7.2	TIME SERIES ANALYSIS	61

7.2.1	OUTLIERS IN MEASRUED SMR	62
7.3	GLOBAL COMPARISONS	65
7.4	CONCLUSION	66
8	Results: Sensitivity of global height-resolved ozone	67
8.1	SINGLE ORBIT ANALYSIS	67
8.2	GLOBAL COMPARISONS	69
9	Summary and recommendation	75
10	Work packages	76

Appendix contents

Appendix A	78
------------	----

List of Figures

Figure 1 Fitting parameter time as function of time (year).	14
Figure 2 Fitting parameter Solar Distance as function of time (year).	15
Figure 3 Fitting parameter OBM Temperature as function of time (year).	15
Figure 4 Fitting parameter linear time-dependent solar azimuth angle as function of time (year).	16
Figure 5 Fitting parameter linear time-dependent solar azimuth angle as function of time (year).	16
Figure 6 Fitting parameter quadratic time-dependent solar azimuth angle as function of time (year).	17
Figure 7 Fitting parameter MgII Index (from GOME2-B) as function of time (year).	17
Figure 8 Fitting parameter F10.7 cm index (from external database) as function of time (year).	18
Figure 9 Standard deviation between model and measurement as function of for different (solar parameters) models.	20
Figure 10 Relative (to default model G2B) Standard deviation between model and measurement as function of for different (solar parameters) models.	21
Figure 11 Standard deviation between model and measurement as function of for different (solar parameters) models.	21
Figure 12 Relative (to default model G2B) Standard deviation between model and measurement as function of for different (solar parameters) models.	22

Figure 13 Standard deviation between model and measurement as function of for different (solar parameters) models.....	22
Figure 14 Relative (to default model G2B) Standard deviation between model and measurement as function of for different (solar parameters) models.....	23
Figure 15 Standard deviation between model and measurement as function of for different (solar parameters) models.....	23
Figure 16 Relative (to default model G2B) Standard deviation between model and measurement as function of for different (solar parameters) models.....	24
Figure 17 Standard deviation between model and measurement as function of for different (solar parameters) models.....	24
Figure 18 Relative (to default model G2B) Standard deviation between model and measurement as function of for different (solar parameters) models.....	25
Figure 19 Difference between shifted_model and model MgII index.....	26
Figure 20 Weight MgII index.....	26
Figure 21 Difference between shifted_model and model F10.7 index.....	27
Figure 22 Weight F10.7 index.....	27
Figure 23 Difference between shifted_model and model as function of wavelength (zoomed in at the Huggins band) and time (year). Impact: $7.71773e^{-5}$	28
Figure 24 Difference between shifted_model and model as function of wavelength (zoomed in at Channel 1) and time (year). Impact: $4.60218 e^{-4}$	28
Figure 25 Difference between shifted_model and model as function of wavelength (zoomed in at Channel 2) and time (year). Impact: $2.49837 e^{-4}$	29
Figure 26 Difference between shifted_model and model as function of wavelength (zoomed in at Channel 3) and time (year). Impact: $1.79239 e^{-4}$	29
Figure 27 Difference between shifted_model and model as function of wavelength (zoomed in at Channel 4) and time (year). Impact: $1.24877 e^{-4}$	30
Figure 28 Detrended SMR measurement for 266.742 nm as function of Day Of the Year (DOY). Each year in different color as indicated on right. In black and dotted the (scaled and offset).....	31
Figure 29 Detrended SMR measurement for 266.742 nm as function of Day Of the Year (DOY). Each year in different color as indicated on right. In black and dotted the (scaled and offset) Azimuth variation over all years. Overpotted in black, the for each year separately scaled azimuth angle.....	32
Figure 30 The fitted scale factor the azimuth angle for each year, as a function of time for 266.742 nm.....	32

Figure 31 Detrended SMR measurement for 266.742 nm as function of azimuth angle. Time is indicated by colors going from blue (early) to yellow to red (late). A clear azimuth dependence is visible that increases over the years.....	33
Figure 32 Detrended SMR measurement for 299.552 nm as function of azimuth angle. Time is indicated by colors going from blue (early) to yellow to red (late). A clear azimuth dependence is visible that increases over the years.....	33
Figure 33 Fitted value of parameter <i>offset</i> as function of pixel number.	34
Figure 34 Fitted value of parameter <i>linear time</i> as function of pixel number.....	35
Figure 35 Fitted value of parameter <i>quadratic time</i> as function of pixel number.....	35
Figure 36 Fitted value of parameter <i>linear SAA</i> as function of pixel number.	36
Figure 37 Fitted value of parameter <i>solar distance</i> as function of pixel number.	36
Figure 38 Fitted value of parameter <i>OBM temperature</i> as function of pixel number.....	37
Figure 39 Fitted value of parameter <i>linear time increase SAA</i> as function of pixel number.	37
Figure 40 Fitted value of parameter <i>quadratic time increase SAA</i> as function of pixel number.	38
Figure 41 Fitted value of parameter <i>MgII index solar activity</i> as function of pixel number.	38
Figure 42 Fitted value of parameter <i>10.7 cm radio flux solar activity</i> as function of pixel number.	39
Figure 43 Derived weights of the various inputs (color-coded as indicated in legend), used to construct the expected solar transmittance, here shown as contribution to the variance (over time) of the model output. The upper plot shows the contribution as function of wavelength. The lower plots shows the same contribution but now as function of pixel nmr.	40
Figure 44 Top: Throughput in the Huggins band in early 2015. Measurement in black, model in red. Bottom: Difference between measurement and model.....	41
Figure 45 Difference between measurement and model as function of wavelength (zoomed in at the Huggins band) and time (year).....	42
Figure 46 Difference between measurement and model as function of wavelength (zoomed in at Channel 1) and time (year).....	42
Figure 47 Difference between measurement and model as function of wavelength (zoomed in at Channel 2) and time (year).....	43
Figure 48 Difference between measurement and model as function of wavelength (zoomed in at Channel 3) and time (year).....	43
Figure 49 Difference between measurement and model as function of wavelength (zoomed in at Channel 4) and time (year).....	44

Figure 50 Top: Throughput at 266 nm as function of time. Measurement in black, model in red. Bottom: Difference between measurement and model.....	44
Figure 51 Top: Throughput at 325 nm as function of time. Measurement in black, model in red. Bottom: Difference between measurement and model.....	45
Figure 52 Comparison between measurements (green), model data (blue) and wavelength interpolated model data (black) for NO ₂ SCD and the resulting RMS.....	47
Figure 53 Gridded daily means of shifted vs not shifted measurement SMR retrievals (01/01/2015). Row 1: Retrieval fit cost & surface albedo. Row 2: Total column ozone. Row 3 & 4: ~0-6km & ~6-12km sub-column ozone. Column 1&3: unshifted SMR values. Column 2&4: Difference with shifted spectra.....	48
Figure 54 Standard deviation between model and measurement reflectance as function of wavelength, averaged over all viewing angles and reference period.....	52
Figure 55 Standard deviation between model and measurement reflectance as function of wavelength (zoom Huggings band), averaged over all viewing angles and reference period.....	52
Figure 56 Standard deviation between model and measurement reflectance as function of wavelength, averaged over select viewing angles and the whole reference period. Different colors indicate different viewing angles averaged over.....	53
Figure 57 Standard deviation between model and measurement reflectance as function of time (since start reference period), averaged over select viewing angles and wavelength (Huggings band). Different colors indicate different viewing angles averaged over.....	53
Figure 58 Standard deviation between model and measurement reflectance as function of wavelength, averaged over all viewing angles and reference period.....	54
Figure 59 Standard deviation between model and measurement reflectance as function of wavelength, averaged over all viewing angles and reference period.....	54
Figure 60 Standard deviation between model and measurement reflectance as function of wavelength, averaged over select viewing angles and the whole reference period. Different colors indicate different viewing angles averaged over.....	55
Figure 61 Standard deviation between model and measurement reflectance as function of time (since start reference period), averaged over select viewing angles and wavelength (Huggings band). Different colors indicate different viewing angles averaged over.....	55
Figure 62 Standard deviation between model and measurement reflectance as function of wavelength, averaged over select viewing angles and the whole reference period. Different colors indicate different viewing angles averaged over.....	56
Figure 63 Standard deviation between model and measurement reflectance as function of wavelength, averaged over select viewing angles and the whole reference period. Different colors indicate different viewing angles averaged over.....	57

Figure 64 Retrieved NO₂ *SCD* using model (blue) and measurement (green) SMR and the corresponding fitting RMS (middle) for one orbit of GOME-2 measurements, as function of latitude. The difference in *SCD* between use of model and measurement SMR is shown in the bottom panel.....59

Figure 65 Difference in stratospheric (*SCD_{strat}*, top) and the residual tropospheric (*SCD_{trop}* = *SCD* – *SCD_{strat}*, bottom) NO₂ slant column between use of the model and measurement SMR for one orbit of GOME-2 measurements, as function of latitude. 60

Figure 66 Comparison of NO₂ *VCD_{trop}* (top) and *VCD_{total}* (bottom) using model and measurement SMR for one orbit of GOME-2 measurements, as function of latitude. Only pixels with cloud radiance fraction less than 50% have been used for the figure. 61

Figure 67 Standard deviation of NO₂ *SCD* retrieval between use of model and measurement SMR as function of time, averaged over the pixels with solar zenith angles less than 80°. The fitting error of *SCD* retrieval from DOAS approach are shown in the figure as well. 62

Figure 68 Comparison of NO₂ *SCD* retrieval between use of modeled, measured and a fixed measured SMR. There are outliers on three days (January 3, 8, 15)..... 63

Figure 69 Standard deviation of NO₂ *SCD_{strat}* (top) and *SCD_{trop}* (bottom) between use of model and measurement SMR as function of time, averaged over the pixels with solar zenith angles less than 80°. Red and black lines indicate the orbital and daily average. 64

Figure 70 Standard deviation of NO₂ $[[VCD]]_{trop}$ between use of model and measurement SMR as function of time, averaged over the pixels with solar zenith angles less than 80°. Red and black lines indicate the orbital and daily average, respectively. 65

Figure 71 Top: Map of averaged NO₂ *VCD_{total}* (left) and *VCD_{trop}* (right) *VCDs* using the measurement SMR. Bottom: Standard deviation of NO₂ *VCD_{total}* (left) and *VCD_{trop}* (right) between use of model and measurement SMR over the whole reference period. Only pixels with cloud radiance fraction less than 50% and SZA less than 80° have used for the figure. 66

Figure 72 Model vs Measurement retrievals for a single orbit (31.03.2015). Figures show the retrieved total and sub-columns ozone after band 1 (top) and final step (middle) with associated difference to cost, no. of iterations ('#it') and surface albedo. Reference retrieval sub-column estimates, L2 cloud fraction and height also shown. 68

Figure 73 Gridded 'cloud free' monthly of model vs measured SMR retrievals (02/01/2015). Row 1: Retrieval fit cost & surface albedo. Row 2: Total column ozone. Row 3 & 4: ~0-6km & ~6-12km sub-column ozone. Column 1/3: Model SMR values. Column 2/4: Difference with measurement 70

Figure 74 Gridded 'cloud free' monthly means of model vs measured SMR retrievals (03/2015). Row 1: Retrieval fit cost & surface albedo. Row 2: Total column ozone. Row 3 & 4: ~0-6km & ~6-12km sub-column ozone. Column 1/3: Model SMR values. Column 2/4: Difference with measurement. 71

Figure 75 Gridded daily means of model vs measured SMR retrievals (11/01/2015). Row 1: Retrieval fit cost & surface albedo. Row 2: Total column ozone. Row 3 & 4: ~0-6km & ~6-12km sub-column ozone. Column 1/3: Model SMR values. Column 2/4: Difference with measurement..... 72

Figure 76 Time series of daily zonal means for ozone total and sub-columns for measured (solid line) and modelled (dashed) SMR	73
Figure 77 Time series of differences for ozone total and sub-columns for measured (solid line) and modelled (dashed) SMR.	74

1 Purpose of this document

This document summarizes the results of the study “Mitigating the loss of solar visibility on GOME-2 reflectance data quality after the end of Metop-A orbit inclination maintenance”.

During WP 1 a model to calculate synthetic mean solar reference spectra (SMR) was developed. Details of this model are described in RD-1 and RD-2. For this WP model data was provided for a certain reference period where also real data is available.

During WP 2 the impact that the loss of solar visibility has on certain products was assessed. Specifically on the reflectance, based in different geographical locations as well as global, and two L2 products, NO₂ and global height resolved ozone. To achieve this, results obtained from model data were compared with results obtained with real data for a certain period of time. These results are described in this document.

1.1 Reference Documents

List of reference Documents:

Document	Reference	Title
RD-1	GOME2-SOL-PR-001	GOME2-SOL-PR-001
RD-2	GOME2-SOL-ATBD-002	Algorithm Theoretical Basis Document
RD-3	GOME2-SOL-PR-002	GOME2-SOL-PR-002

2 Objective of the study

Due to the end of life of the Metop-A satellite its orbit configuration will change slowly, putting the satellite in relative positions where it loses direct line of sight to the sun. Direct sun visibility is necessary for the GOME-2 instrument in order to maintain its correct calibration, which depends on recording sun spectra for reference (SMR, solar mean reference spectra).

A wealth of data products is derived from GOME-2 measurements and a number of them rely on the continuous availability of SMR, i.e. reflectance, sensitive level2 products. In order to maintain the best possible quality for those products as long as possible it is necessary to determine strategies how to deal with degraded SMRs or in the worst case how to deal with situations where the original SMR is unavailable, due to the loss of direct line of sight to the sun. Also, a quantitative estimate of the impact on the products in question has to be made, based on documented assumptions and a model of the degradation of the sensor. To achieve this sensitivity studies on SMR, reflectance and Level-2 products are the measures of choice.

Key aspects of this work include:

- Develop a model to simulate the evolution of the SMR during non-vis periods.
- Produce virtual SMRs and apply them in studies to compare the results with products derived under nominal conditions.

A major instrument related issue is degradation to the reflectivity of optical surfaces in the instrument, due to build-up of a contaminating layer. This depends strongly on wavelength and time, and is seen differently in the direct-sun and Earthshine optical paths.

The availability and quality of the SMR is a crucial element for the quality of remote sensing products derived from GOME-2, i.e. reflectance, trace gas profiles and columns. To achieve satisfactory quality in retrieved products, the effect of degradation on the sun-normalized uv radiance spectrum has to be accounted for carefully.

In order to compensate for those issues as long as possible and to ensure functionality of GOME-2 as a valuable scientific measurement system as long as possible it is necessary to evaluate and propose mitigating actions with respect to GOME-2 on Metop-A, addressing:

- reflectance data quality
- level-2 product quality

To enable a study of the above subjects it is necessary to develop a model for the gradual change of the sensor during the times of no sun-visibility and to compare the propagated effects of those changes to a nominal situation.

3 Model

First all measurements are shifted from the supplied wavelength grid to a common wavelength grid. Next all, measurements are divided by the first available in-flight measurement resulting in the relative degradation since (close to) launch.

The signal at the lower wavelengths can be foremost described by an exponential decay (in time, t), likely due to a linear (in time) growth of contaminant on the various optical surfaces causing exponential absorption (Krijger et al, 2014).

Investigation of the signals in Channel 1 clearly indicates a dependence on solar azimuth angle (α). See Section 3.4. This dependence seems to be exponentially growing in time. Explanation again is likely linear growth (in time) of contaminant causing an increasing dependence on azimuth angle.

Given the need for empirically deriving the weights of all terms and the tendency of exponential function to arrive to extremely high values and thus not converge in any fitting algorithm, the choice was made to approximate the exponential decays with quadratic functions. This also allows the higher wavelengths, where exponential decay is being counter-acted by interference effects, to be fitted by the same function.

Solar variation is especially important at the lower wavelengths. See section 3.2. The solar variation is described by two indices, the F10.7 cm radio index ($F10.7_{Index}$) and the the MgII index ($MgII_{Index}$). The MgII index is derived from GOME2-B. The model is fitted independently for each wavelength.

Instrumental temperature effects are captured by the provided instrumental (OBM) temperatures.

Finally any remaining solar distance dependence (d_{solar}^2) is described by a free fit to the power of the solar distance. This gives 10 fitting parameters (P_{1-10}). Note that P_7 is no longer considered, see Section 3.2.2. for justification.

$$I = P_0 + P_1 * t + P_2 * t^2$$

$$I = I + P_3 * \alpha + P_4 * \alpha * t + P_5 * \alpha * t^2$$

$$I = I * (1 + P_6 * F10.7_{Index})$$

$$I = I * (1 + P_8 * MgII_{Index})$$

$$I = I * (d_{solar}^2)^{P_9}$$

$$I = I * (1 + P_{10} * Temperature)$$

More recent periods and periods with large azimuth angles (which will be the case during solar visibility loss period) have a large fitting weight, as for future extrapolation we are not interested in early periods or other azimuth angles. The measurement for these periods do add information to the fit and are thus taken into account, however with smaller weight so the fits do not attempt to find a compromise for all periods.

3.1 Fitting Parameters

The following images show the different employed fitting parameters as a function of time

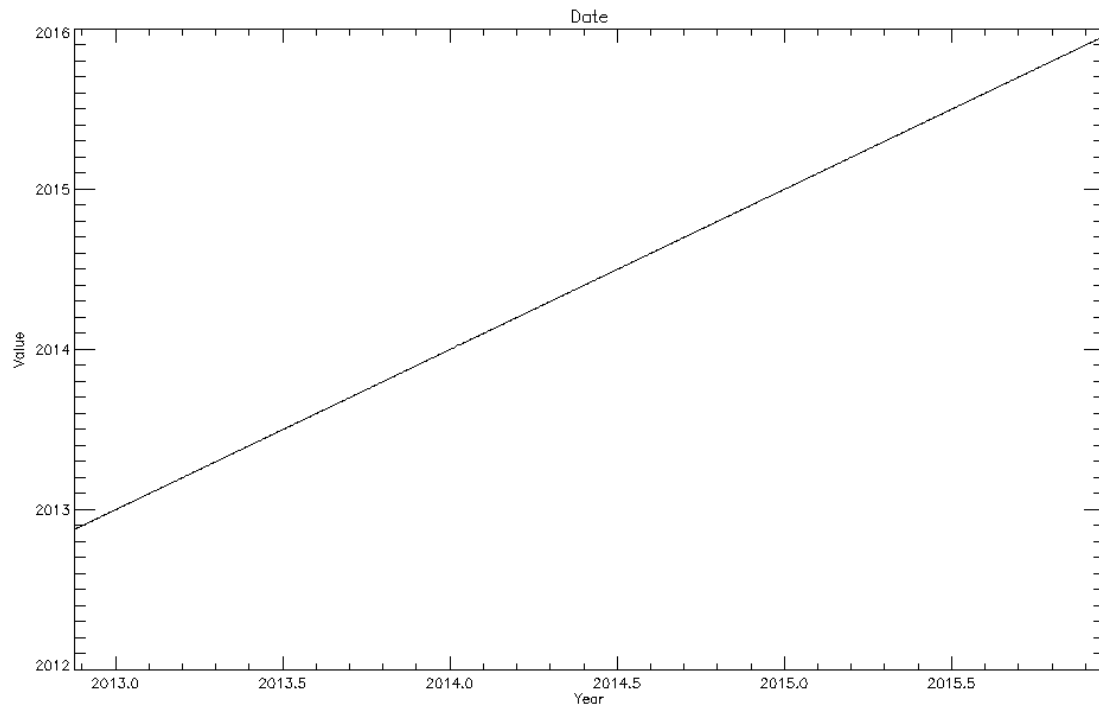


Figure 1 Fitting parameter time as function of time (year).

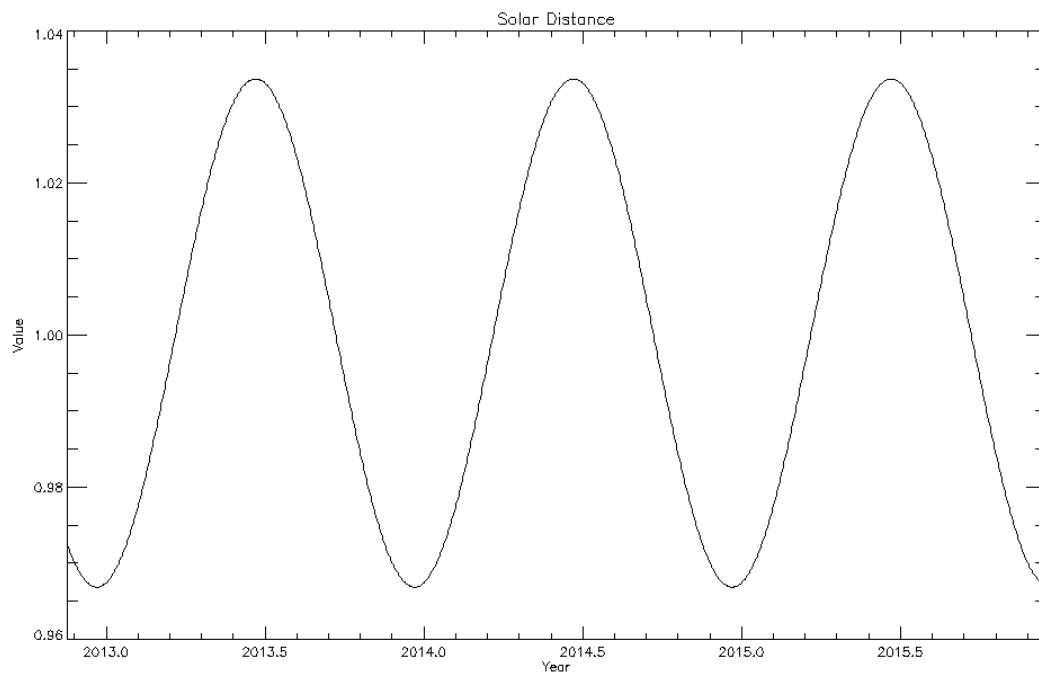


Figure 2 Fitting parameter Solar Distance as function of time (year).

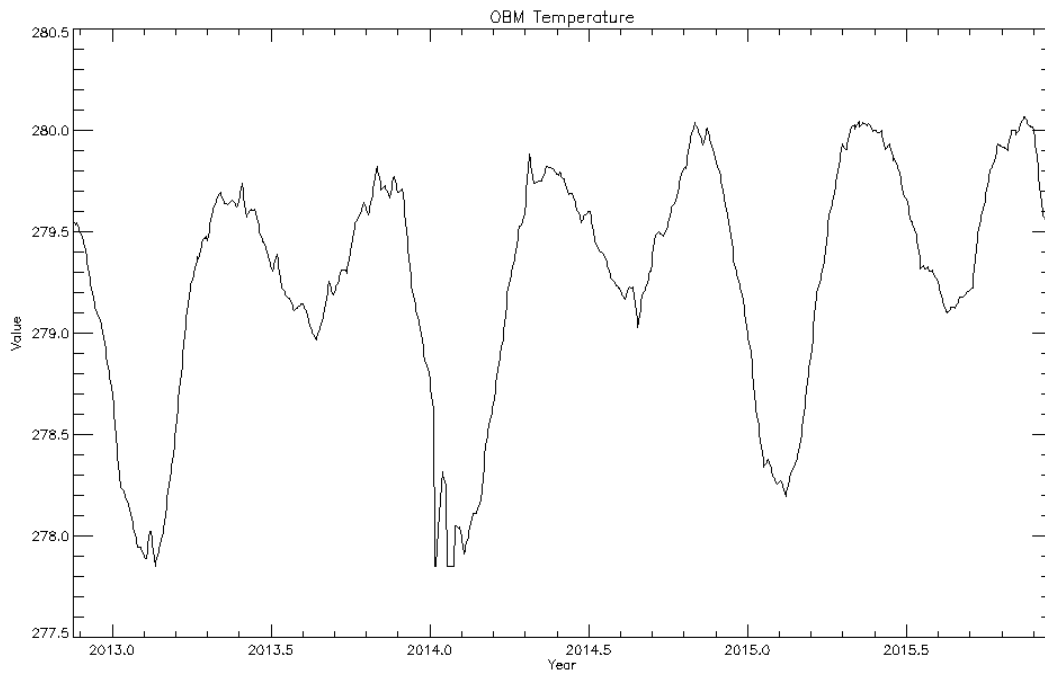


Figure 3 Fitting parameter OBM Temperature as function of time (year).

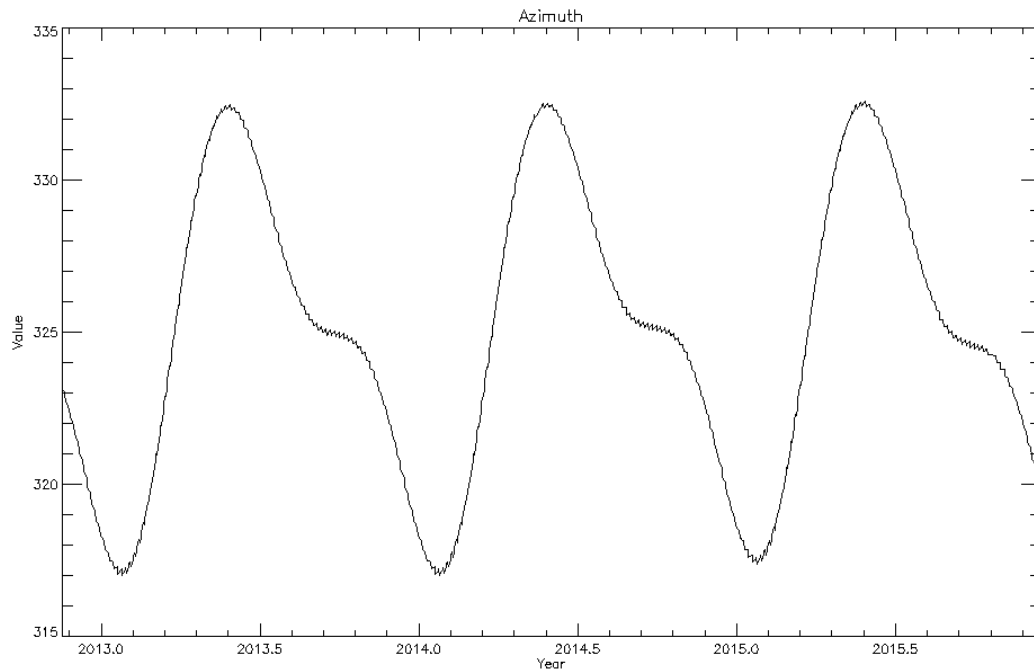


Figure 4 Fitting parameter linear time-dependent solar azimuth angle as function of time (year).

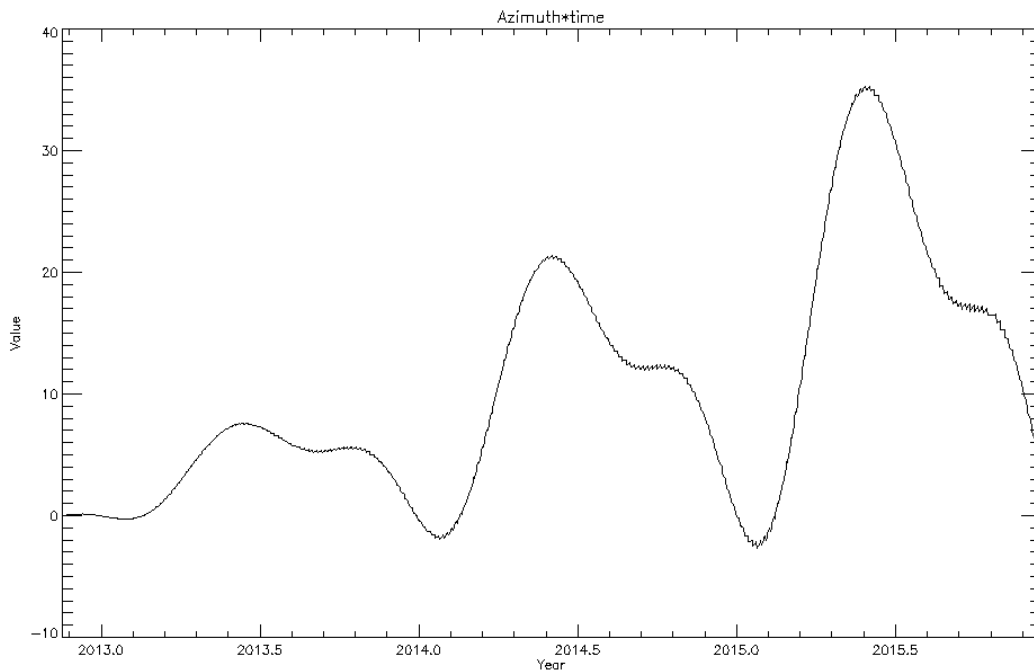


Figure 5 Fitting parameter linear time-dependent solar azimuth angle as function of time (year).

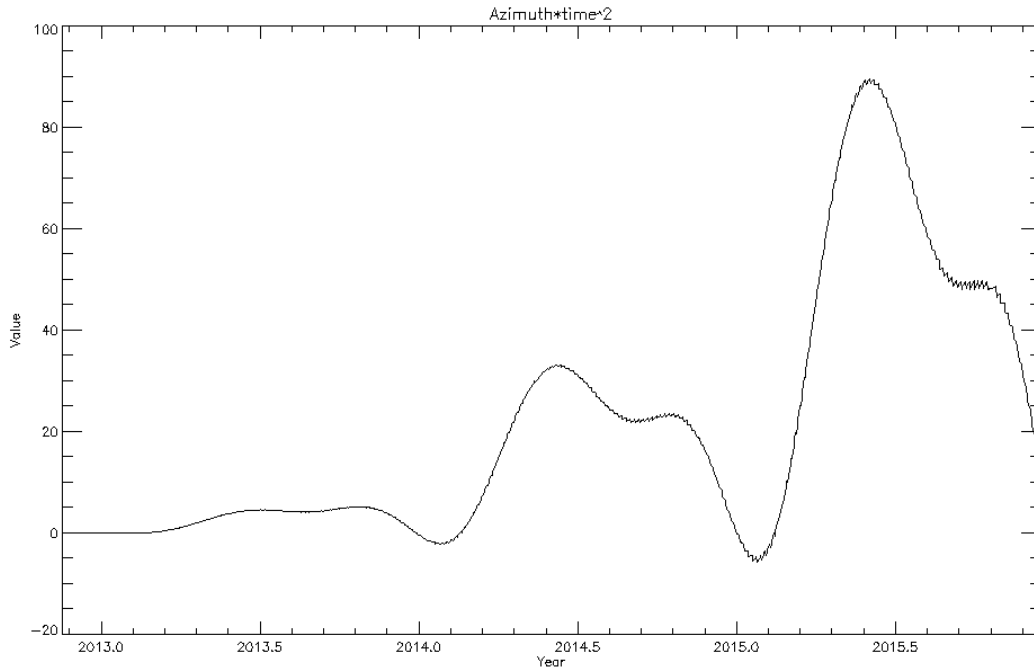


Figure 6 Fitting parameter quadratic time-dependent solar azimuth angle as function of time (year).

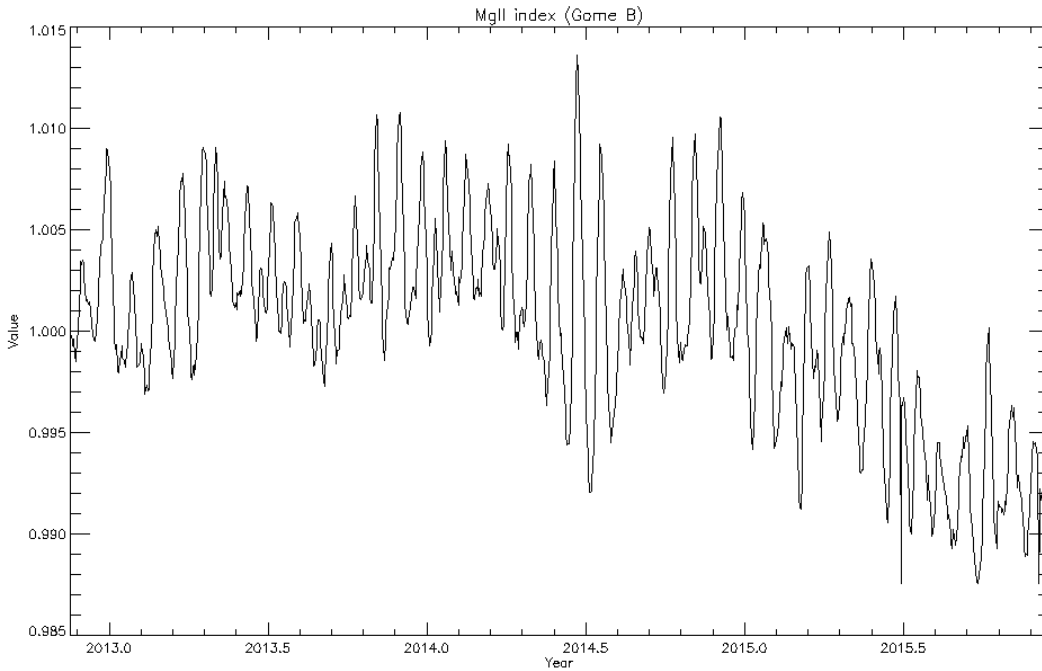


Figure 7 Fitting parameter MgII Index (from GOME2-B) as function of time (year).

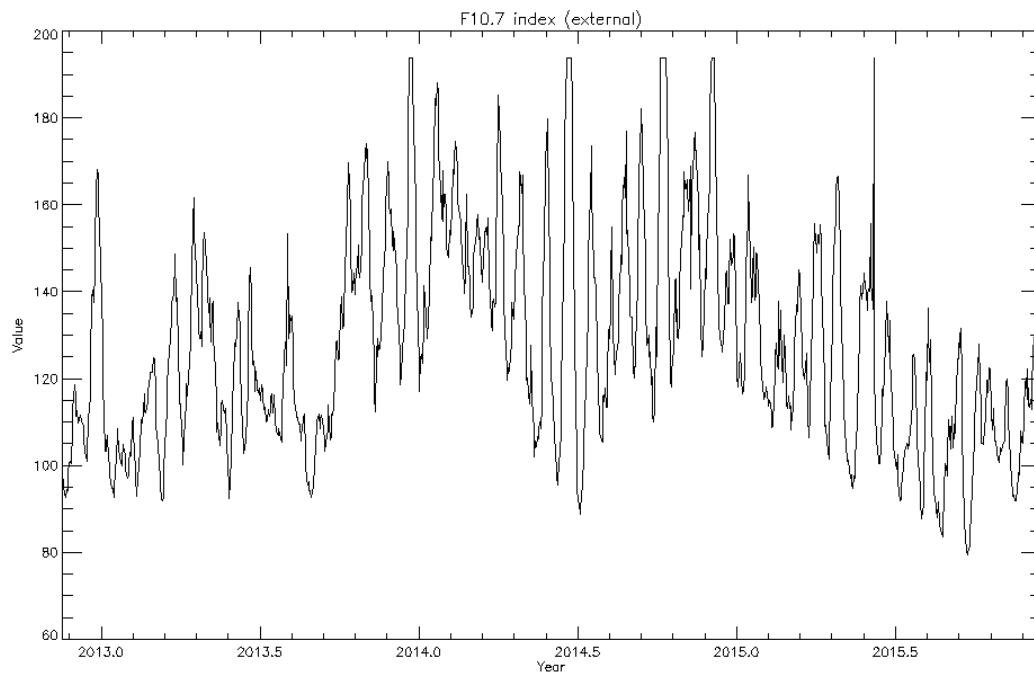


Figure 8 Fitting parameter F10.7 cm index (from external database) as function of time (year).

3.2 Solar variation

Solar variation is especially important at the lower wavelengths. Similar to the works of by M. Weber and J. Paragan, the solar variation can be very well approximated by different indices with different weights for each wavelength.

We have employed two indices in this study:

- The MgII Index
- The F10.7 cm radio index,

The F10.7 cm radio index, is external information, downloaded from the SPDF OMNIWeb Plus service at <http://omniweb.gsfc.nasa.gov/>.

The Omniweb information is kept up to date, and is expected to be still available during the period of solar visibility loss. However, we studied the scenario where this information is no longer available (scenario 'NoExternal'). As expected the accuracy of the results decrease.

3.2.1 MGII INDEX

The *MgII* index is derived according Snow, 2014.

The spectrum is smoothed over 33 wavelength pixels, and calculated as follows:

$$\text{Index} = \frac{(4 * E(279.8\text{nm}) + E(280.0\text{nm}) + E(280.2\text{nm}))}{(3 * E(276.6\text{nm}) + E(276.8\text{nm}) + E(283.2\text{nm}) + E(283.4\text{nm}))}$$

With E the solar irradiance in photons per nm sec cm² at the indicated wavelengths.

This can be done for GOME2-A, but as GOME2-A solar measurements are not available during the solar visibility loss periods the GOME2-B measurements will be taken instead. Studying the *MgII* index of GOME2-A and GOME2-B shows that the ratio between them is constant (for now) and thus can be used to transform the GOME2-B *MgII* index into GOME2-A *MgII* index.

However, as done here, the GOME2-B *MgII* index can also be used directly to empirically derive the GOME2-A signal.

3.2.2 DIFFERENT SCENARIOS FOR MODELLING SOLAR ACTIVITY

The *MgII* index we derive from GOME2-B, as GOME2-A solar measurements are not available during the solar visibility loss period. We have studied how the results improve employing GOME2-A *MgII* index directly (scenario 'G2A-MgII') compared to the suggested model (scenario 'G2B-MgII'). As expected the results improve slightly. In addition we have studied not employing the *MgII* index at all, on the chance all solar variability can be described employing F10.7 cm index only (scenario 'NoMgII'). As expected the results decrease.

Additionally we studied the effect of not fitting F10.7 cm index (scenario 'noF10'). For some wavelength not fitting F10.7 cm might decrease the standard deviation.

As verification we studied a scenario which does not describe any solar variability (scenario 'nosolar'). Results decrease significantly.

During the course of the study it became apparent that the F10.7cm flux and the sunspot index are not needed both. One of these parameters can be neglected. Since the F10.7 can be provided more reliably and accurately (sunspot counting is still a human endeavor), it was decided to take it into account when calculating model data, but not the sunspot index.

The following figures show the standard deviation as a function of wavelength for the different channels and bands of interest, both absolute and relative to the employed model (scenario 'G2B').

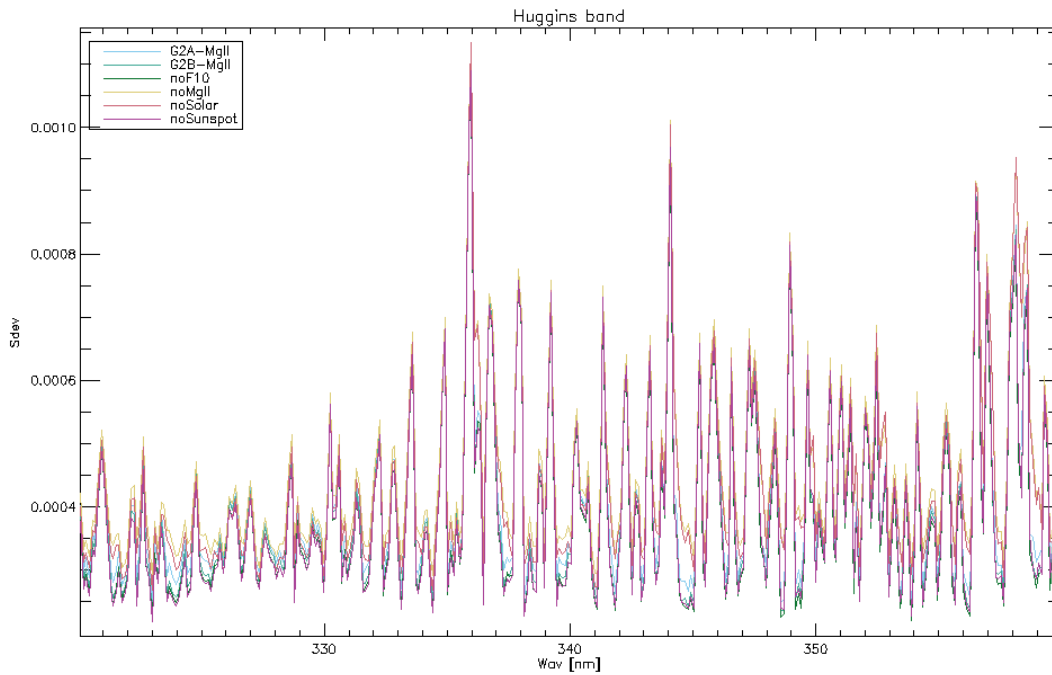


Figure 9 Standard deviation between model and measurement as function of for different (solar parameters) models.

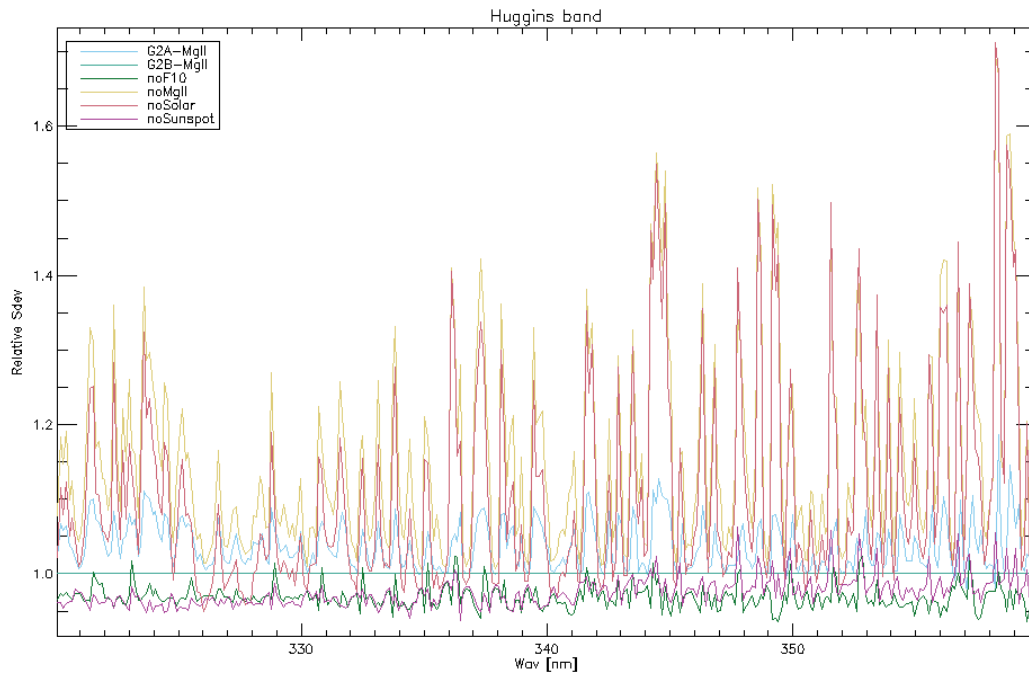


Figure 10 Relative (to default model G2B) Standard deviation between model and measurement as function of for different (solar parameters) models.

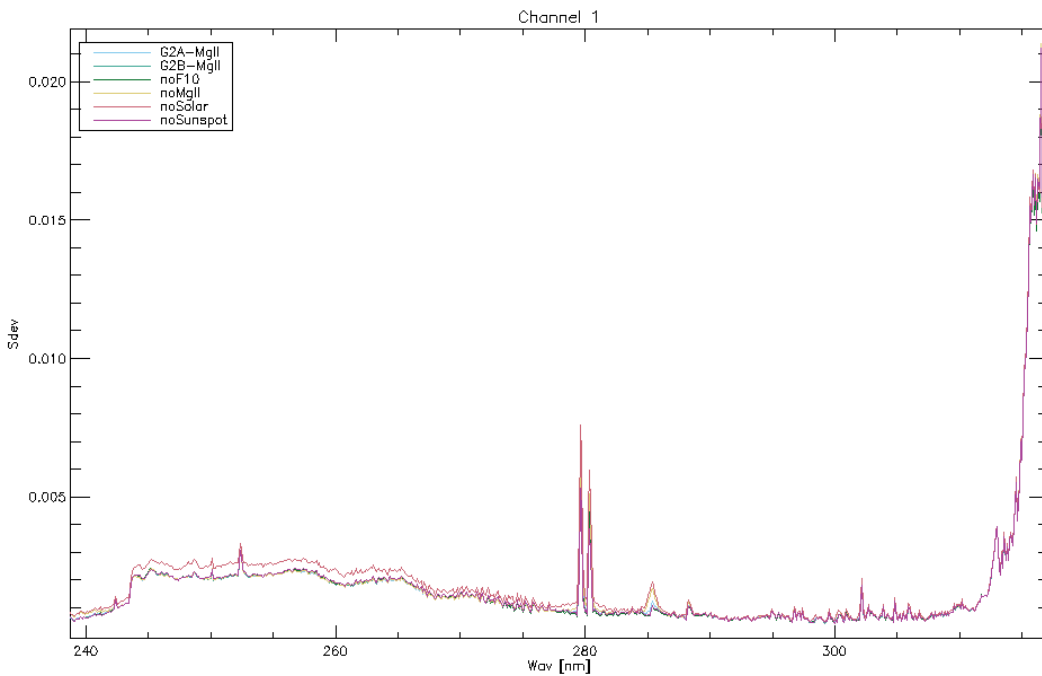


Figure 11 Standard deviation between model and measurement as function of for different (solar parameters) models.

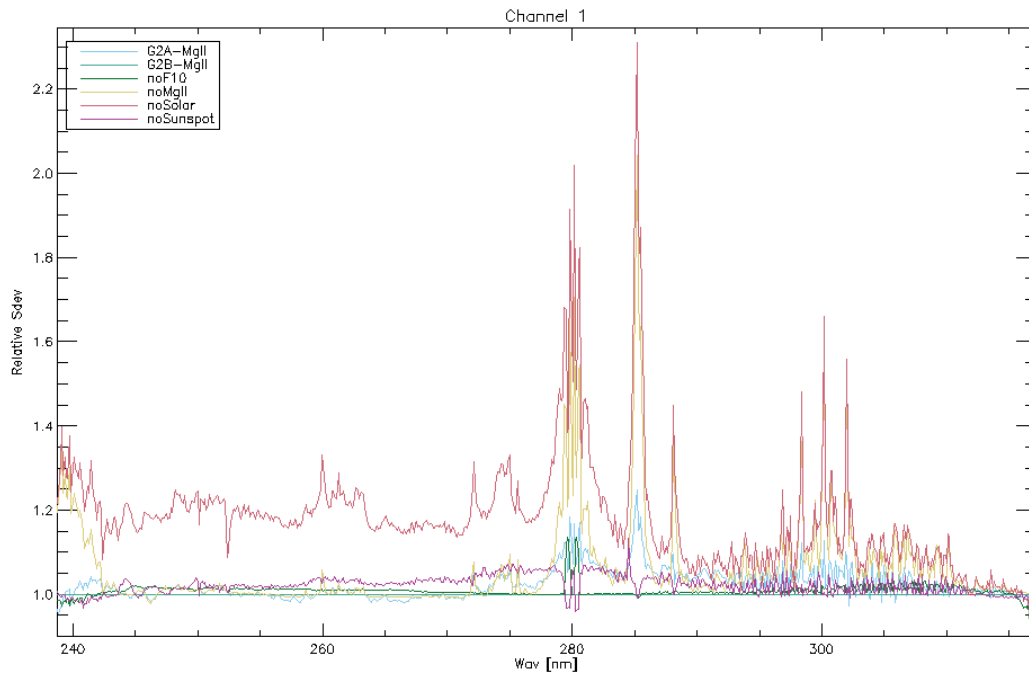


Figure 12 Relative (to default model G2B) Standard deviation between model and measurement as function of for different (solar parameters) models.

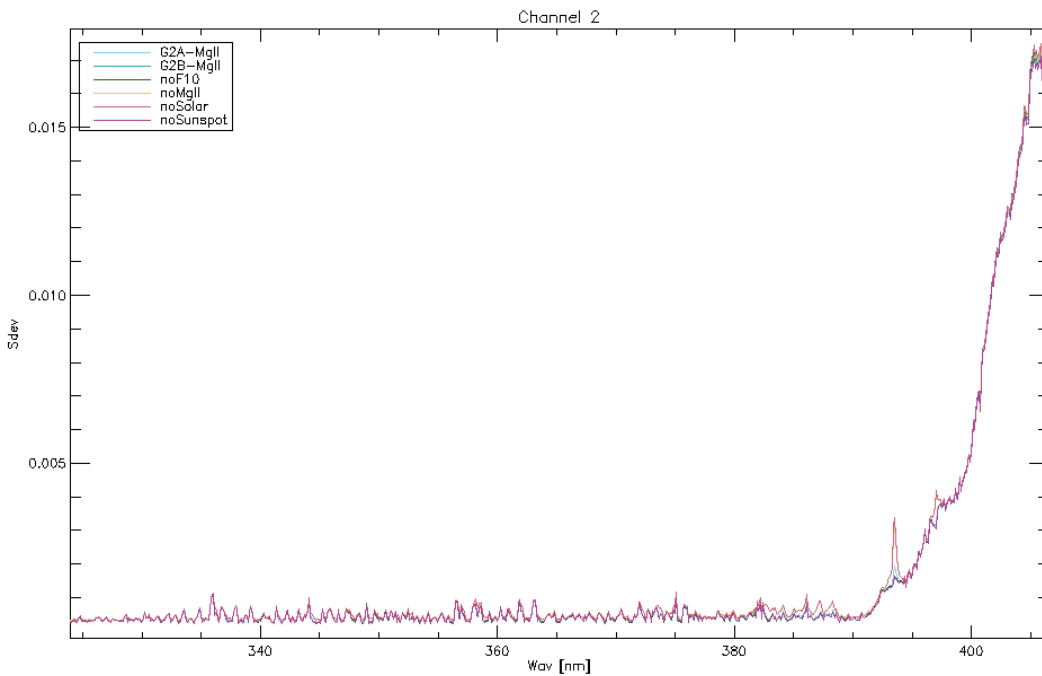


Figure 13 Standard deviation between model and measurement as function of for different (solar parameters) models.

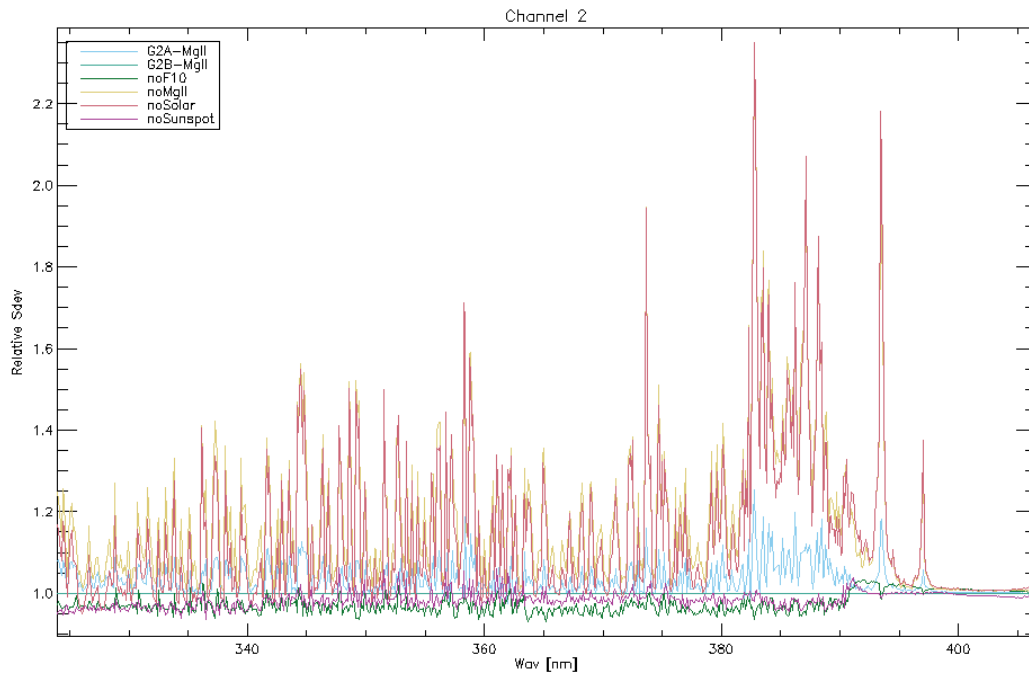


Figure 14 Relative (to default model G2B) Standard deviation between model and measurement as function of for different (solar parameters) models.

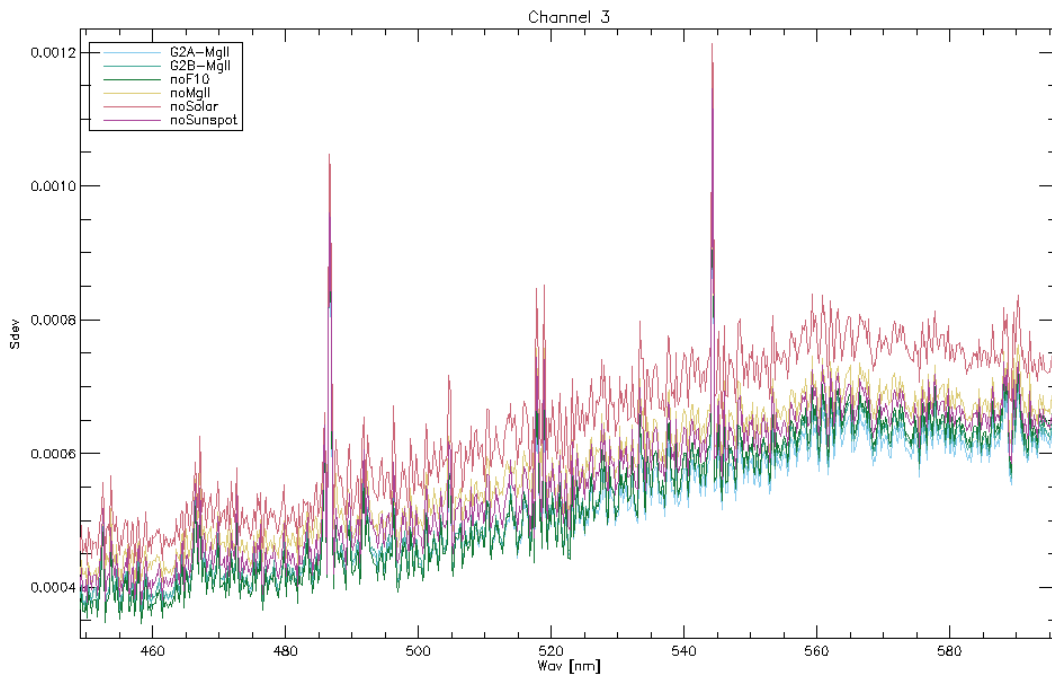


Figure 15 Standard deviation between model and measurement as function of for different (solar parameters) models.

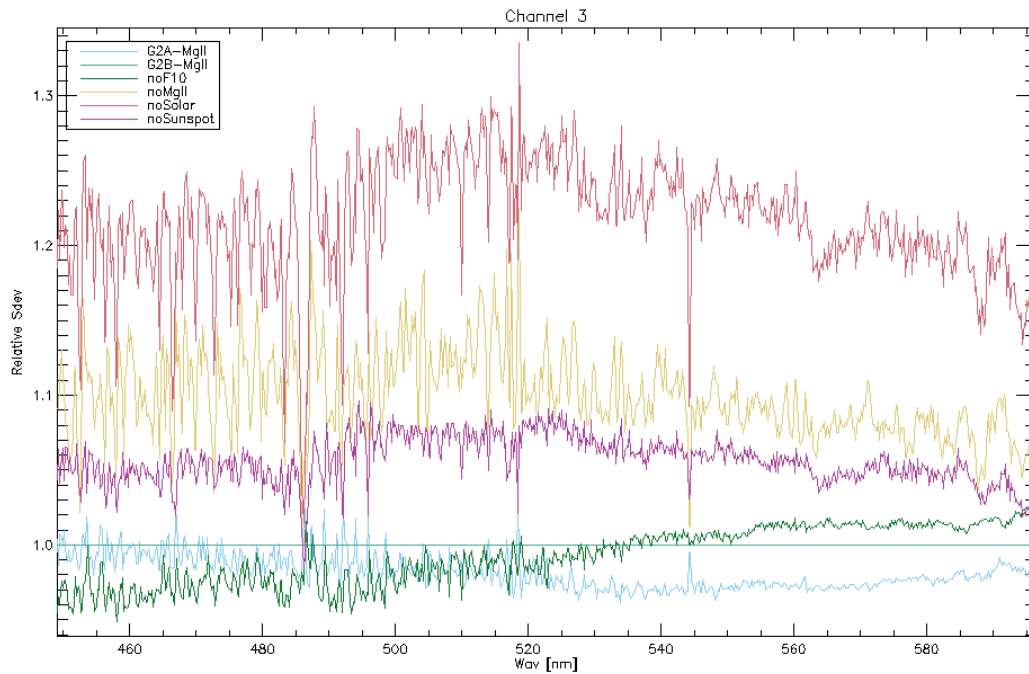


Figure 16 Relative (to default model G2B) Standard deviation between model and measurement as function of for different (solar parameters) models.

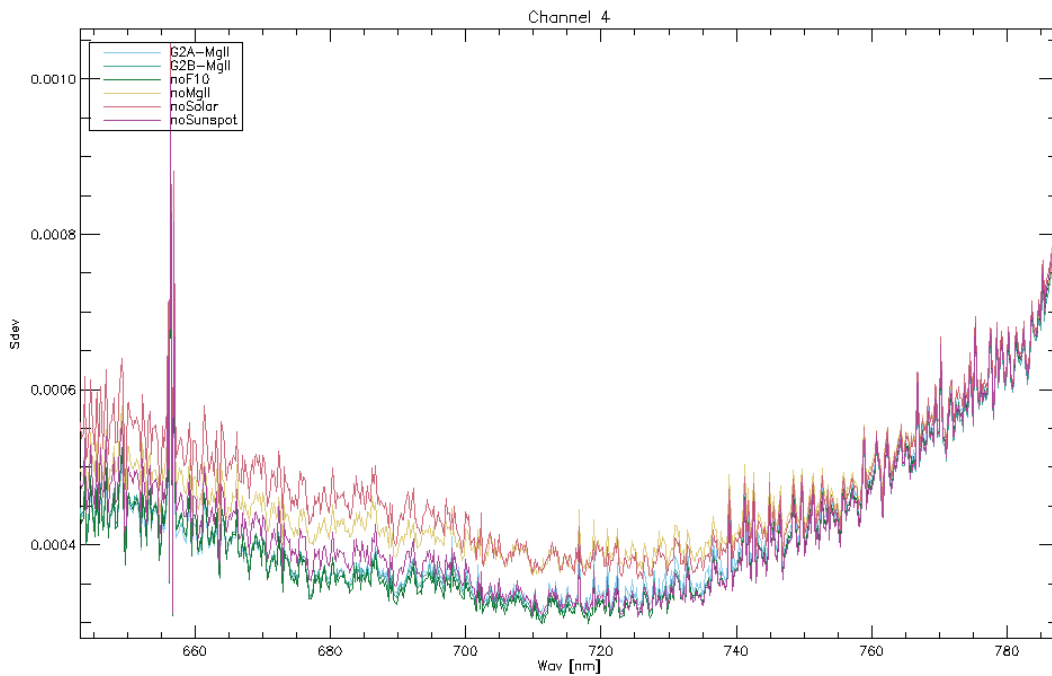


Figure 17 Standard deviation between model and measurement as function of for different (solar parameters) models.

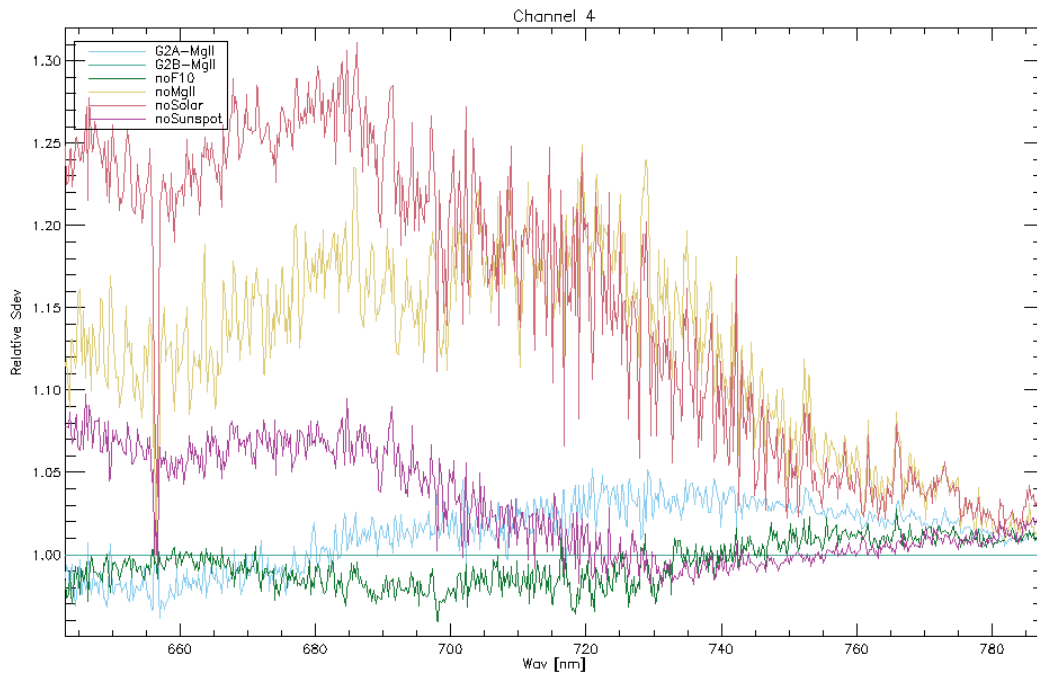


Figure 18 Relative (to default model G2B) Standard deviation between model and measurement as function of for different (solar parameters) models.

3.2.3 TIME DEPENDANCE OF SOLAR INDICES

It is not guaranteed that MGII index and F10.7 are not available in real time. In such cases, it is necessary to use data that is about one day old. The model was re-run using this older data. The effect is not negligible; in fact, the RMS is $\sim 1-2e^{-4}$. It is thus recommended to employ solar observations indices taken as close as possible to actual observation.

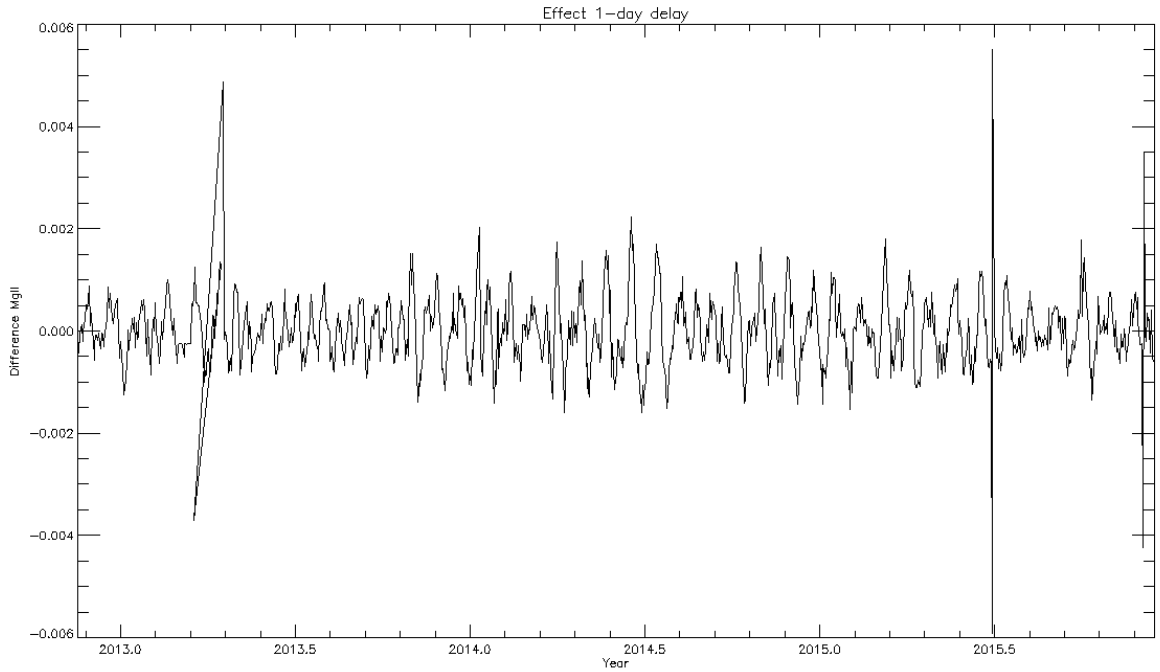


Figure 19 Difference between shifted_model and model MgII index.

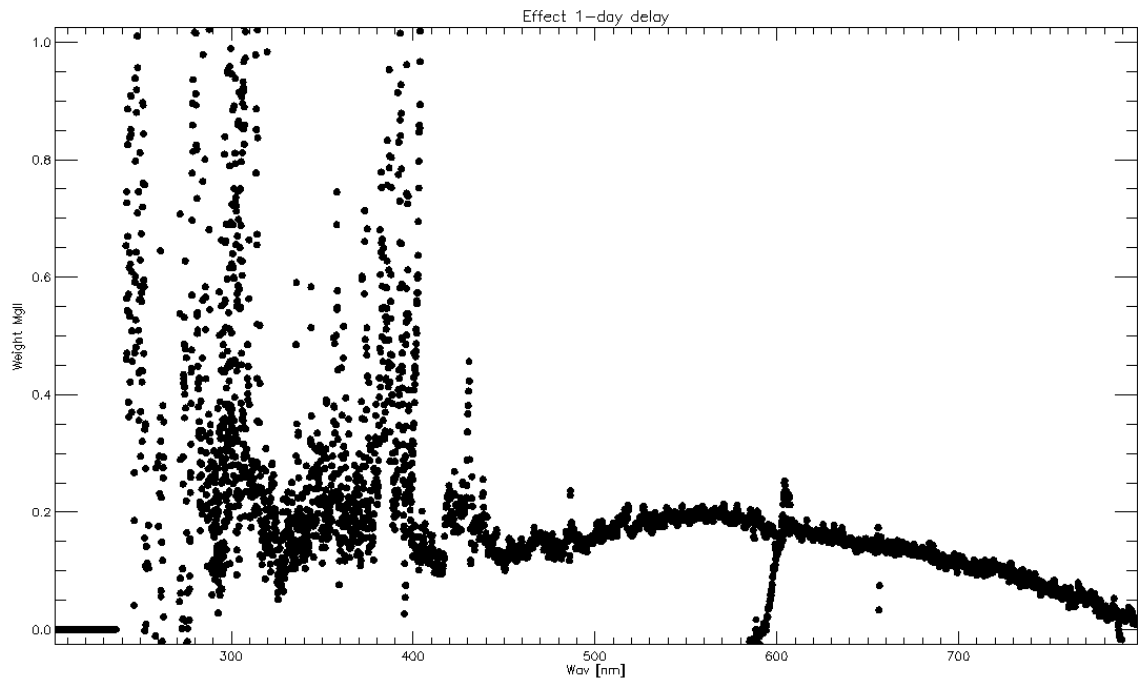


Figure 20 Weight MgII index.

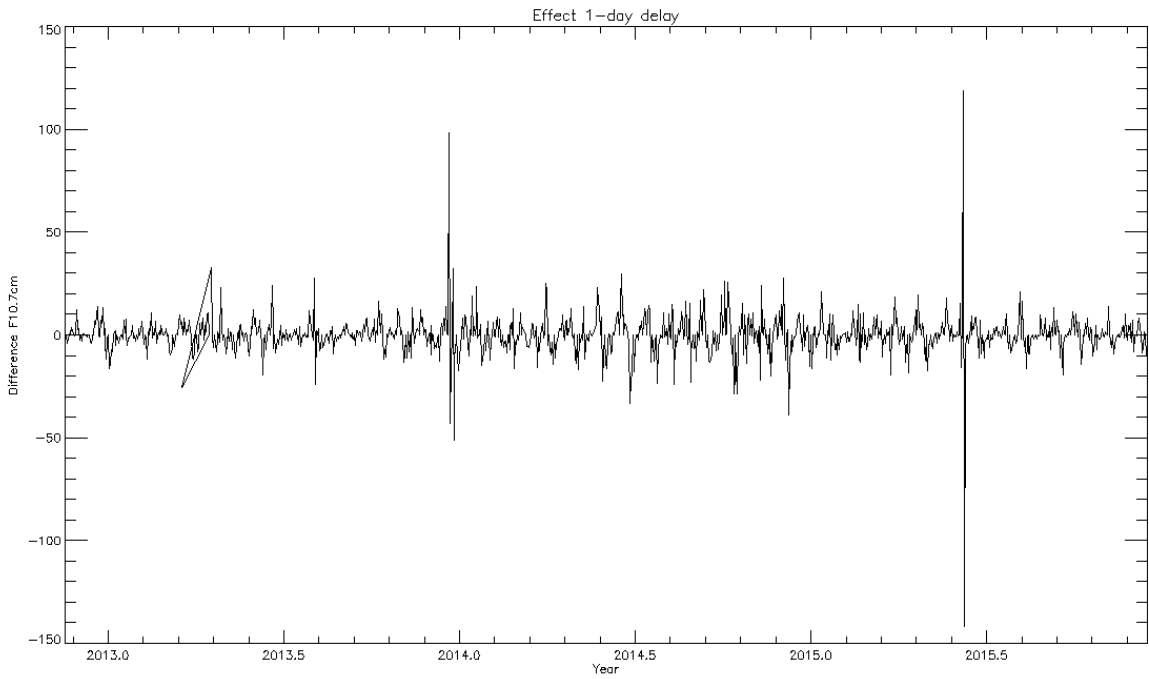


Figure 21 Difference between shifted_model and model F10.7 index

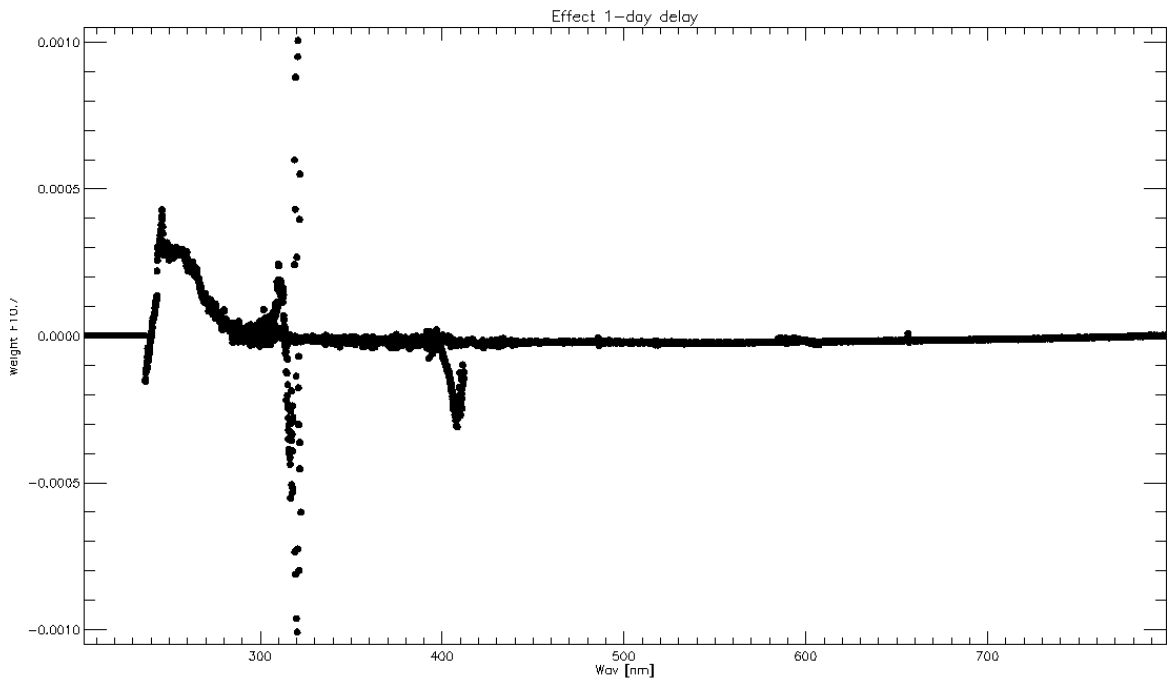


Figure 22 Weight F10.7 index

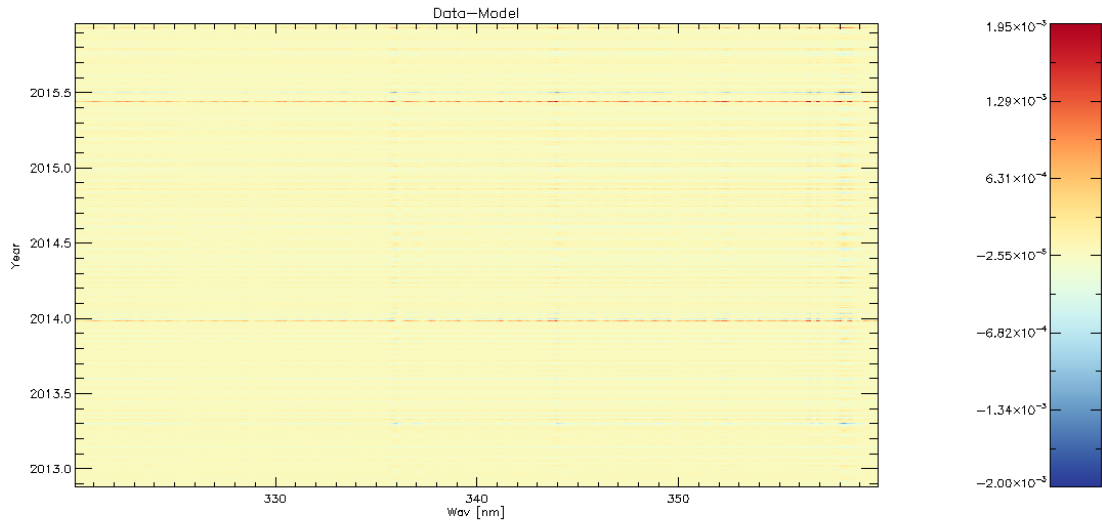


Figure 23 Difference between shifted_model and model as function of wavelength (zoomed in at the Huggins band) and time (year). Impact: $7.71773e^{-5}$.

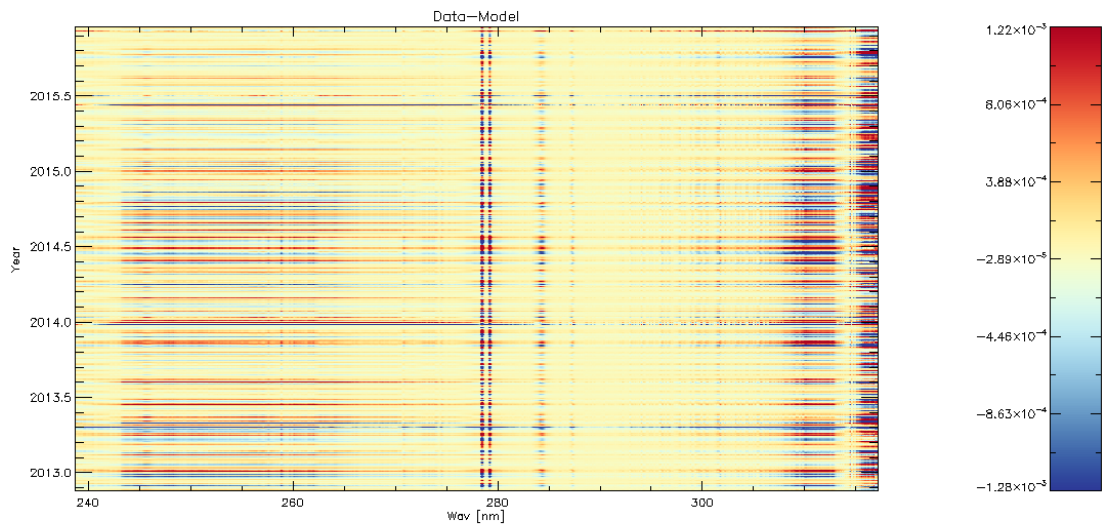


Figure 24 Difference between shifted_model and model as function of wavelength (zoomed in at Channel 1) and time (year). Impact: $4.60218 e^{-4}$.

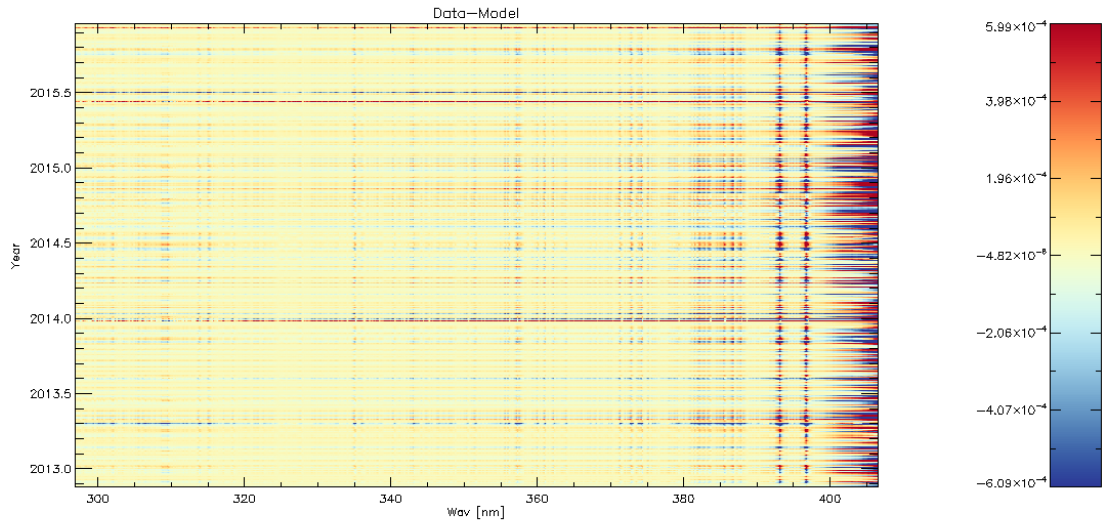


Figure 25 Difference between shifted_model and model as function of wavelength (zoomed in at Channel 2) and time (year). Impact: 2.49837 e^{-4} .

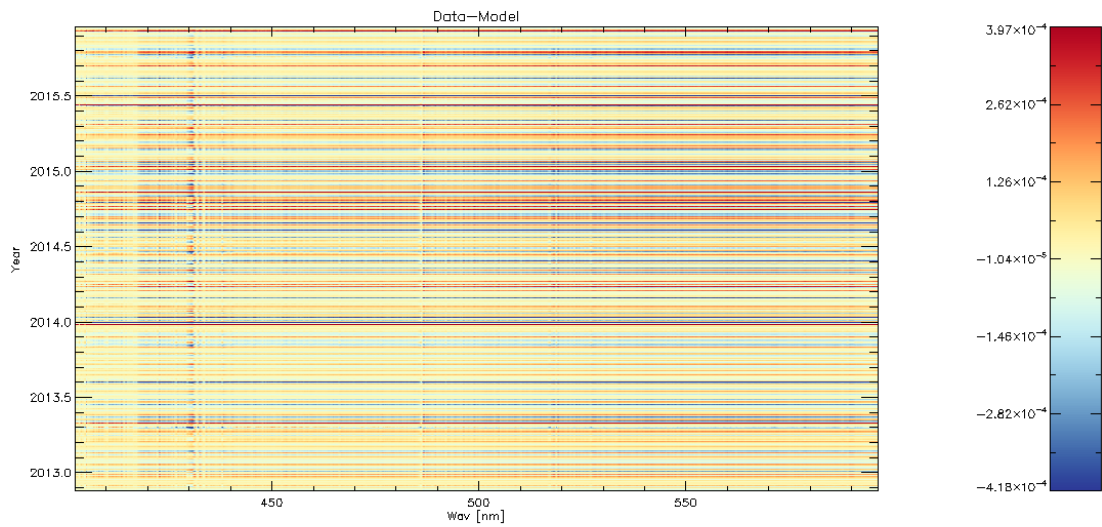


Figure 26 Difference between shifted_model and model as function of wavelength (zoomed in at Channel 3) and time (year). Impact: 1.79239 e^{-4} .

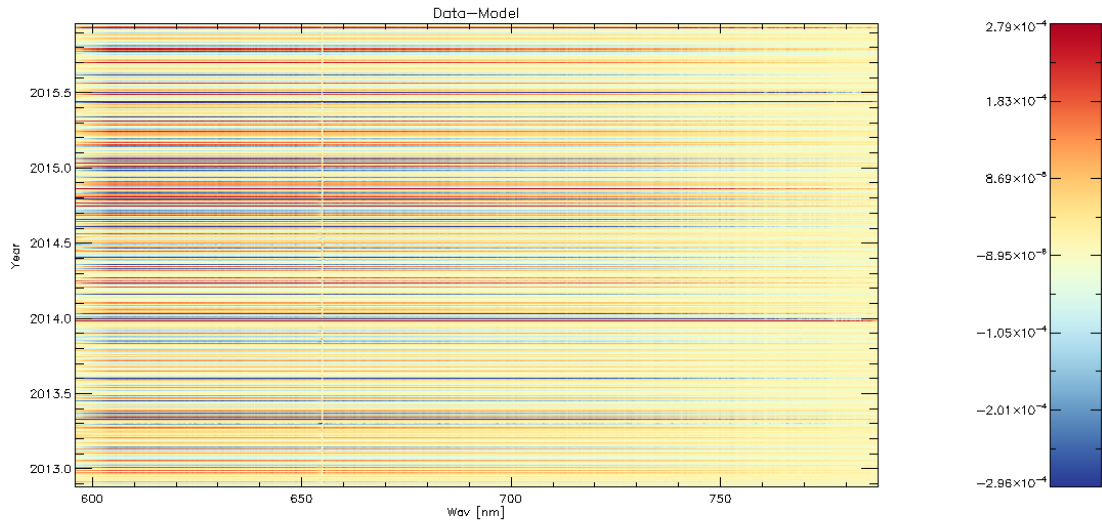


Figure 27 Difference between shifted_model and model as function of wavelength (zoomed in at Channel 4) and time (year). Impact: 1.24877 e^{-4} .

3.3 Degradation

The degradation of GOME2 is caused by a linear (in time) growth of contaminant on the various optical surfaces causing exponential absorption (Krijger et al, 2014). Longer wavelength show a recovery, most likely caused by constructive interference from the contaminant together with any coatings reaching an effective thickness of around $\frac{1}{4} \lambda$ of the longer wavelengths in question. The slow growth of the contaminant causes longer and longer wavelengths to fall into this domain and thus show recovery. The exact timing when a wavelength starts to show recovery confirms this slow growth.

As we are mostly focused on short term degradation (<3 year) we can describe this throughput degradation due to contaminant as a second order polynomial. This method both captures exponential decay and recovery depending on the wavelength of interest.

3.4 Solar Azimuth Variation

The signal in channel 1 (after polynomial degradation correction) shows a clear dependence on solar azimuth angle. In Figure 28 we show the detrended (each year individually) signal for each year for a wavelength in the middle of channel 1. Each year has a different color. In black we show the solar azimuth variation (for all years combined). The correlation is striking. Figure 29 is the result of fitting each yearly

signal to its solar azimuth variation individually with a simple offset and multiplication factor or weight. In Figure 30 the found weight for each year is plotted together with a second order polynomial fit.

In Figure 31 we investigate this further. Instead of a weight for each year we now plot the weight for each yearly detrended measurement together with a second order polynomial fit and an exponential fit. The exponential fit is clearly the most correct description; however a second order polynomial can be employed for the later period (as is the case here).

Explanation for this is likely linear growth (in time) of contaminant causing an increasing dependence on azimuth angle.

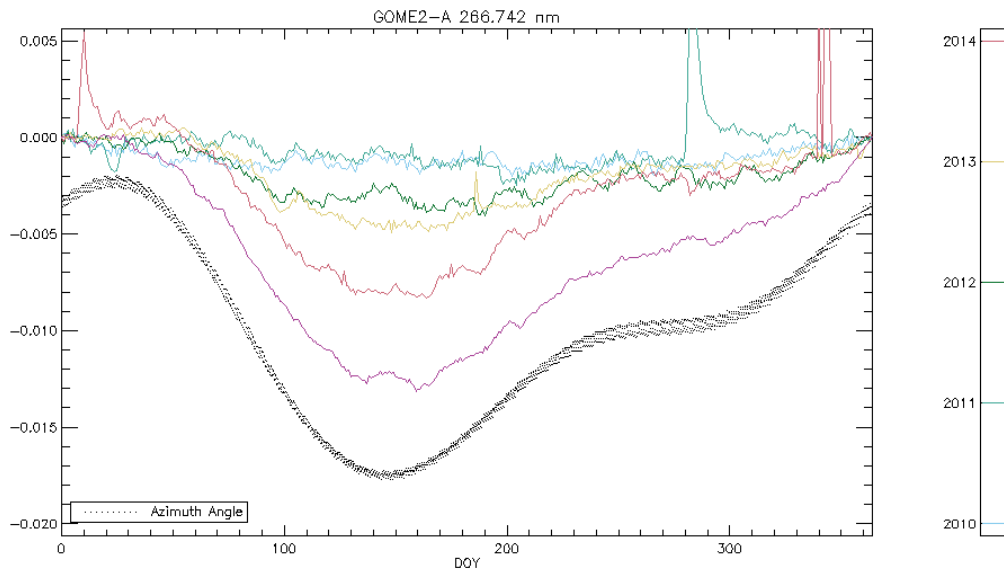


Figure 28 Detrended SMR measurement for 266.742 nm as function of Day Of the Year (DOY). Each year in different color as indicated on right. In black and dotted the (scaled and offset).

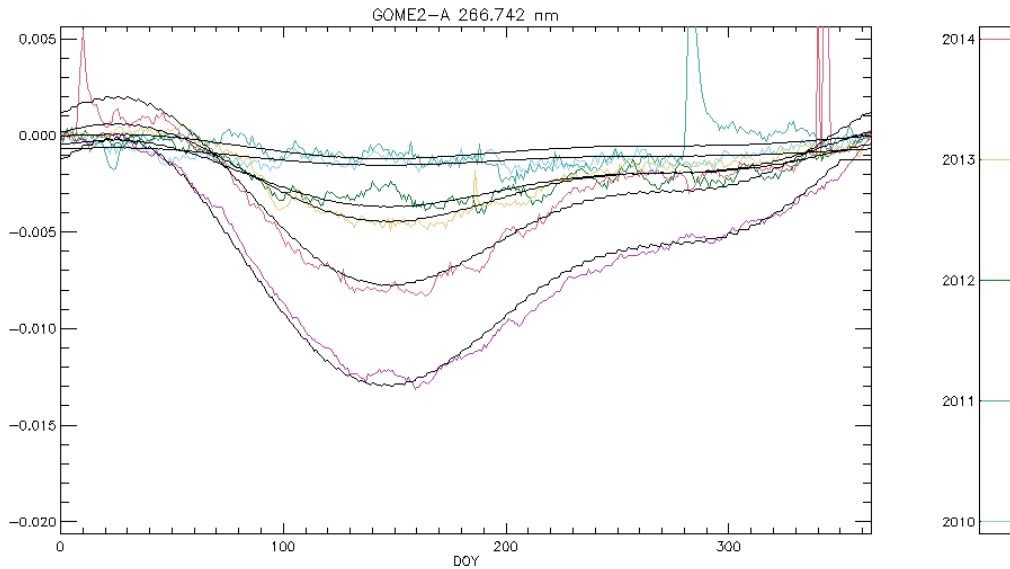


Figure 29 Detrended SMR measurement for 266.742 nm as function of Day Of the Year (DOY). Each year in different color as indicated on right. In black and dotted the (scaled and offset) Azimuth variation over all years. Overpotted in black, the for each year separately scaled azimuth angle.

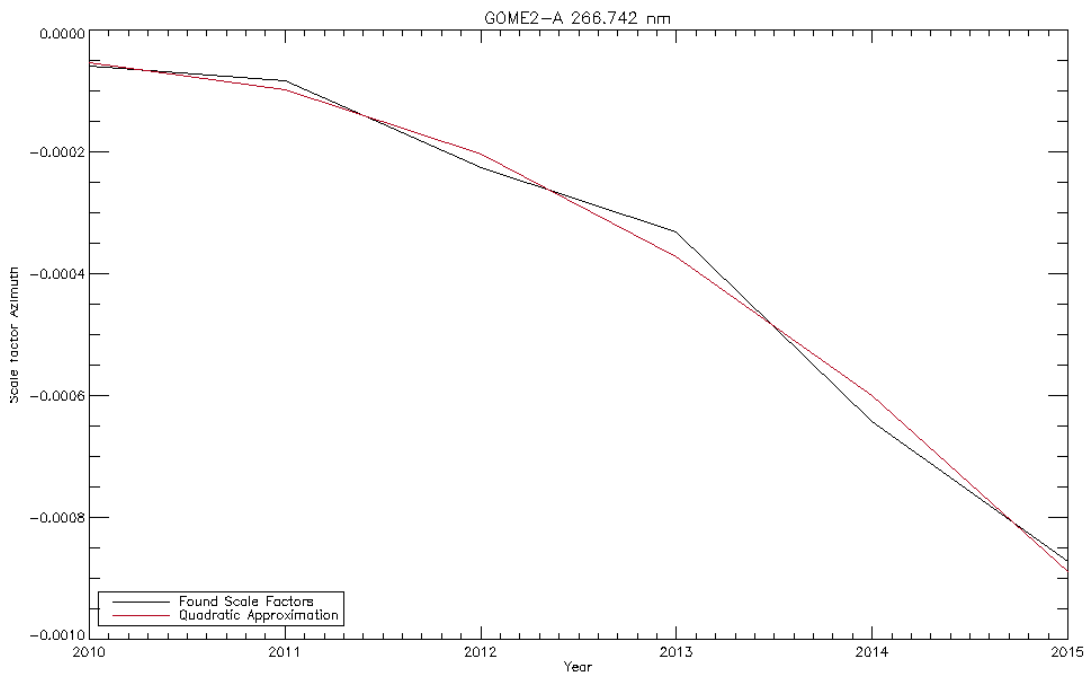


Figure 30 The fitted scale factor the azimuth angle for each year, as a function of time for 266.742 nm.

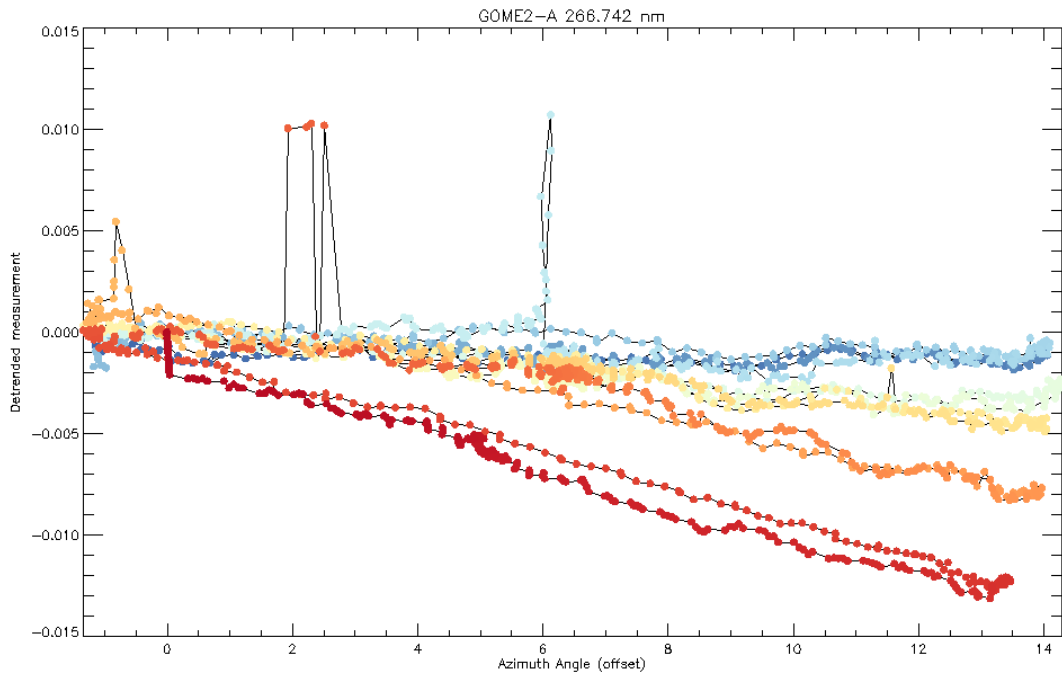


Figure 31 Detrended SMR measurement for 266.742 nm as function of azimuth angle. Time is indicated by colors going from blue (early) to yellow to red (late). A clear azimuth dependence is visible that increases over the years.

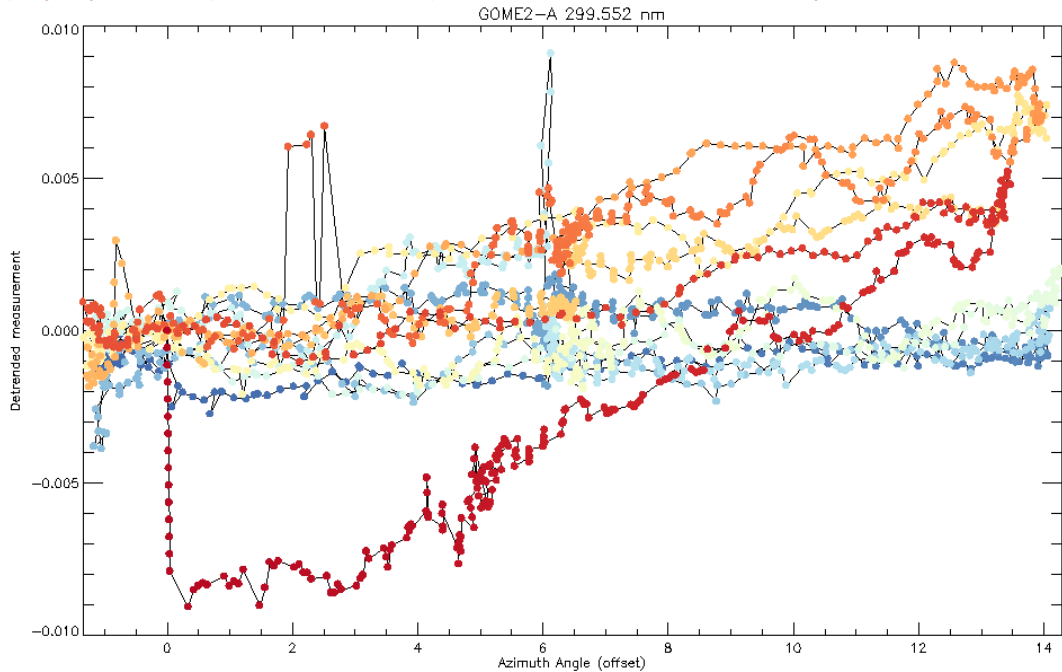


Figure 32 Detrended SMR measurement for 299.552 nm as function of azimuth angle. Time is indicated by colors going from blue (early) to yellow to red (late). A clear azimuth dependence is visible that increases over the years.

3.5 Model results

3.5.1 FIT VALUES

The following images show the found fitting weights for the different fitting parameters as a function of virtual detector pixel.

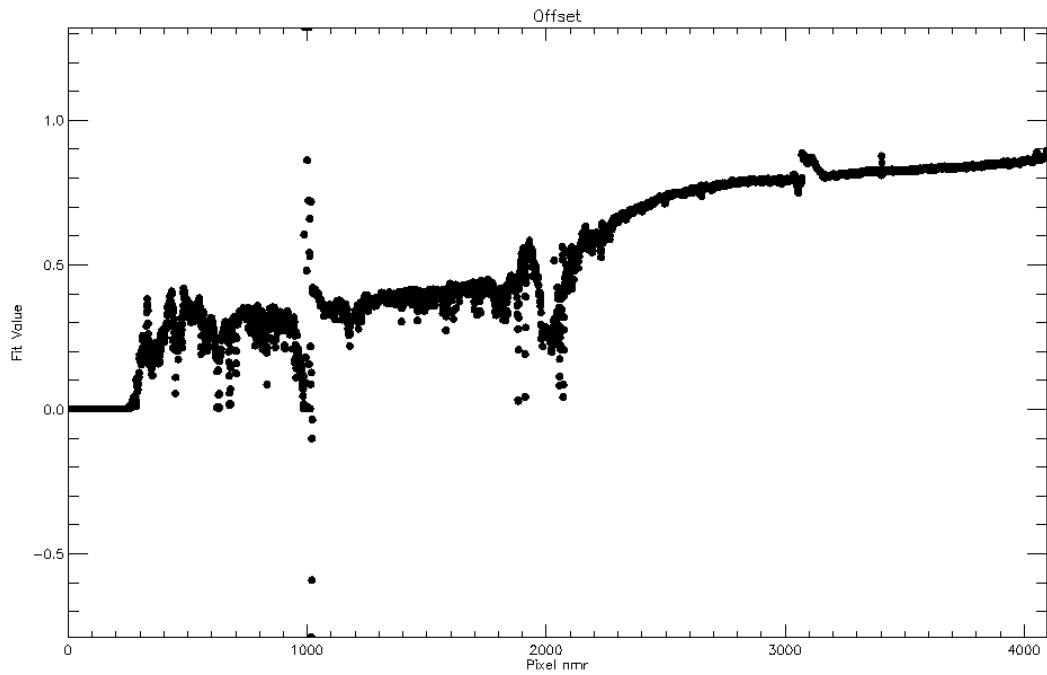


Figure 33 Fitted value of parameter *offset* as function of pixel number.

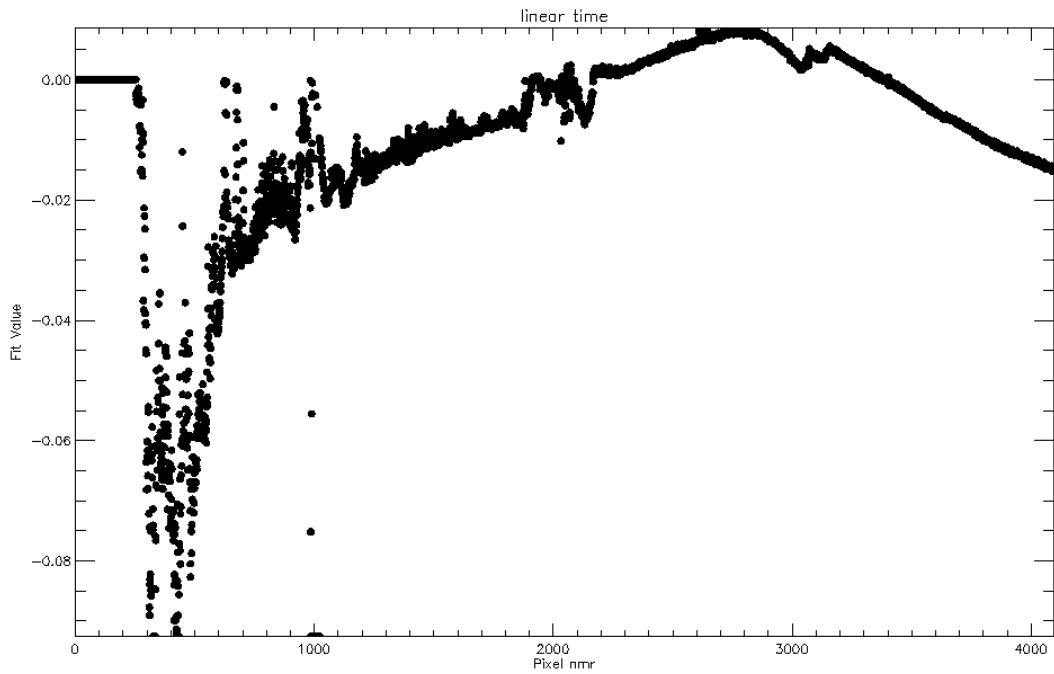


Figure 34 Fitted value of parameter *linear time* as function of pixel number.

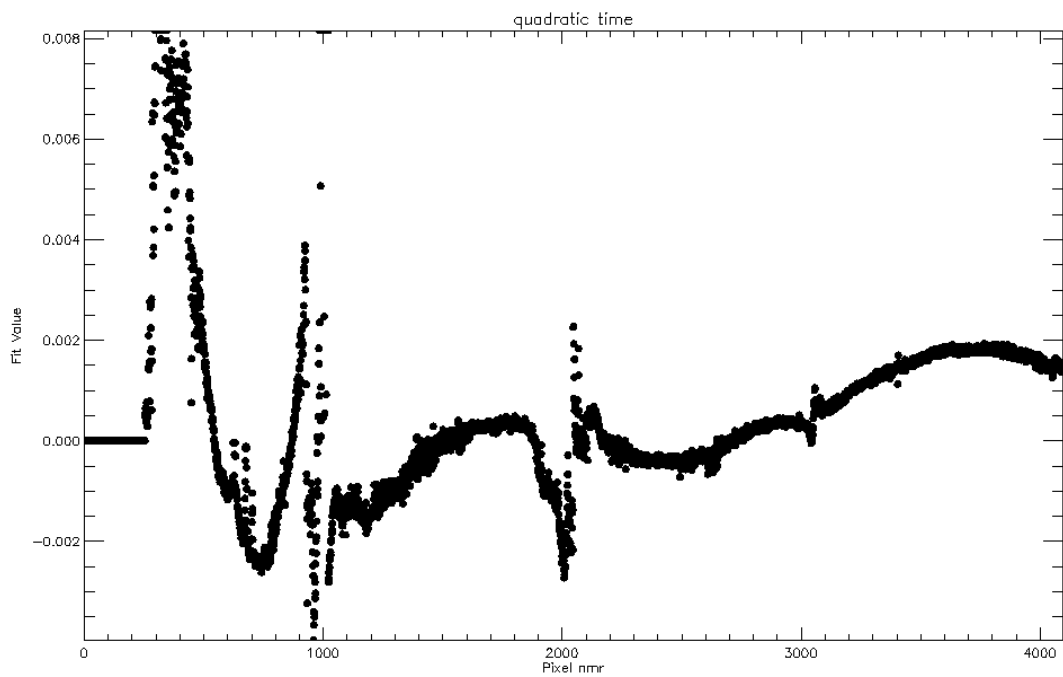


Figure 35 Fitted value of parameter *quadratic time* as function of pixel number.

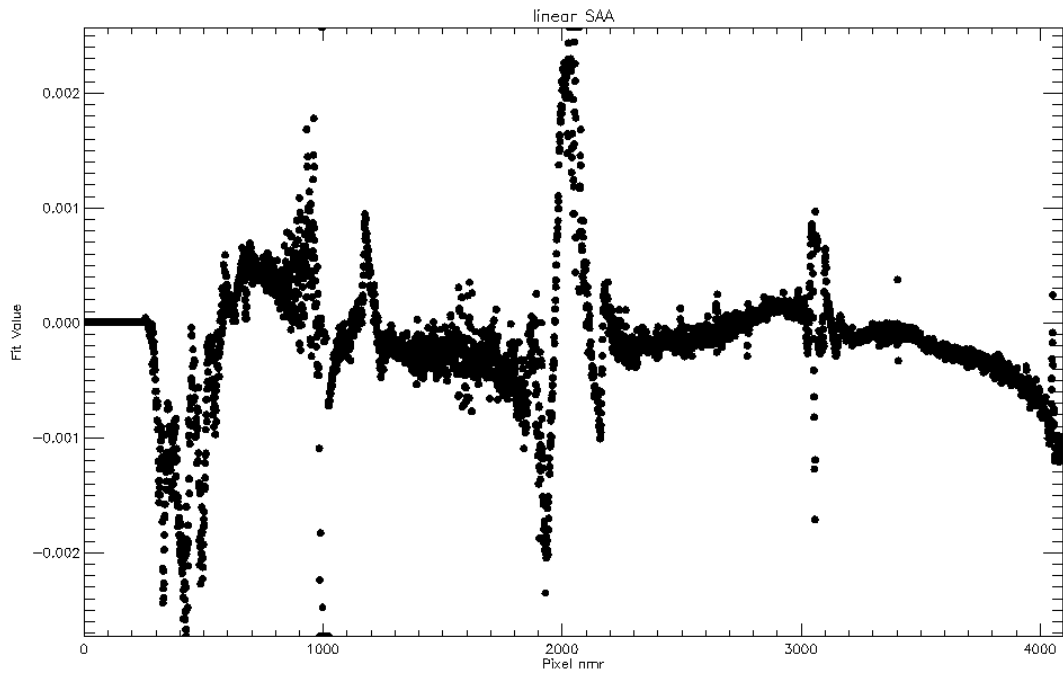


Figure 36 Fitted value of parameter *linear_SAA* as function of pixel number.

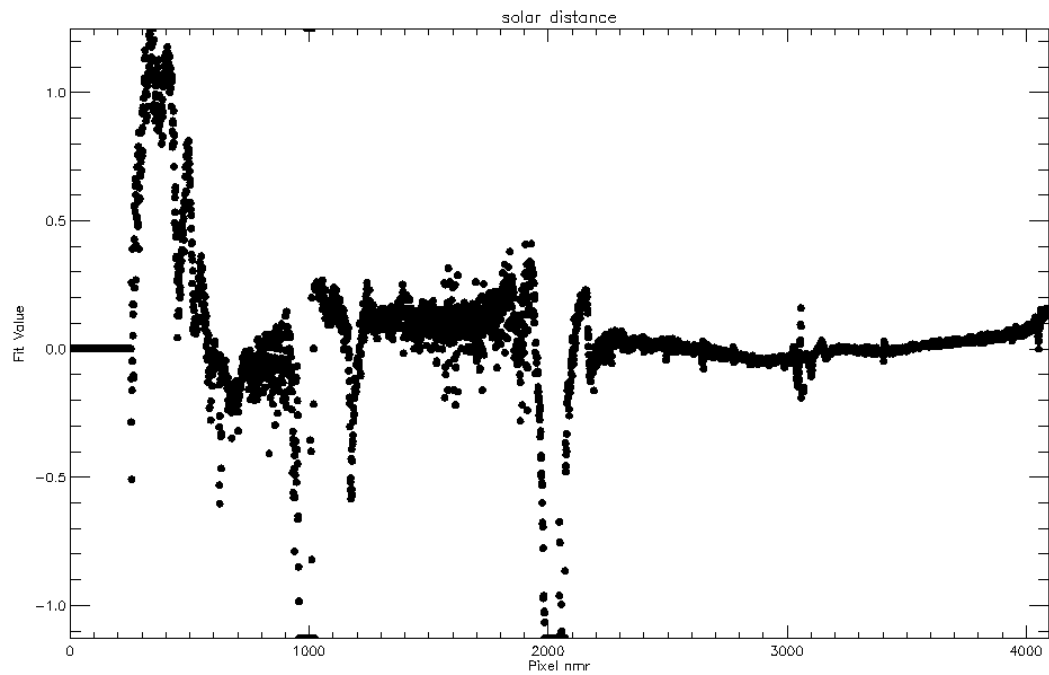


Figure 37 Fitted value of parameter *solar distance* as function of pixel number.

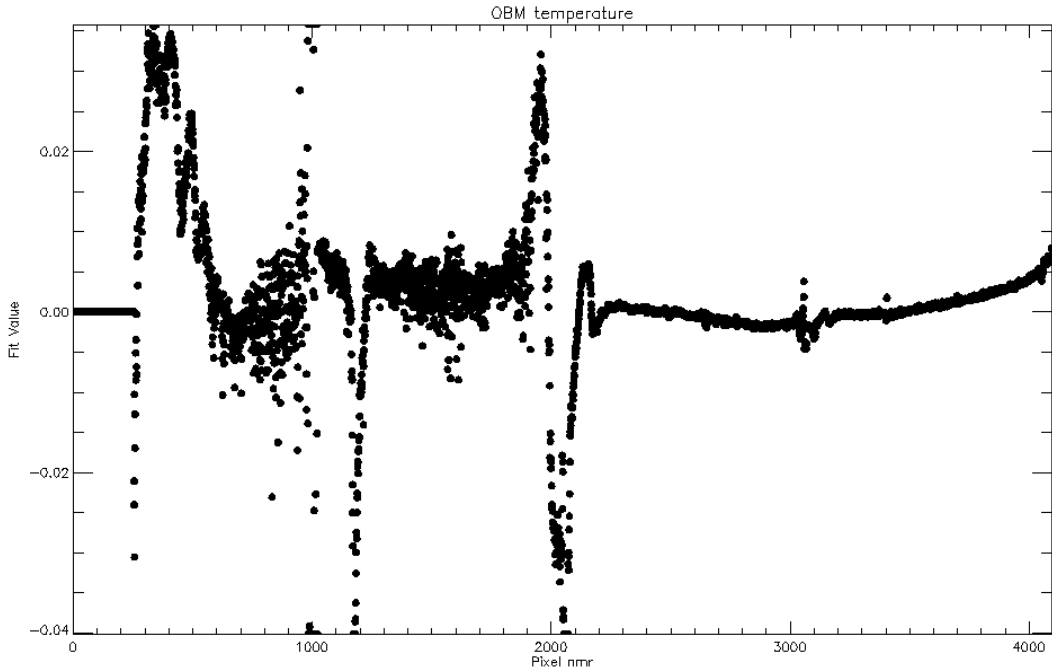


Figure 38 Fitted value of parameter *OBM temperature* as function of pixel number.

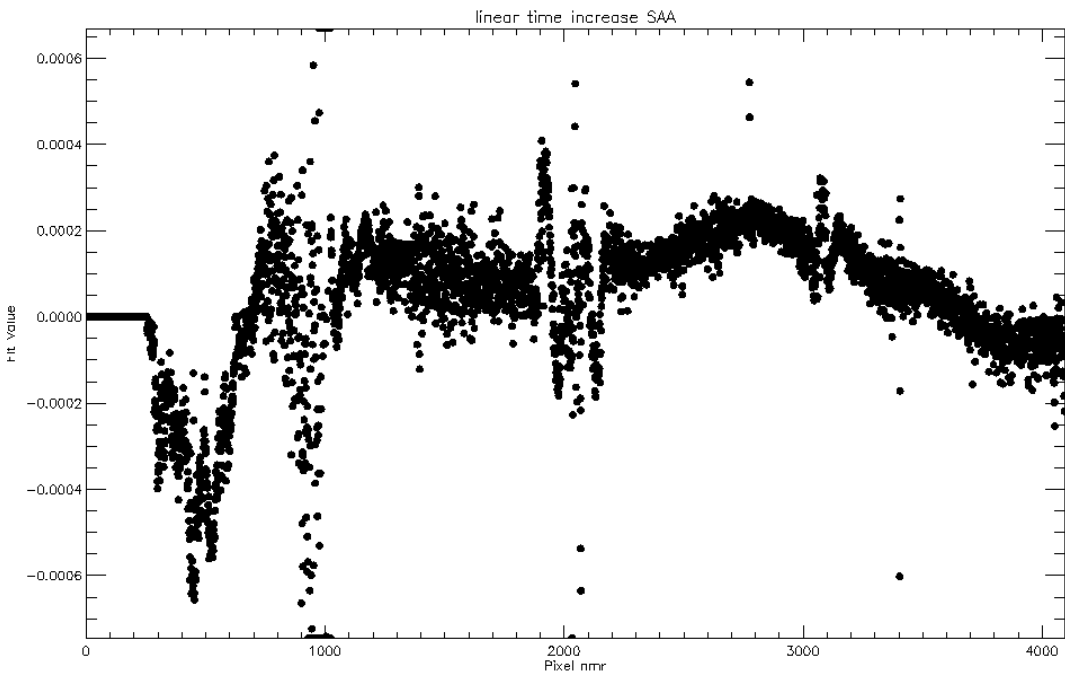


Figure 39 Fitted value of parameter *linear time increase SAA* as function of pixel number.

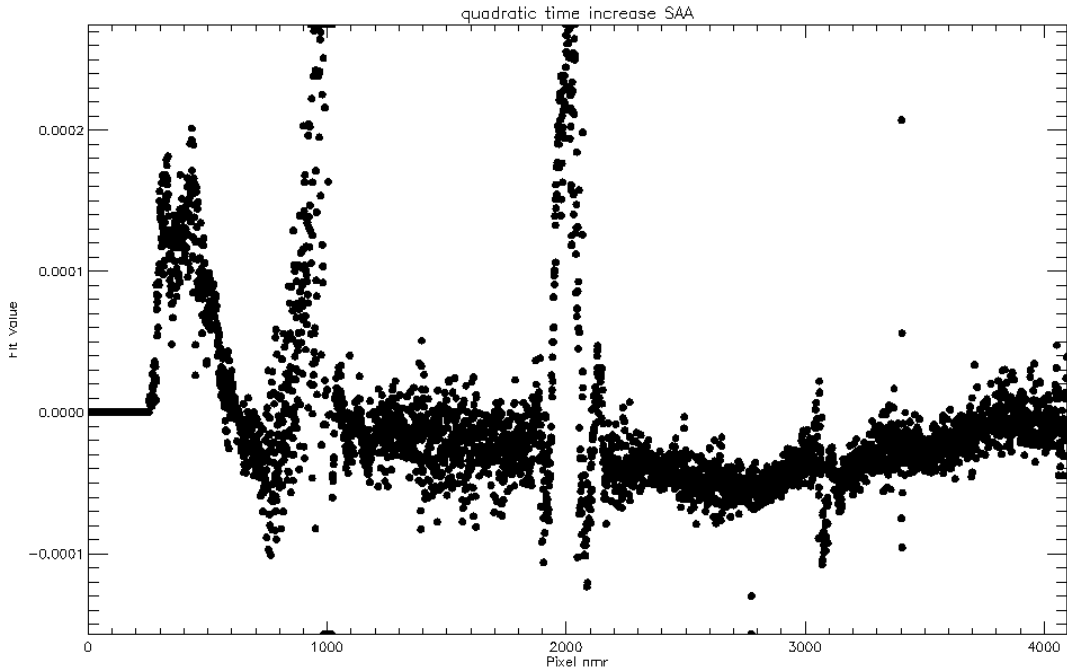


Figure 40 Fitted value of parameter *quadratic time increase SAA* as function of pixel number.

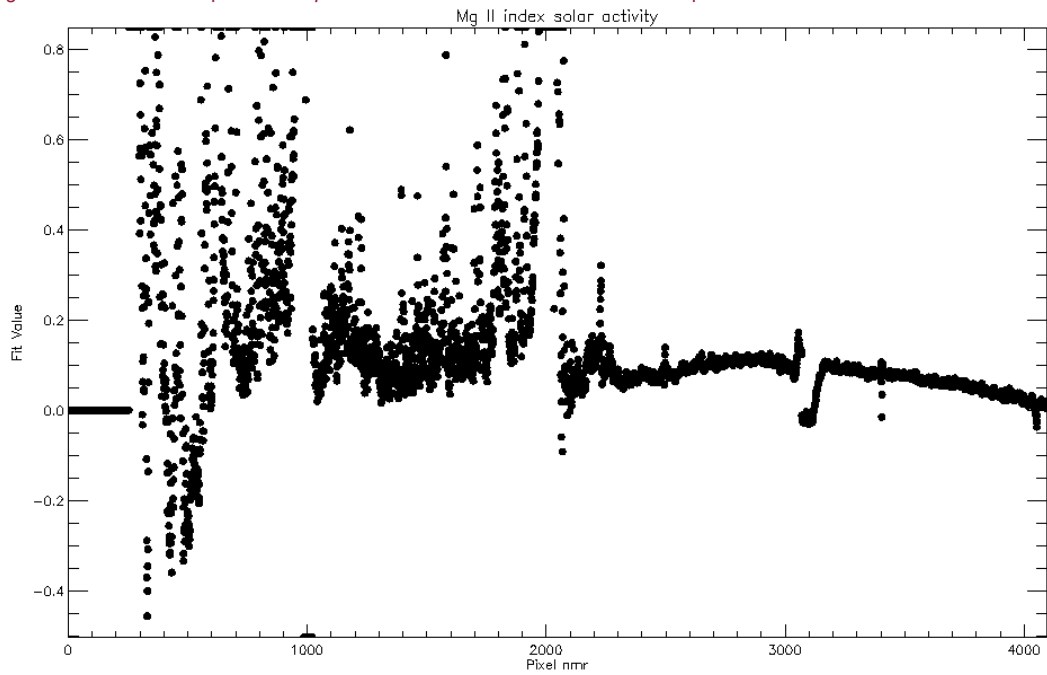


Figure 41 Fitted value of parameter *MgII index solar activity* as function of pixel number.

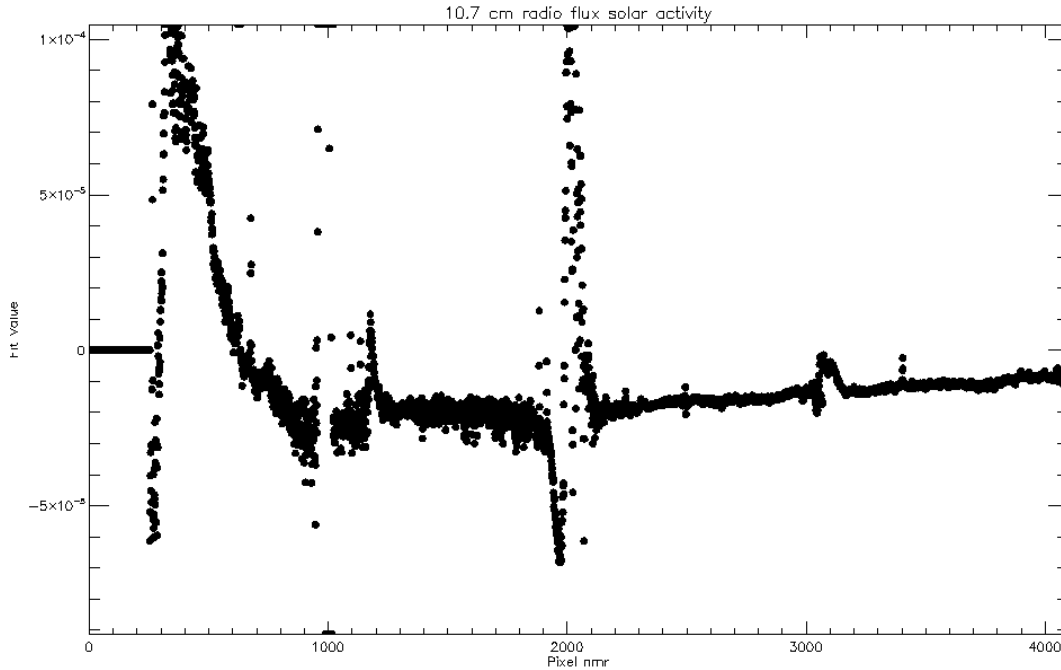


Figure 42 Fitted value of parameter *10.7 cm radio flux solar activity* as function of pixel number.

3.5.2 FIT CONTRIBUTIONS

The following images show the various contributions to the model as derived weights of the various inputs, used to construct the expected solar transmittance. Contribution is defined here as the contribution to the variance (over time) of the model output. Note these are absolute weights, e.g., the lower wavelengths degrade more, hence have a larger variance, and so the weights are larger for the lower wavelengths.

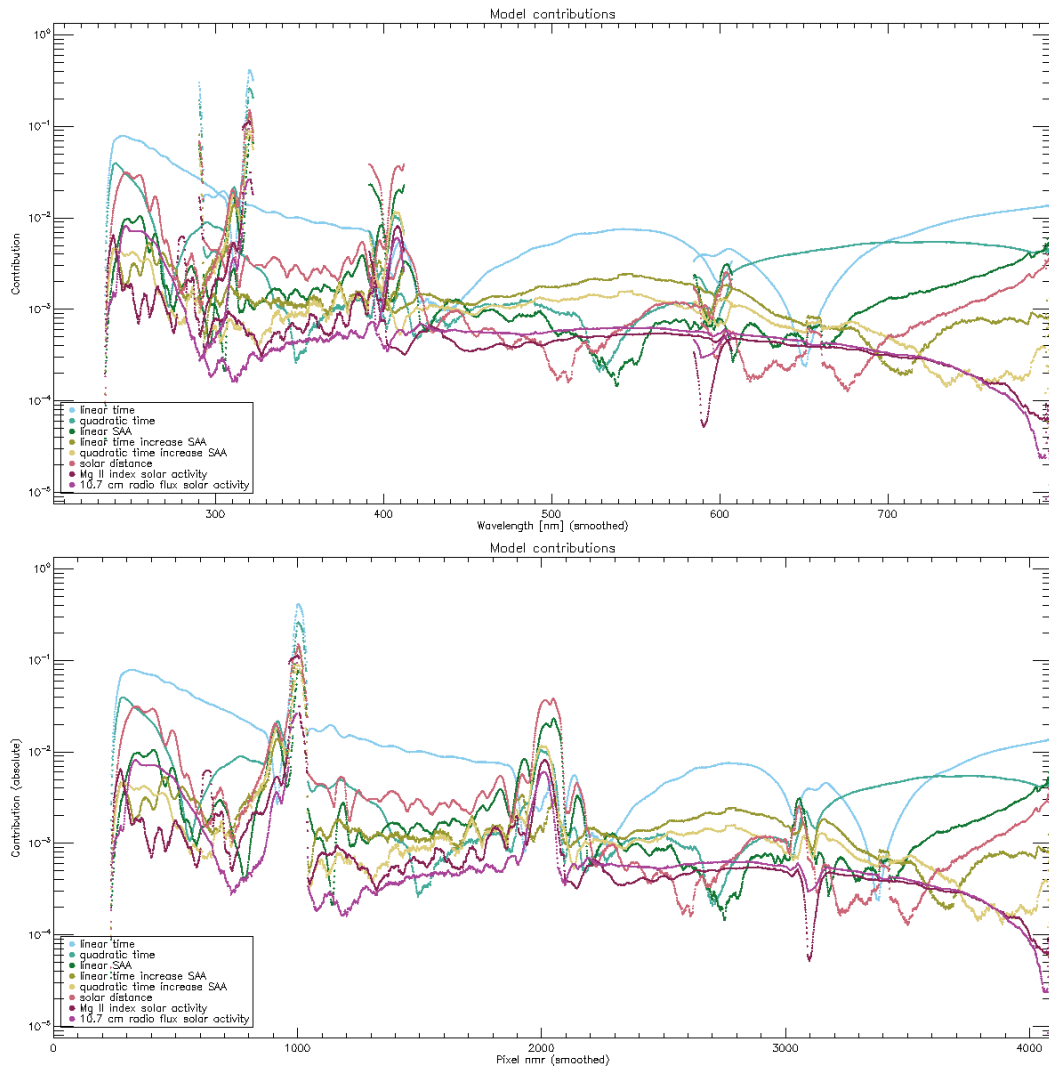


Figure 43 Derived weights of the various inputs (color-coded as indicated in legend), used to construct the expected solar transmittance, here shown as contribution to the variance (over time) of the model output. The upper plot shows the contribution as function of wavelength. The lower plots shows the same contribution but now as function of pixel nmr.

3.5.3 ACCURACY

The following images show the difference (standard deviation) between actual measurement and the fully modeled or virtual measurement for different wavelengths over certain periods of time, or as color in a 2D image as a function of time and detector pixel (wavelength). We have chosen to focus here on the period 2015.0 till 2015.216 (2015-01-01 – 2015-03-18) which best represent the future solar visibility loss periods in all viewing parameters.

Channel 2-4 differences are very small in the order $1e-4$, channel 1 has for certain periods a slightly larger deviation between actual measurement and virtual measurement. No attempt has been made to describe the signal below 237nm, as the solar observations are too noisy at these wavelengths.

See also standard deviation plots in Section 3.2.2 (Different Scenarios).

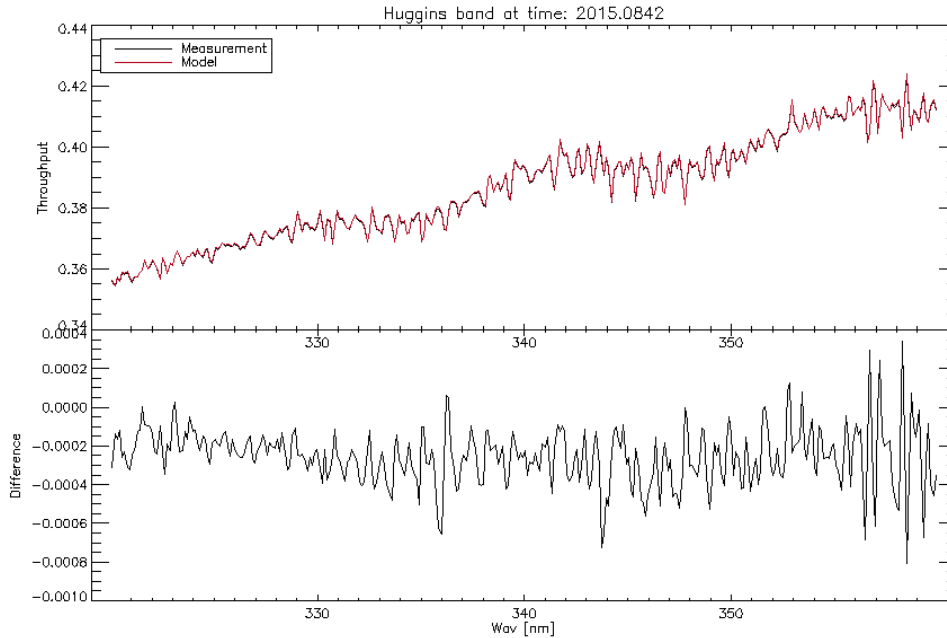


Figure 44 Top: Throughput in the Huggins band in early 2015. Measurement in black, model in red. Bottom: Difference between measurement and model.

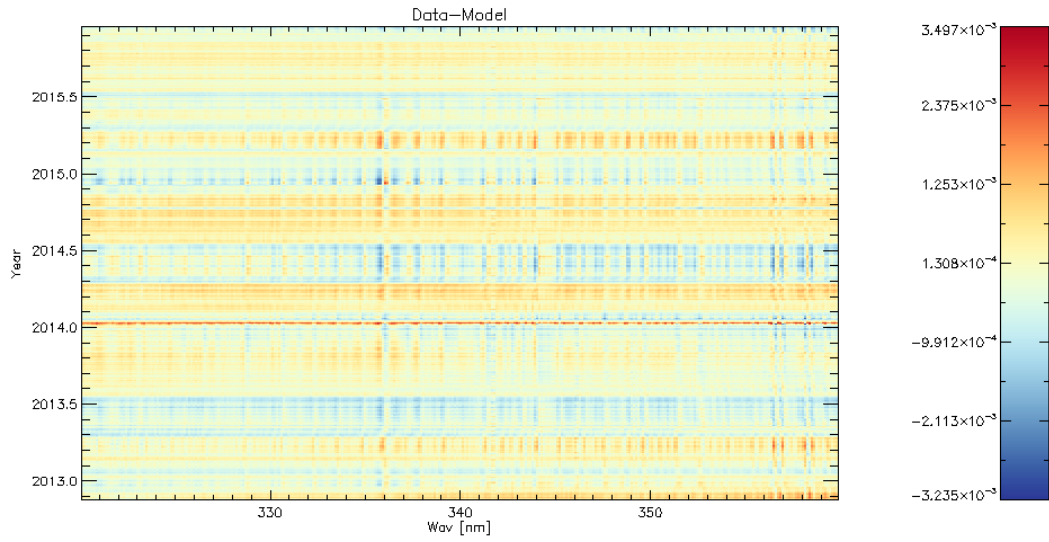


Figure 45 Difference between measurement and model as function of wavelength (zoomed in at the Huggins band) and time (year).

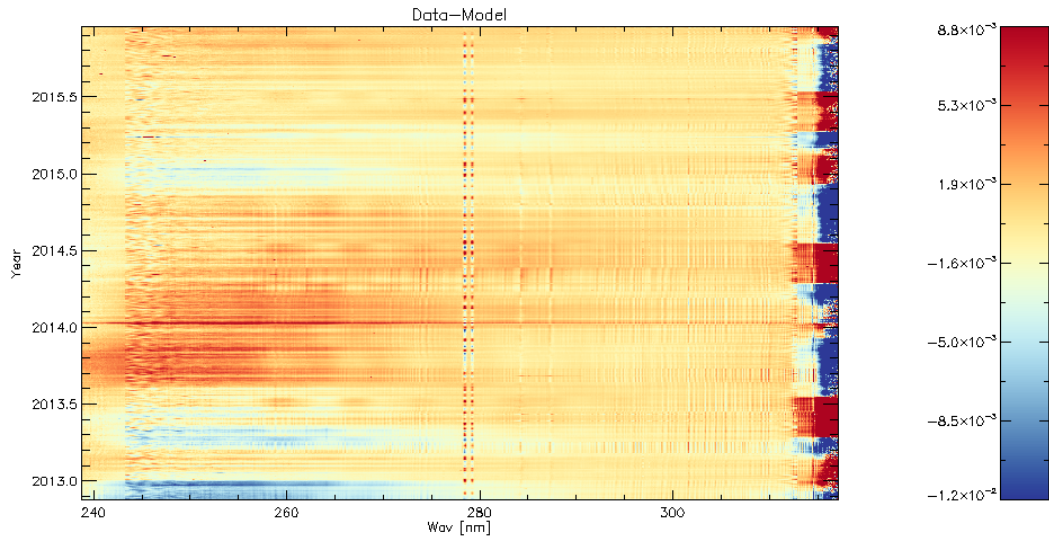


Figure 46 Difference between measurement and model as function of wavelength (zoomed in at Channel 1) and time (year).

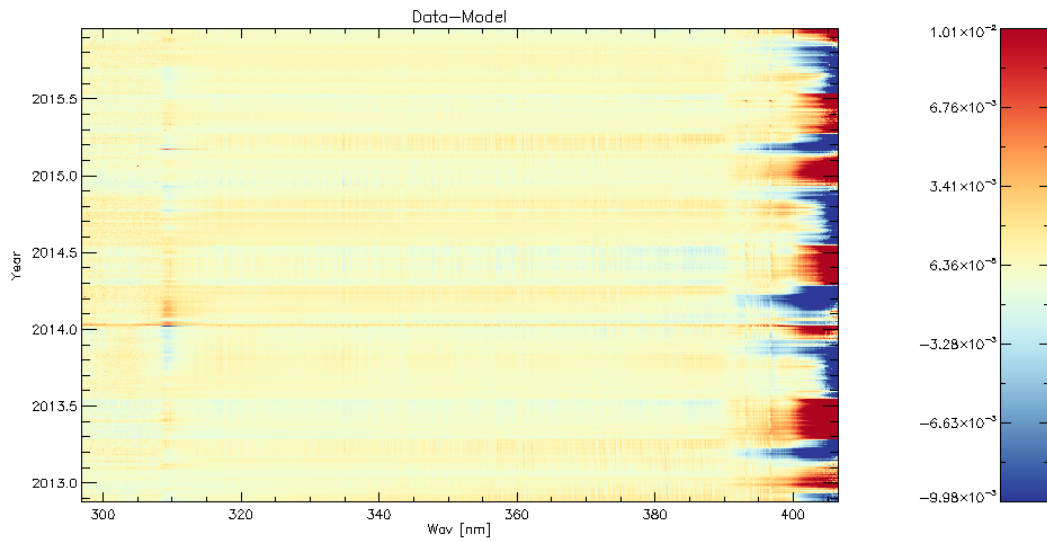


Figure 47 Difference between measurement and model as function of wavelength (zoomed in at Channel 2) and time (year).

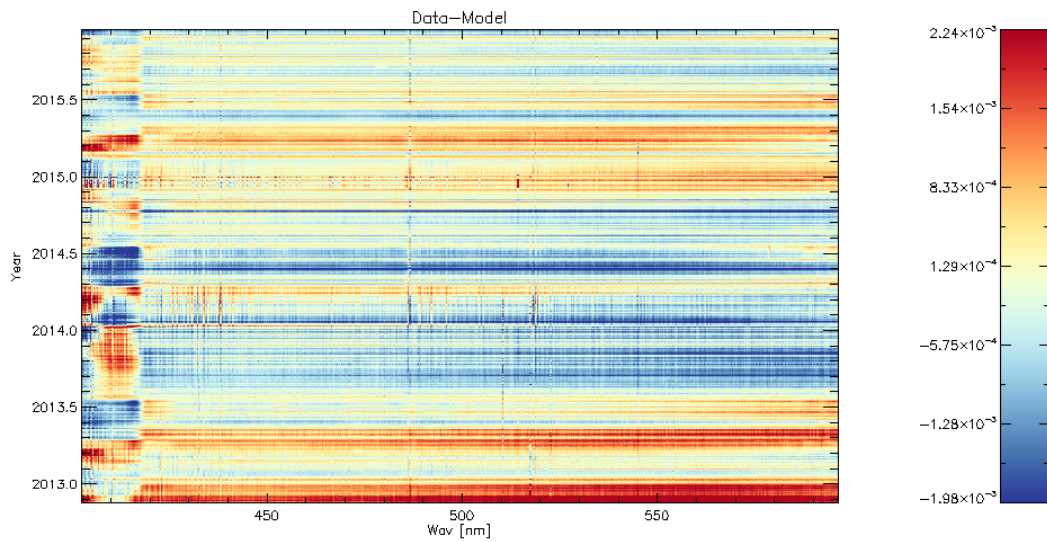


Figure 48 Difference between measurement and model as function of wavelength (zoomed in at Channel 3) and time (year)

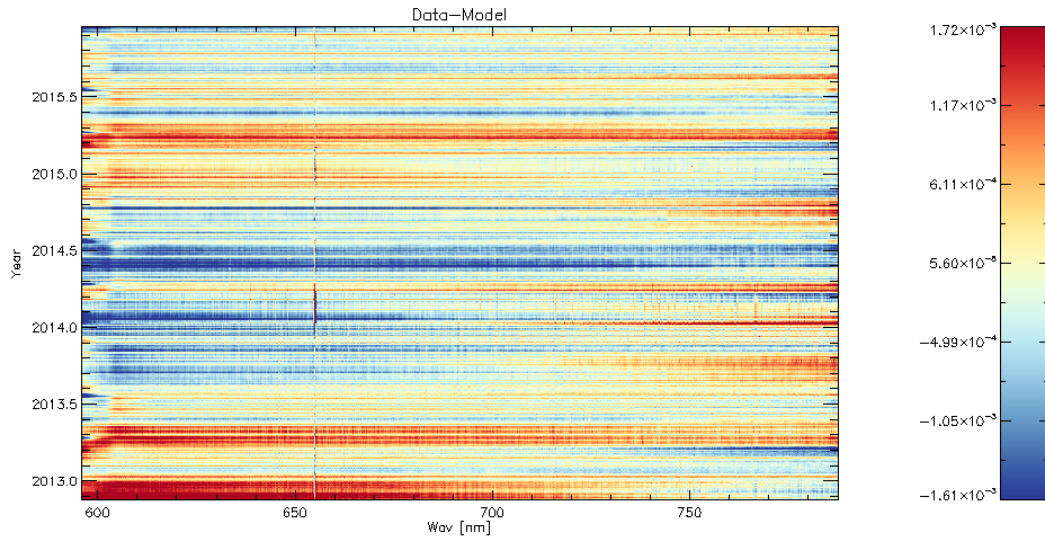


Figure 49 Difference between measurement and model as function of wavelength (zoomed in at Channel 4) and time (year).

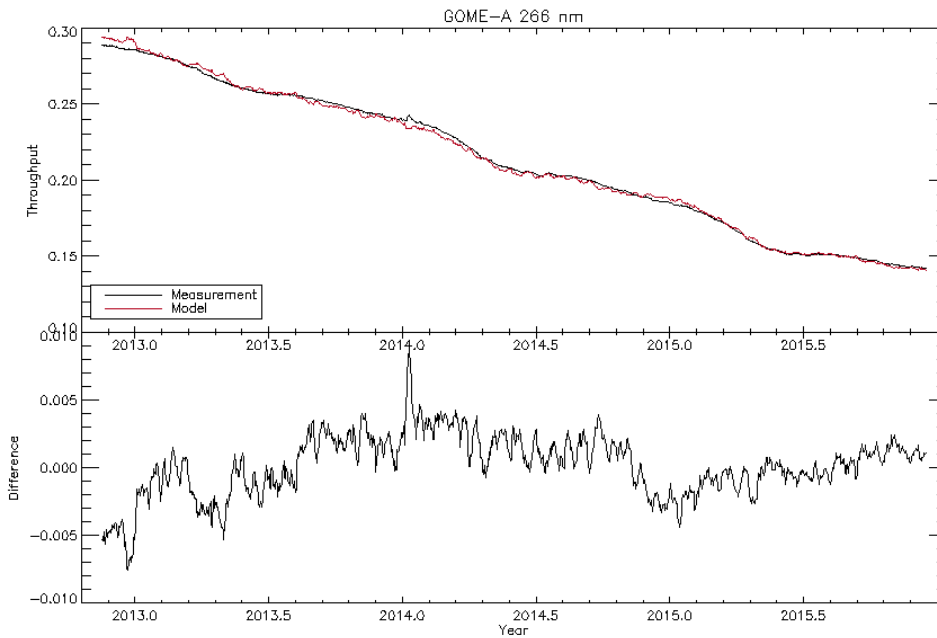


Figure 50 Top: Throughput at 266 nm as function of time. Measurement in black, model in red. Bottom: Difference between measurement and model.

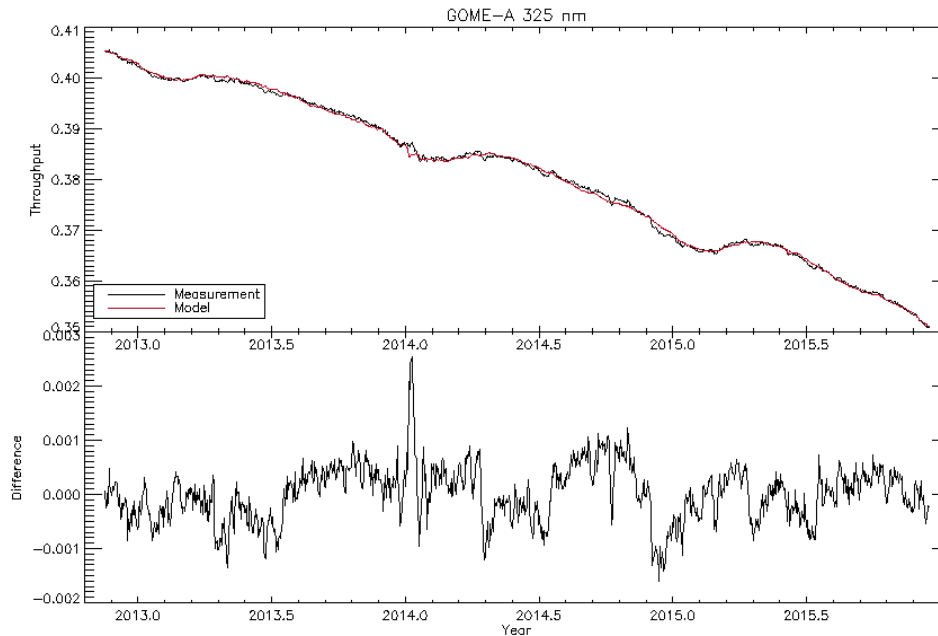


Figure 51 Top: Throughput at 325 nm as function of time. Measurement in black, model in red. Bottom: Difference between measurement and model.

3.6 Instrument anomalies and step function

The current model is only valid for GOME-2A in its current state. The (future) driver for the accuracy of the model is, as shown, the solar azimuth dependence which is currently strongly (exponentially) increasing. Therefore, the model parameters should be re-determined as close as possible to the solar visibility loss period. This will guarantee the best possible azimuth dependence correction. If new key data is adapted for this dependence at any point, the model parameters must also be determined again for the newly calibrated solar observations.

Any instrument anomaly between now and the period of solar visibility loss that affects the throughput after the anomaly has been resolved, e.g. step-like throughput loss, or azimuth dependence will invalidate the model. It is possible to determine the model parameters again with only observations after the anomaly, but at least a year of observations is needed to validate the new parameters over all viewing conditions. Given the currently exponential growth of the azimuthal dependence, any change in or determination of this (exponential) growth rate would require likely at least 2-3 years of observations, as the most extreme effects are experienced only during a short period of the year (which regrettably coincides with the period of visibility loss). If not enough time is available to re-determine all parameters, assumptions must be made which parameters likely did not change, fix those and attempt to re-determine only the suspected changed parameters. If the anomaly and its effects are understood (eg sudden single event detector degradation) the observations before or after the anomaly could be altered in such a way

as if the anomaly never took place by introducing a step function in the measurements. The current model does not fit step functions itself, so the measurements must be corrected for any step-function.

Any anomaly affecting throughput during the period of solar visibility loss cannot be (straightforward) corrected for during the period of solar visibility loss. Potentially from the earthshine a throughput correction could be derived and similarly applied to the solar observations. However this will likely take as long as the period of solar visibility loss, and at that point in time the (new) solar observations themselves can be corrected, with a retro-active correction for the observations during the solar visibility loss.

Another option is making a solar measurement by rotating the instrument, however too little information can be derived from a single measurement to re-establish all model parameters. A single measurement can only be used as an updated offset (P_0) or step-function between expected model measurement and the new actual measurement, with all other parameters remaining fixed. A second measurement can either be used to increase the precision of the offset or determine either the linear degradation or azimuthal dependence. Three measurements should allow offset, linear degradation and azimuthal dependence to be redetermined, but with extremely low precision, however in case anomaly this might be the only option. More measurements will allow more parameters to be redetermined or increase precision. Each measurement however must be carefully hand treated to determine the change in parameter.

3.7 Wavelength-shifted vs. not shifted dataset

During the project two options were investigated. Either interpolating all measurements to a common wavelength grid ("Shift") or leaving all measurements & wavelengths as-is and model the measurement (with their slightly varying wavelengths) as-is ("NoShift"). The preferred option would be to employ a common wavelength grid and take the varying slit function of GOME-2A into account. However the required information to model the slit function was not available. Hence modeled solar observations for the two mentioned options were both determined.

Investigation on the Lv2 data shows clearly that the non-interpolated ("NoShift") solar observations are the preferred option. Please refer to sections 7 and 8 for a more detailed description about the retrieval of level-2 data of NO₂ and ozone respectively. This can be seen clearly in Figure 52 in the NO₂ SCD and the corresponding RMS. The non-interpolated model data much better fits the real measurements than the interpolated model data.

The nadir profile scheme is known to be sensitive fine scale spectral structure at the 0.1% reflectance due to the fit precision required to extract tropospheric ozone information. The spectra structure introduced by interpolation on to the common grid exceed this level. Figure 53 shows RAL retrieval diagnostics comparison of retrievals using the nominal measurement and wavelength shifted SMR. As expected, there is a significant impact introduced in the band 2b retrieval step, affecting both the total column and sub-column values, beyond the level considered acceptable.

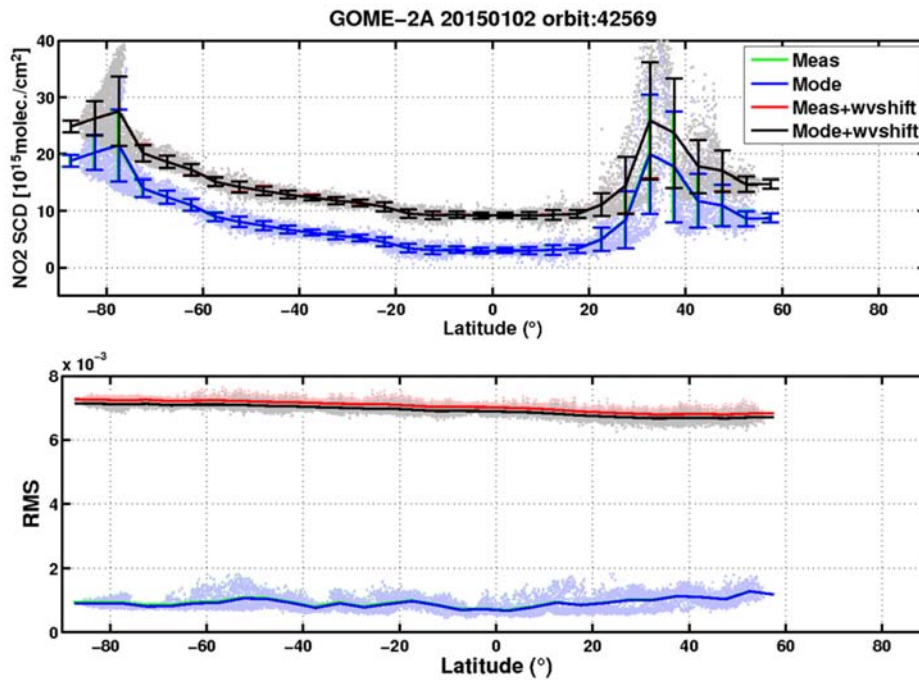


Figure 52 Comparison between measurements (green), model data (blue) and wavelength interpolated model data (black) for NO₂ SCD and the resulting RMS.

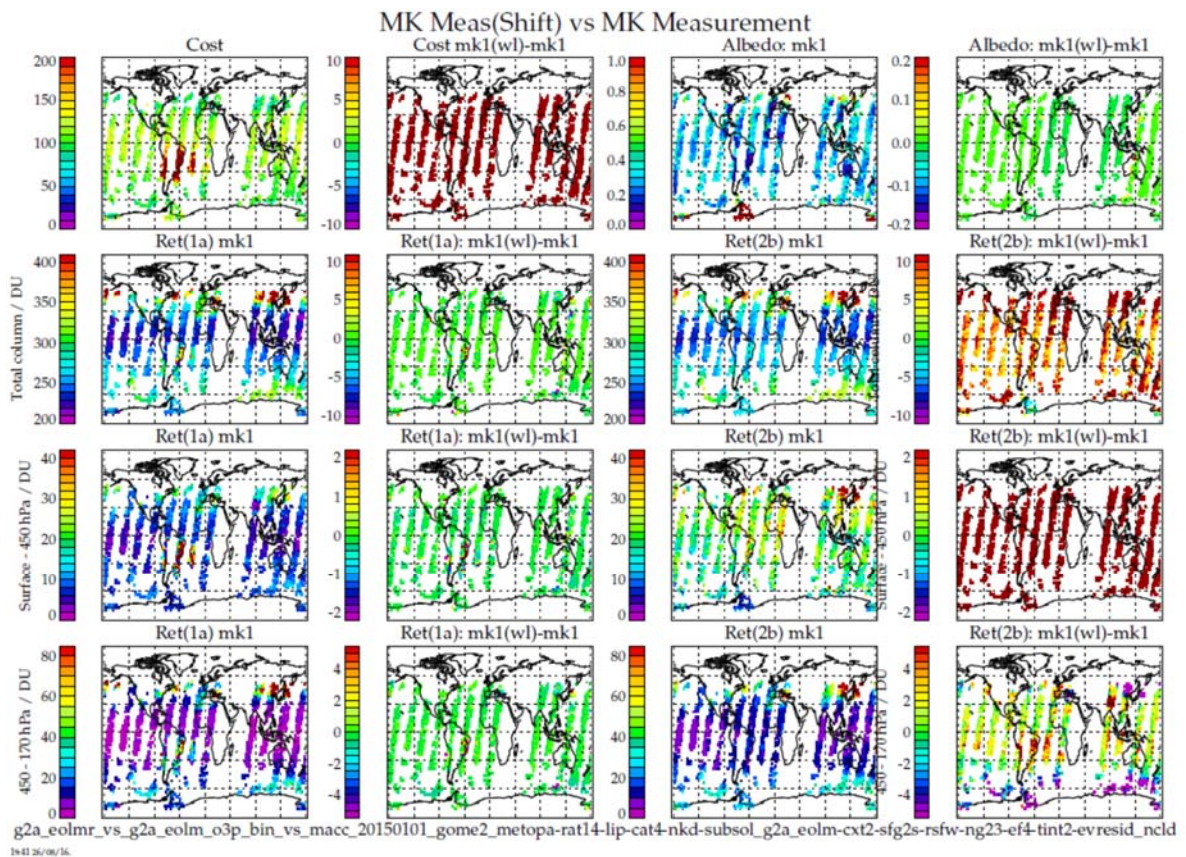


Figure 53 Gridded daily means of shifted vs not shifted measurement SMR retrievals (01/01/2015). Row 1: Retrieval fit cost & surface albedo. Row 2: Total column ozone. Row 3 & 4: ~0-6km & ~6-12km sub-column ozone. Column 1&3: unshifted SMR values. Column 2&4: Difference with shifted spectra.

Given the strong need of a proper determined slit function, this is not unexpected, as interpolating measurements (“Shift”) is equivalent to a broader slit function that varies wavelength to wavelength, as interpolation often implies some smoothing.

With this result and in order to avoid confusion, it was determined to only include the non-interpolated (“NoShift”) modeled observations in this report.

3.8 Summary ATBD like document

For a complete description of the model and how to use it, we refer the reader to RD-2. In the following we provide a brief summary of the key model elements, the model in- and outputs.

The model as described in Chapter 3 is fitted independently for each wavelength using Levenberg-Marquardt least-squares minimization, resulting in 11 model parameters for each wavelength. As it was decided not to employ the ISN index in the final version, only 10 out of 11 are used.

Various model inputs are used. In order to balance the weight between parameters, each input has an arbitrary offset that is subtracted from the input before being used in the model.

Description	Offset	Source
Time (t)	733068	Julian Date (relative to 0-0-0)
Solar azimuth angle (α)	325	GOME2A
Solar Distance squared (d_{solar}^2)	0	Astronomical Almanac (1984)
MgII Index	0.32	GOME2B
F10.7 cm radio index	131	SPDF OMNIWeb
OBM Temperature	279	GOME2A

Time is additionally divided by 365.25 in order to get the input size in the same order of magnitude as the other inputs.

More recent periods and periods with large azimuth angles (which will be the case during solar visibility loss period) have a large fitting weight, as for future extrapolation we are not interested in early periods or other azimuth angles. The measurement for these periods do add information to the fit and are thus taken into account, however with smaller weight so the fits do not attempt to find a compromise for all periods.

The measurements employed for the model parameter derivation are the diffuser key-data corrected Solar Mean Reference (SMR) data spectra, SMR_NewAIRR, 2007-01-25 TO 2015-12-31, based on GOME-2 R2 (PPF 5.3.0) and R2 5.3.0 interim data and provided as part of the Level-1C degradation matrices provided by EUMETSAT for the GOME-2 instruments¹.

Since the MgII index is derived from GOME2-B, we restrict ourselves to dates for which both GOME2-A and GOME2B data is available (>JD 735204). Added bonus is that earlier GOME2-A decontaminations that upset any fitting are also not used in the fitting here.

Both GOME2-A and GOME2-B data is divided by their first observed SMR (for GOME2-B only important because of later MgII index derivation).

The model with the found model parameters, combined with the model input for desired date result in a virtual SMR for the desired date.

The further away the model input values are from the original input values used for finding the model parameters, the more inaccurate the model likely becomes. As such it is recommended to update the model parameter derivation when more input data (also known as measurements) become available, most optimally just before the period of solar visibility loss. The parameter derivation is relatively fast and can be done within 20-200 min depending computer hardware.

To update and run the model, please follow the steps described in the Appendix B of RD-2.

¹ The data is available on <ftp://ftp.eumetsat.int/pub/out/EPS/out/lang/Level1C/>.

4 Reference Period

It was decided to take 01/01/2015 to 31/03/2015 as reference period, because this is the most recent period with available observations with the same period of the year as the future solar loss periods and with similar viewing geometries.

4.1 Solar Loss Periods

The last OOP manoeuvre happened on 31.08.2016. This lead to the following expected scenario for non-visibility (as of 30.09.2016):

- The FOV is considered as 8.05° times 2.47° (i.e. full sun disk in FOV).

Start time	End time	Duration (days)
26.01.2018	19.02.2018	24.4
28.12.2018	20.03.2019	82.8

5 Results: Quality impact in time based on region

We define the impact of the different Sun Mean References as the standard deviation of the difference between the reflectance derived with the measured Sun Mean Reference and the reflectance derived with the modelled Sun Mean Reference

$$\sigma = \sqrt{\sum_{i=0}^n \left(\frac{\pi I_i}{S_i^{meas} \cos \theta_{SZA}} - \frac{\pi I_i}{S_i^{model} \cos \theta_{SZA}} \right)^2 \frac{1}{n}}$$

With θ_{SZA} the solar zenith angle of the radiance observation, S_i^{meas} is the solar signal of interest, S_i^{model} is the corresponding modelled solar signal and I_i is the matching calibrated (real) solar signal.

5.1 Sahara & pristine equatorial Pacific

Concluding the standard deviation is in the order of 10^{-5} and behaves as expected.

The data is examined in both the spectral, temporal and scan-angle domains.

There is no significant temporal variation.

The spectral behavior shows the higher expected noise at the lower wavelengths.

A scan angle dependence is found (stronger in the Sahara than in Pacific). This is (regrettably) as expected because we study an inverse difference (as we divide by the Sun Mean Reference). In an inverse difference, the found difference is the original difference scaled with the measured signal. So higher radiance will result in higher found difference. As GOME2-A is degrading with a scan angle dependent component, indeed the measured signals vary consistently with scan angle with higher signals for the higher scan angles. This difference in average radiance thus also causes a difference in the found standard deviation.

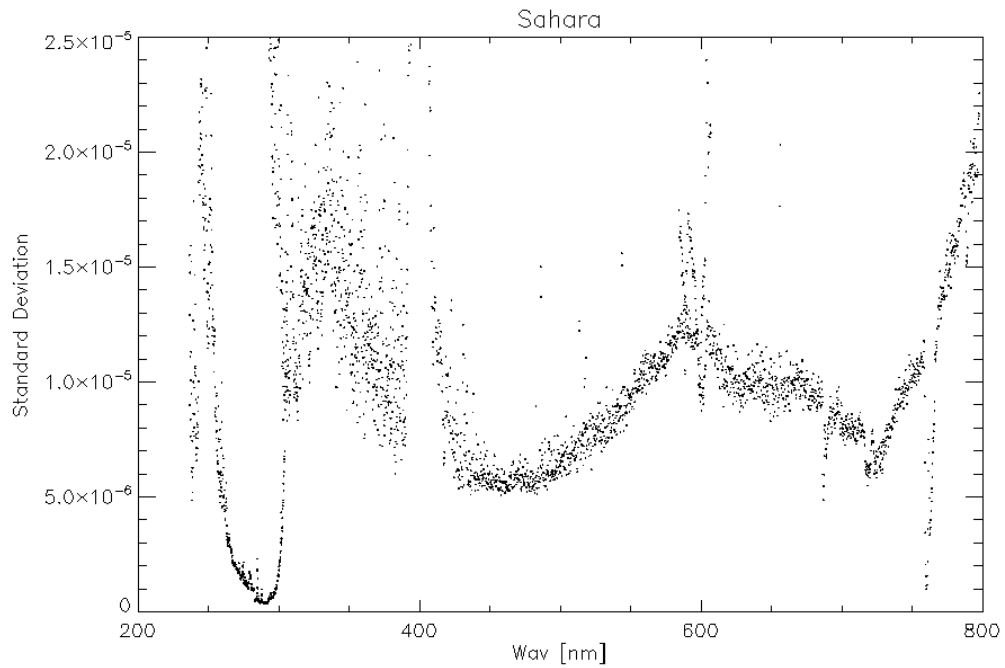


Figure 54 Standard deviation between model and measurement reflectance as function of wavelength, averaged over all viewing angles and reference period.

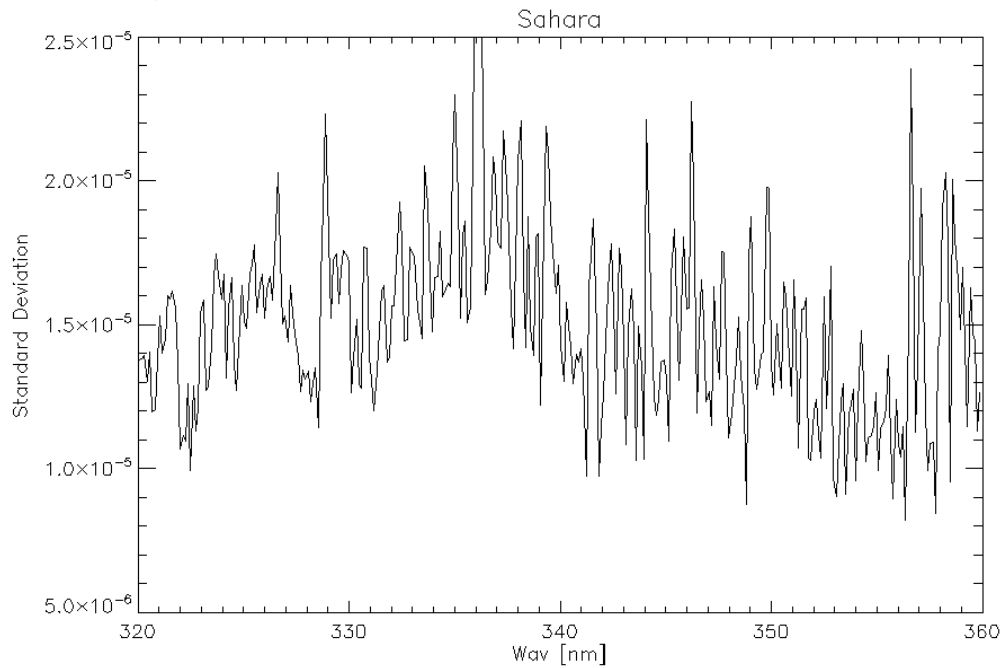


Figure 55 Standard deviation between model and measurement reflectance as function of wavelength (zoom Huggings band), averaged over all viewing angles and reference period.

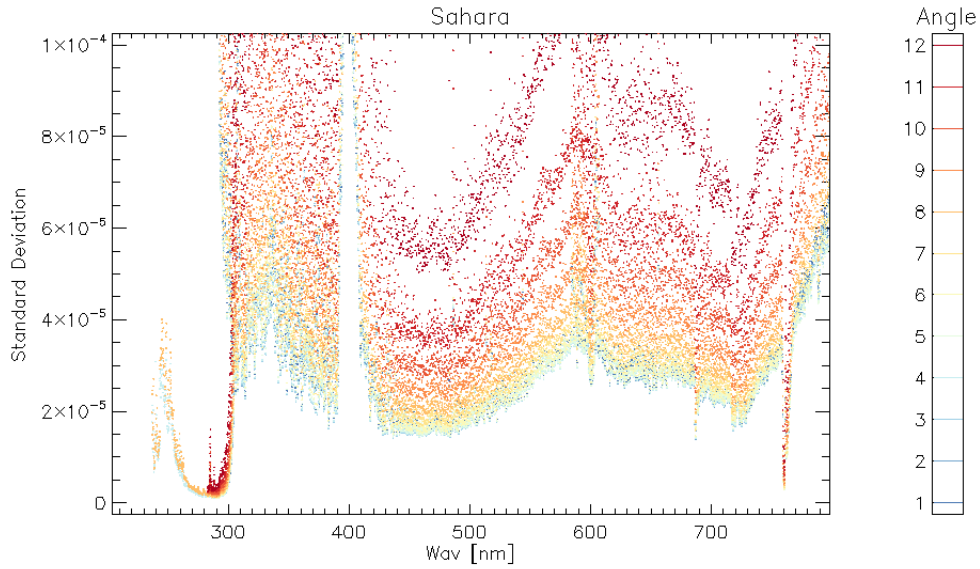


Figure 56 Standard deviation between model and measurement reflectance as function of wavelength, averaged over select viewing angles and the whole reference period. Different colors indicate different viewing angles averaged over.

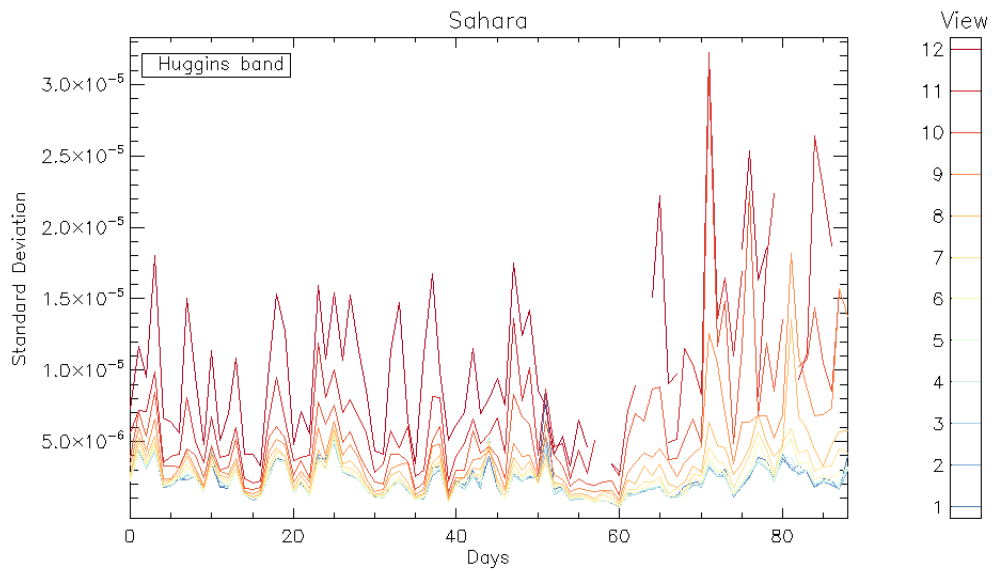


Figure 57 Standard deviation between model and measurement reflectance as function of time (since start reference period), averaged over select viewing angles and wavelength (Huggins band). Different colors indicate different viewing angles averaged over.

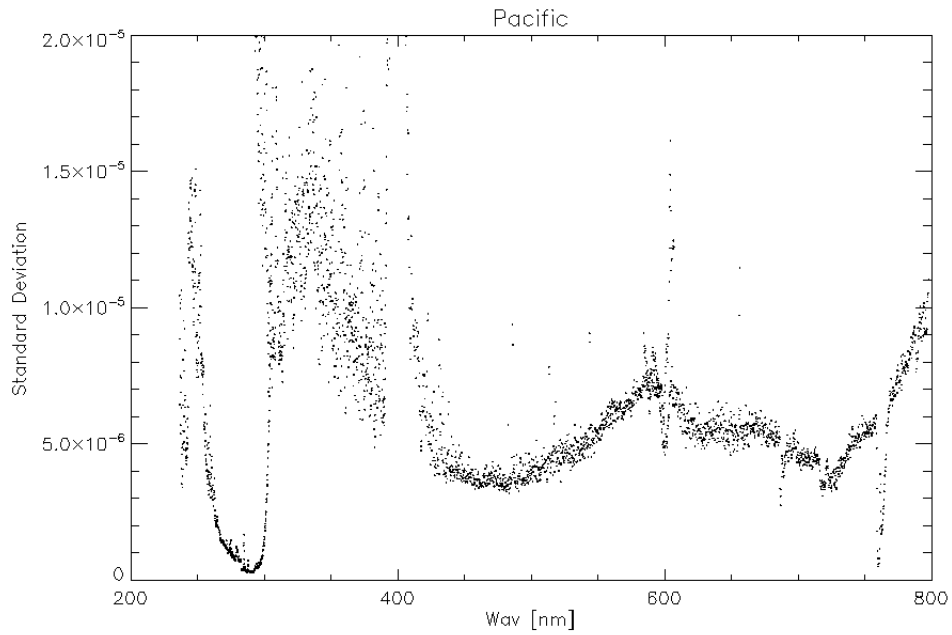


Figure 58 Standard deviation between model and measurement reflectance as function of wavelength, averaged over all viewing angles and reference period.

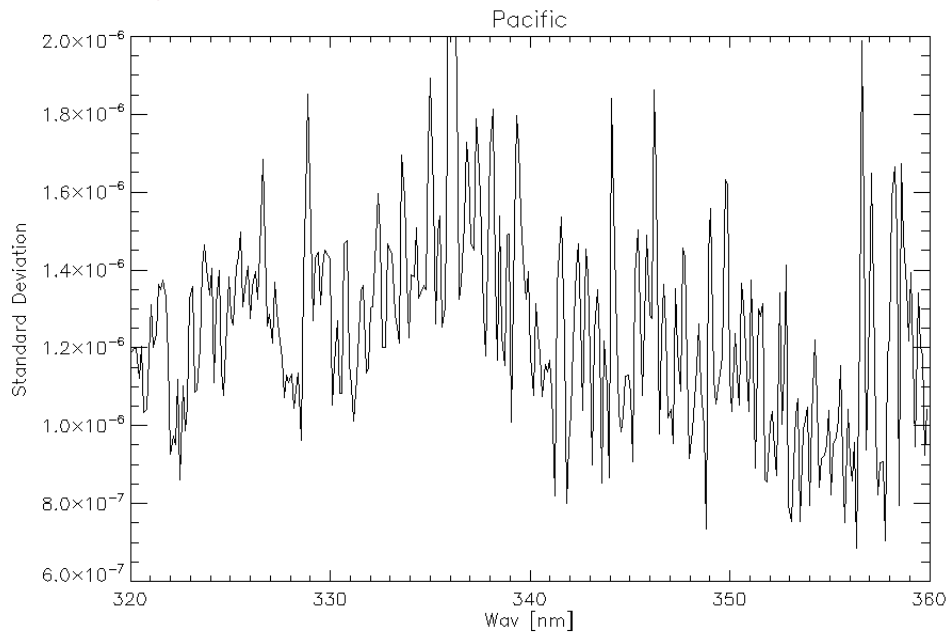


Figure 59 Standard deviation between model and measurement reflectance as function of wavelength, averaged over all viewing angles and reference period.

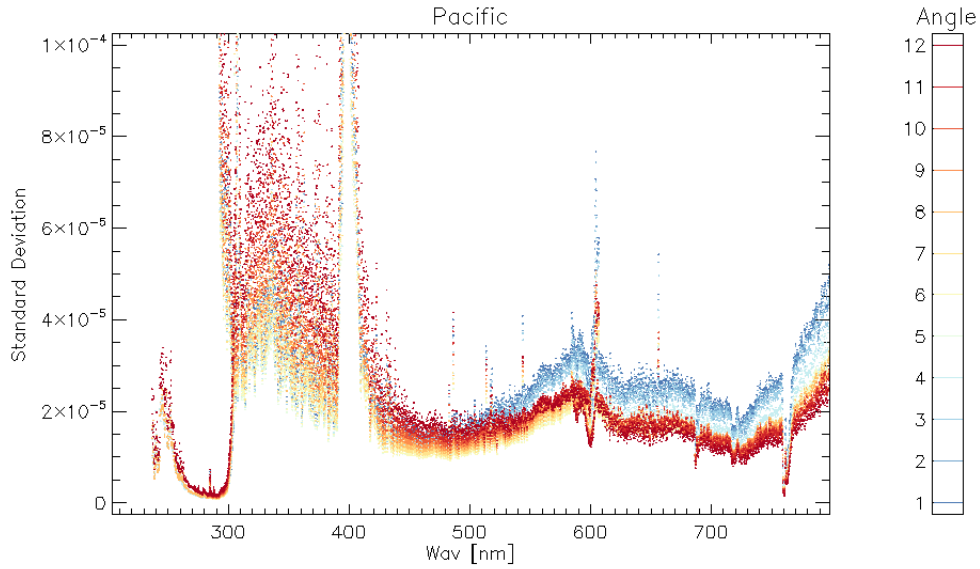


Figure 60 Standard deviation between model and measurement reflectance as function of wavelength, averaged over select viewing angles and the whole reference period. Different colors indicate different viewing angles averaged over.

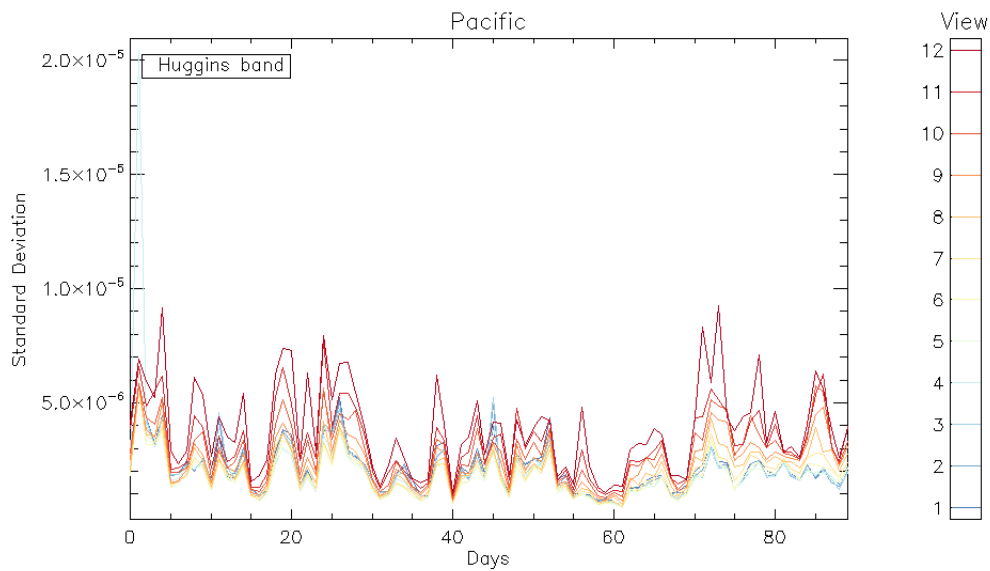


Figure 61 Standard deviation between model and measurement reflectance as function of time (since start reference period), averaged over select viewing angles and wavelength (Huggins band). Different colors indicate different viewing angles averaged over.

6 Results: Global quality impact based on shorter periods

The same conclusions as for the Sahara and Pacific regions can be made to the global observations for a subset of the reference period, namely the 6th day of each month for the reference period. Given the short period the temporal variation is not shown here (but does not vary significantly). Again a scan angle variation is found. In order to verify the earlier mentioned radiance dependence, also the cloud-free global radiance results are shown, and the scan angle-angle dependence has decreased. The reason is that the high radiance clouds have been omitted. Same order of standard deviation is found as for the regional studies.

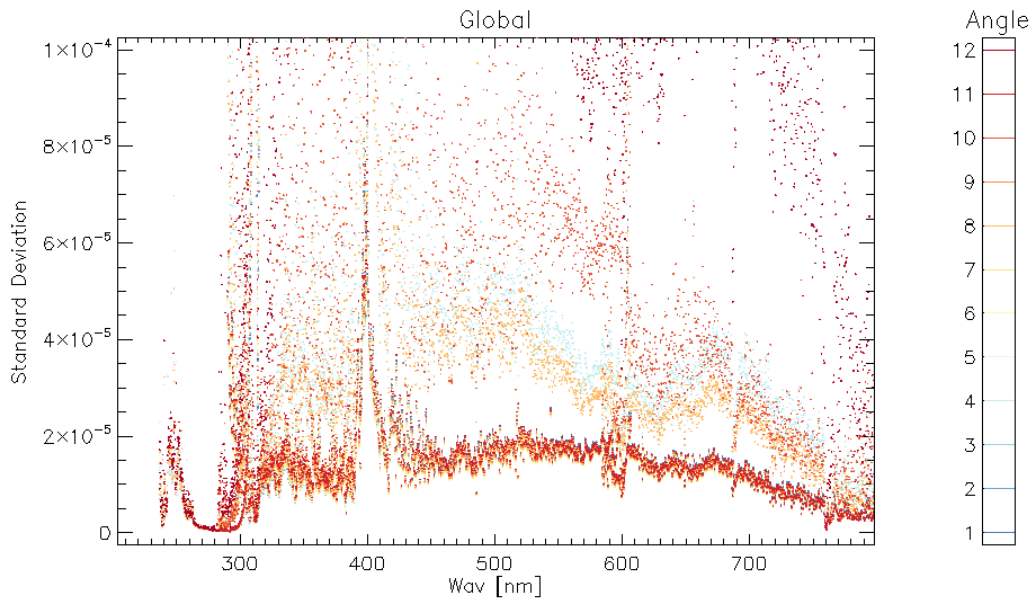


Figure 62 Standard deviation between model and measurement reflectance as function of wavelength, averaged over select viewing angles and the whole reference period. Different colors indicate different viewing angles averaged over.

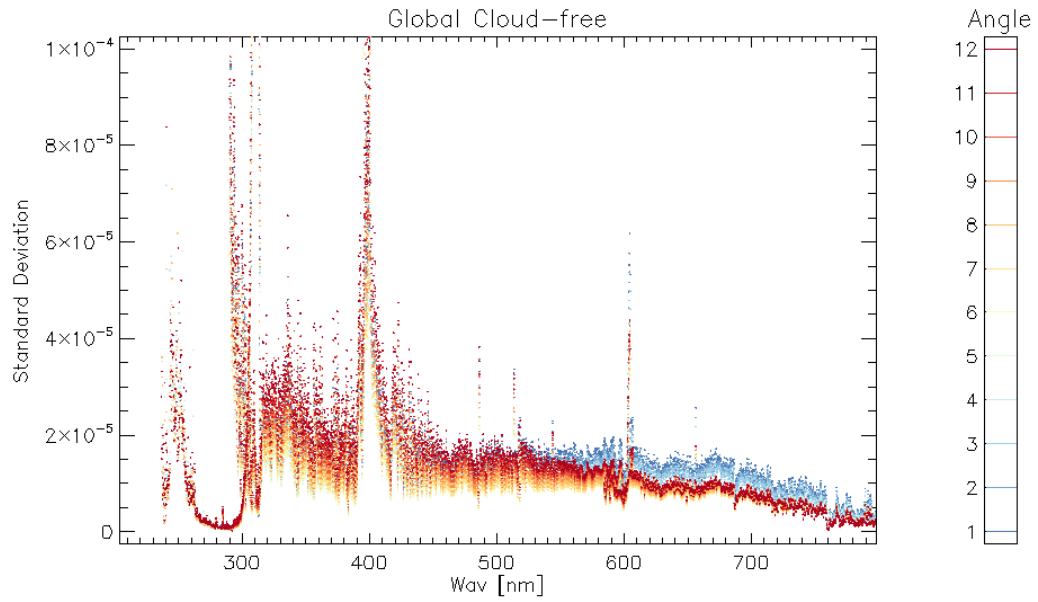


Figure 63 Standard deviation between model and measurement reflectance as function of wavelength, averaged over select viewing angles and the whole reference period. Different colors indicate different viewing angles averaged over.

7 Results: Sensitivity of L2 NO₂ products

In order to assess the impact on the NO₂ tropospheric L2 product, BIRA NO₂ retrieval scheme has been performed on selected GOME-2A L1b data, using subsequently modelled and measured SMR.

BIRA NO₂ retrieval algorithm is very similar with the O3MSAF operational product (Valks et al., 2011), and it consists of the following steps: (1) determination of the NO₂ slant column density (SCD) using DOAS fitting; (2) estimation of the stratospheric component of the NO₂ SCD using a spatial filtering approach: Over clean regions, the satellite's view of NO₂ are mainly from stratosphere, and we assume the contribution from troposphere is negligible over these regions, stratospheric NO₂ over polluted regions are interpolated from the stratospheric field over clean regions. (3) the conversion of the residual tropospheric slant column (SCD_{trop}) into a tropospheric vertical column, using a tropospheric air mass factor AMF_{trop} . The three retrieval steps can thus be summarized as follows:

$$VCD_{trop} = \left(\frac{SCD - SCD_{strat}}{AMF_{trop}} \right)$$

Finally, total NO₂ column density (VCD_{total}) is the sum of stratospheric (VCD_{strat}) and tropospheric (VCD_{trop}) component.

The main effect of SMR on NO₂ retrieval is in the first algorithm component --- DOAS fit, which both BIRA retrieval and operational product use the same fitting window (425-450nm) and the same absorbers (NO₂, O₃, H₂O, O₂-O₂ and Ring) in the fitting, and results show perfect agreement (Pinaridi, et al., 2013).

In this study, the effect of the choice of SMR on the NO₂ retrieval will be investigated step by step, subsequently looking at a single orbit measurement, the full time series, and finally global measurements.

7.1 Single orbit analysis

First of all, the results of the two types of NO₂ retrievals (using modelled and measured SMR, respectively) are compared along a single orbit of GOME-2 measurements. From inspection of **Error! Reference source not found.**, **Error! Reference source not found.** and **Error! Reference source not found.**, we conclude the following:

- (1) The model SMR introduces a constant bias in the SCD retrieval with a slightly different RMS.
- (2) The systematic bias on SCD is almost completely transferred to SCD_{strat} , and the residual tropospheric slant columns are therefore equivalent, except over high latitudes.
- (3) Except for a few outliers, the difference in VCD_{trop} is in the order of 10^{14} molec/cm².

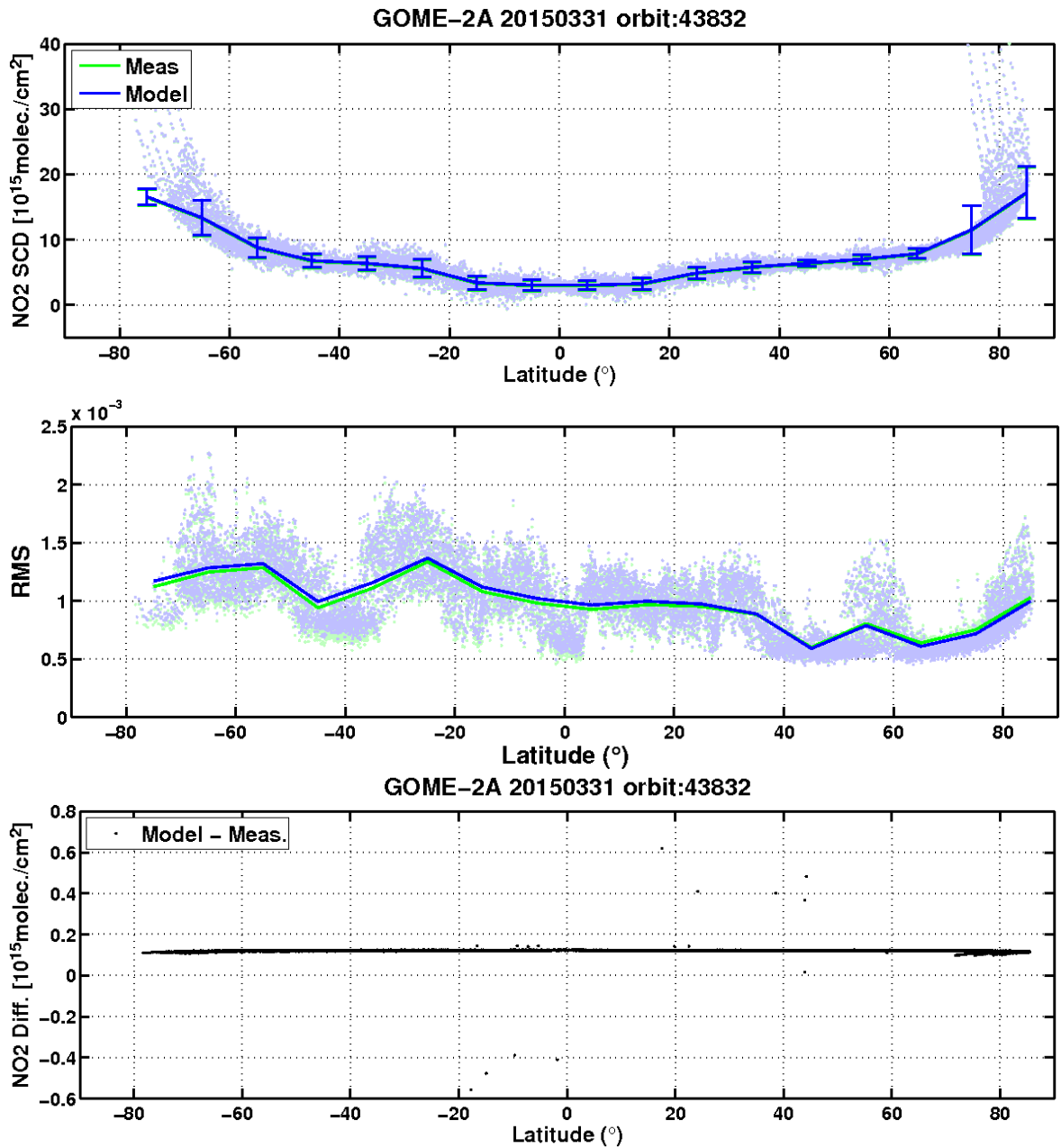


Figure 64 Retrieved NO₂ SCD using model (blue) and measurement (green) SMR and the corresponding fitting RMS (middle) for one orbit of GOME-2 measurements, as function of latitude. The difference in SCD between use of model and measurement SMR is shown in the bottom panel.

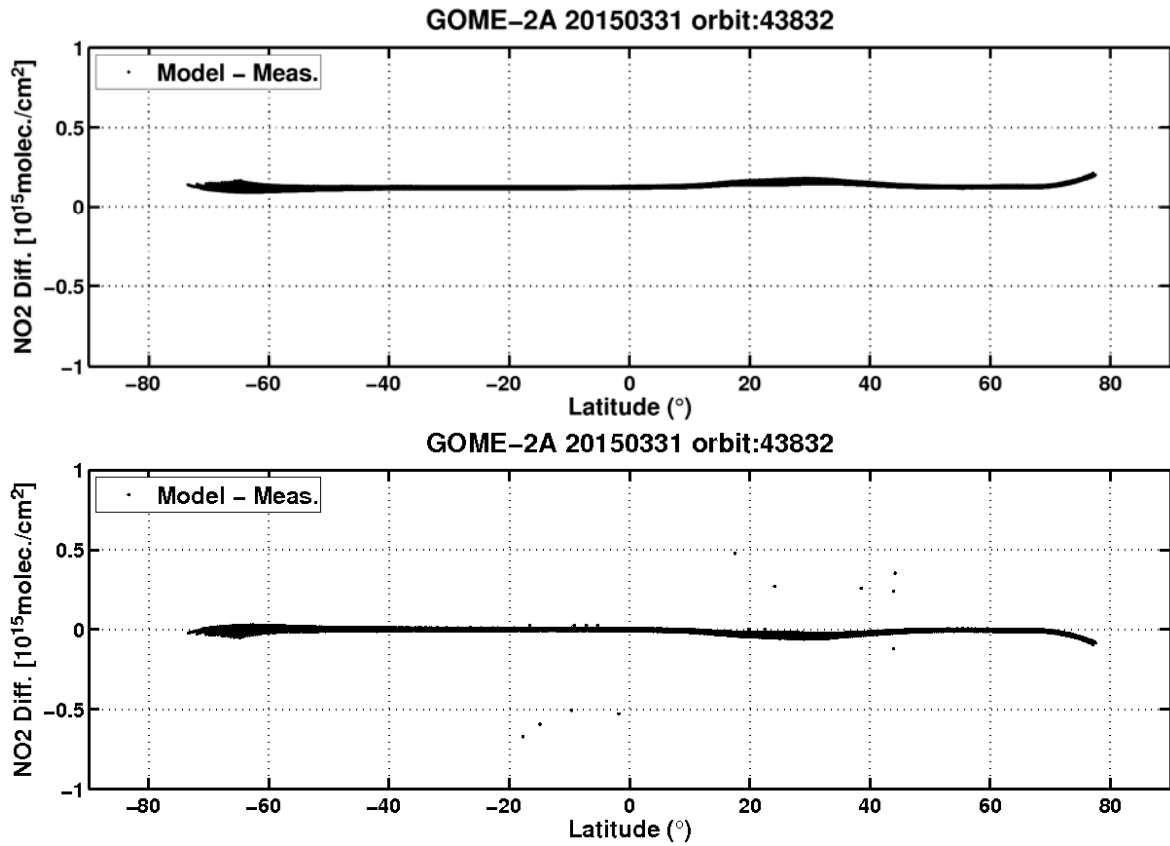


Figure 65 Difference in stratospheric (SCD_{strat} , top) and the residual tropospheric ($SCD_{trop} = SCD - SCD_{strat}$, bottom) NO_2 slant column between use of the model and measurement SMR for one orbit of GOME-2 measurements, as function of latitude.

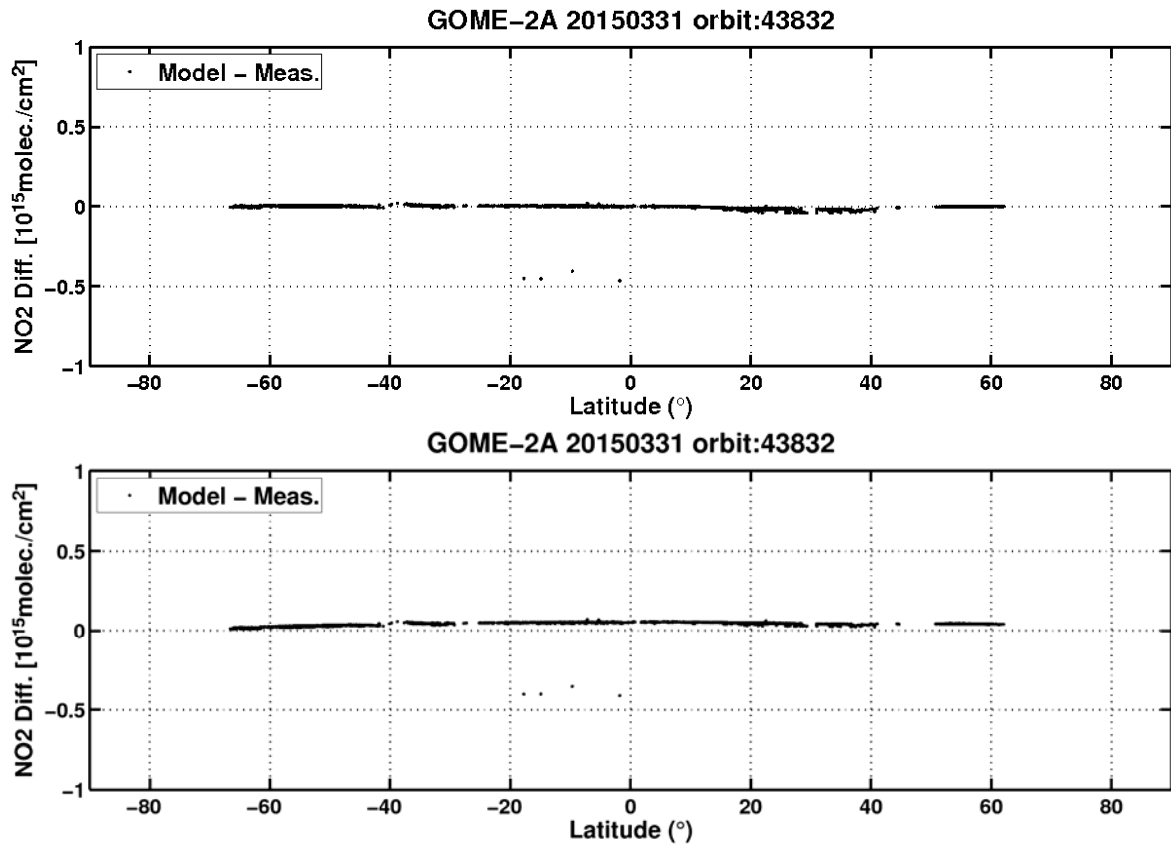


Figure 66 Comparison of NO₂ VCD_{trop} (top) and VCD_{total} (bottom) using model and measurement SMR for one orbit of GOME-2 measurements, as function of latitude. Only pixels with cloud radiance fraction less than 50% have been used for the figure.

7.2 Time series analysis

Data have been examined over the whole reference period (see Chapter 4) for each of the retrieval steps (**Error! Reference source not found.**, **Error! Reference source not found.** and **Error! Reference source not found.**). The main conclusions can be summarized as follows:

- (1) Effects on SCD are mostly in the order of 10^{14} molec/cm², which is 10 times less than the fitting error of the DOAS approach. But there are a few days with up to 10^{15} mole/cm² of differences at the beginning of January 2015, and the outliers are mainly due to the measured SMR.
- (2) The approach of stratospheric correction could not completely remove the bias in SCD , the relatively large standard deviation of SCD between model and measurement will introduce a larger difference in SCD_{trop} .
- (3) Standard deviations of SCD_{trop} and VCD_{trop} are mostly within 10^{14} molec/cm², except for a few orbits in the beginning of the reference period, which is consistent with the period with a large bias in SCD .

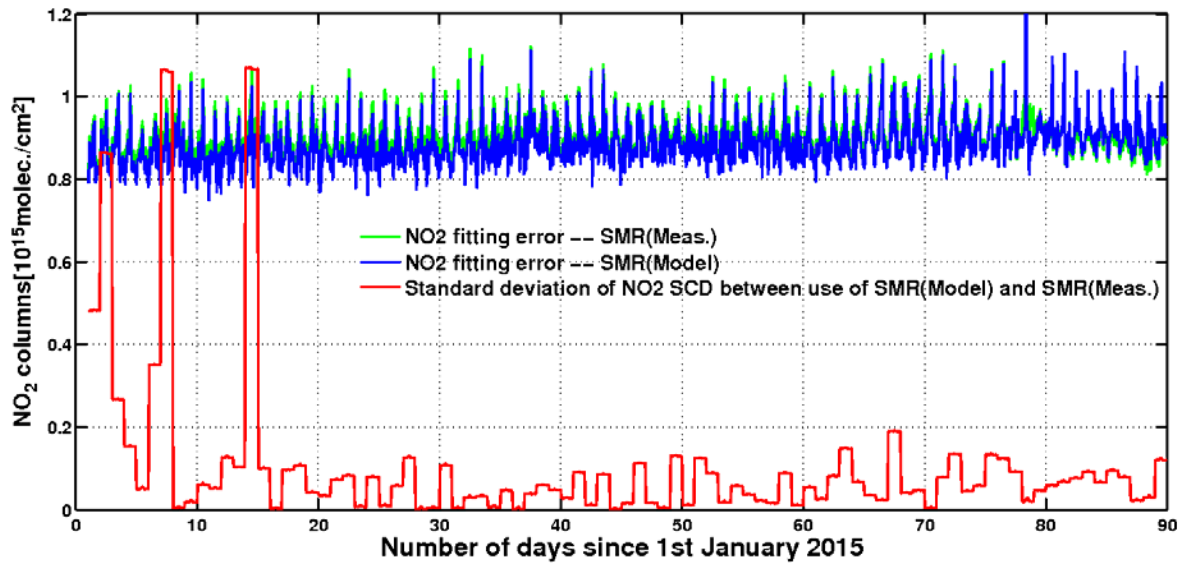


Figure 67 Standard deviation of NO_2 SCD retrieval between use of model and measurement SMR as function of time, averaged over the pixels with solar zenith angles less than 80° . The fitting error of SCD retrieval from DOAS approach are shown in the figure as well.

7.2.1 OUTLIERS IN MEASRUED SMR

While comparing NO_2 retrieval between use of the simulated and real GOME-2 measured SMR, it becomes apparent that the differences are very small except for 3 days (January 3, 8, 15).

In order to test if these differences are due to the real measurements or effects if the model, the NO_2 retrieval was compared for measured daily SMRs and a fixed SMR (using one SMR measured at 31st March 2015 for NO_2 retrieval over the whole period). The large differences still exist. This means that NO_2 retrieval using daily measured SMR may introduce a bias of 10^{15} molec/cm² due to the daily variability of SMR measurement.

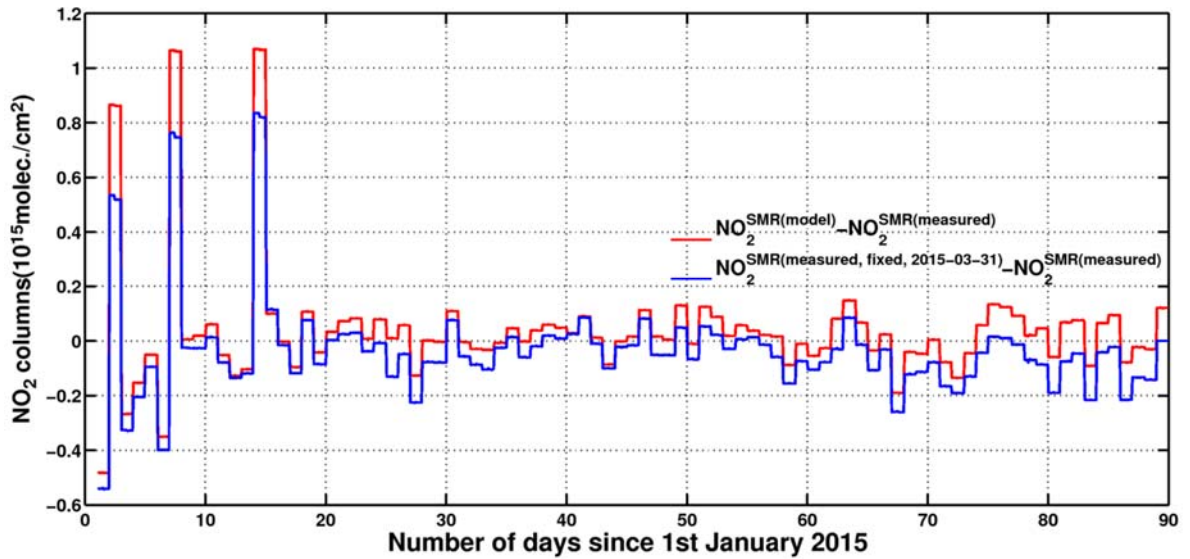


Figure 68 Comparison of NO₂ SCD retrieval between use of modeled, measured and a fixed measured SMR. There are outliers on three days (January 3, 8, 15).

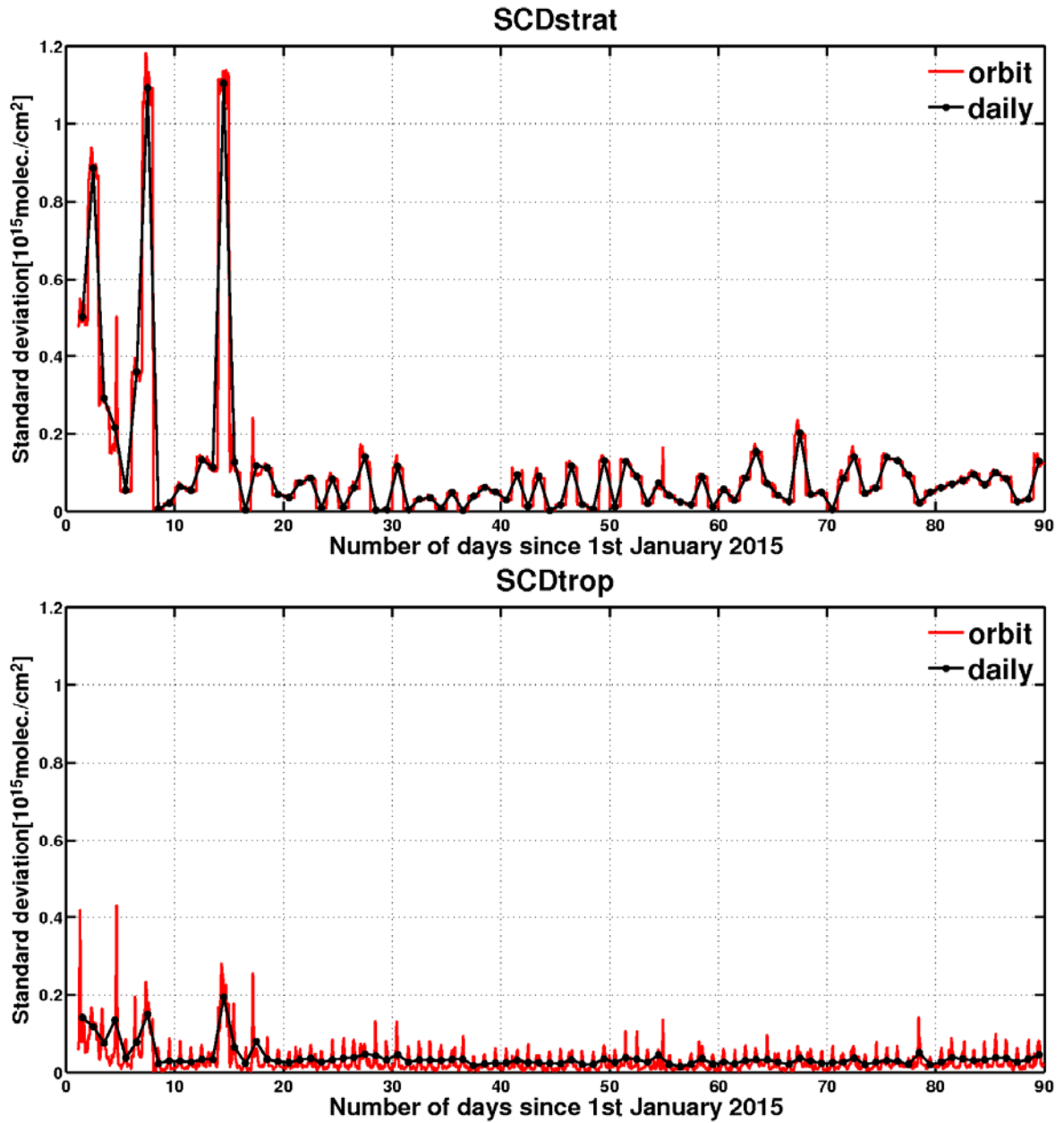


Figure 69 Standard deviation of NO₂ SCD_{strat} (top) and SCD_{trop} (bottom) between use of model and measurement SMR as function of time, averaged over the pixels with solar zenith angles less than 80°. Red and black lines indicate the orbital and daily average.

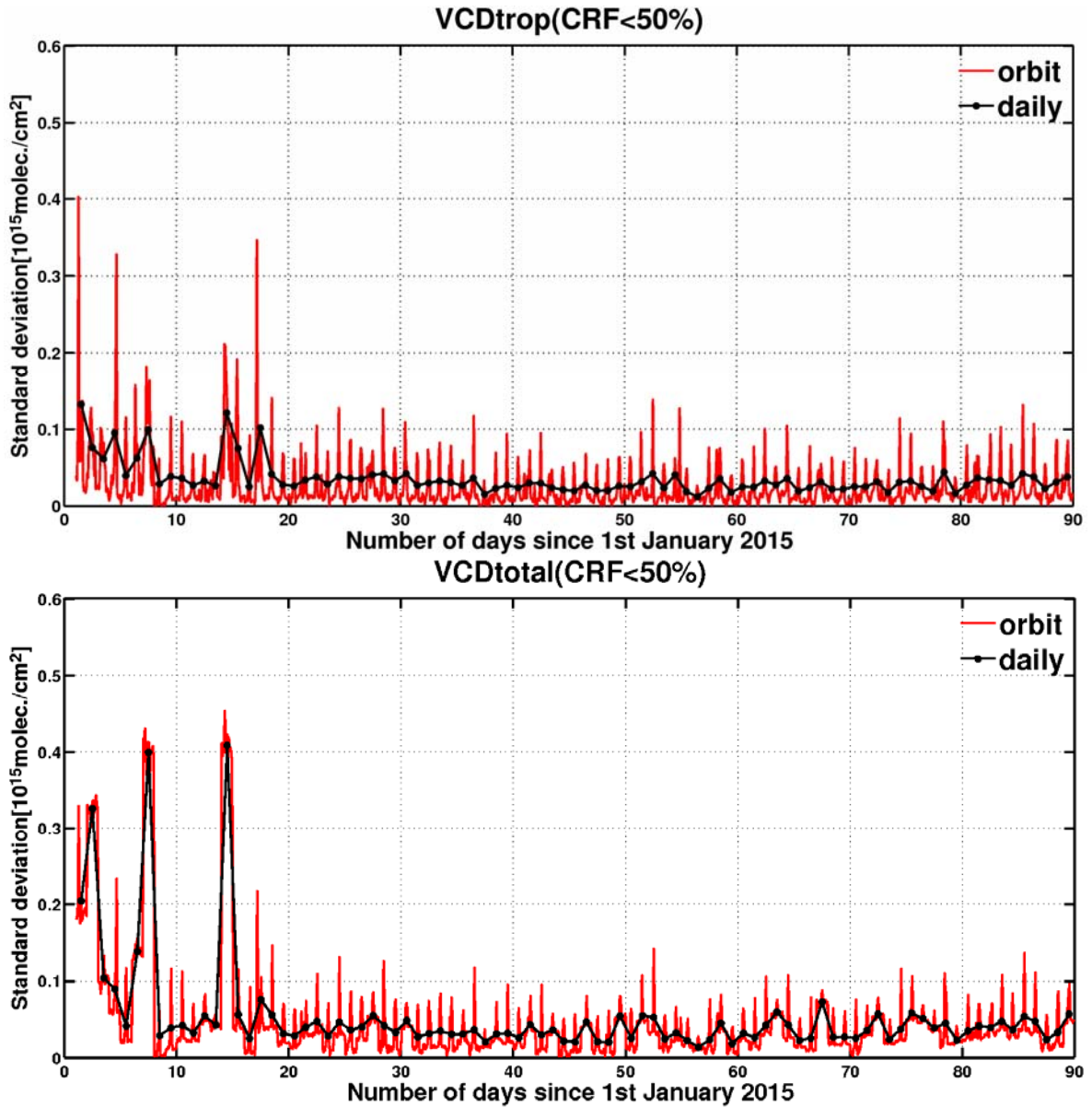


Figure 70 Standard deviation of NO2 $[[VCD]]_{trop}$ between use of model and measurement SMR as function of time, averaged over the pixels with solar zenith angles less than 80° . Red and black lines indicate the orbital and daily average, respectively.

7.3 Global comparisons

Finally, global maps of averaged NO_2 VCD_{total} and VCD_{trop} , as well as the standard deviation of $VCDs$ between use of model and measurement SMR over the whole reference period are shown.

VCD_{total} shows a systematic bias with the value of $\sim 10^{14}$ molec/cm², corresponding to a few percent of VCD_{total} over background region.

Large standard deviations (in order of 10^{14} molec/cm²) of VCD_{trop} occur mainly over the polluted regions, while the standard deviation of VCD_{trop} is lower than 10^{13} molec/cm² over background areas. This is probably due to the approach of stratospheric-tropospheric-separation (See Section 6).

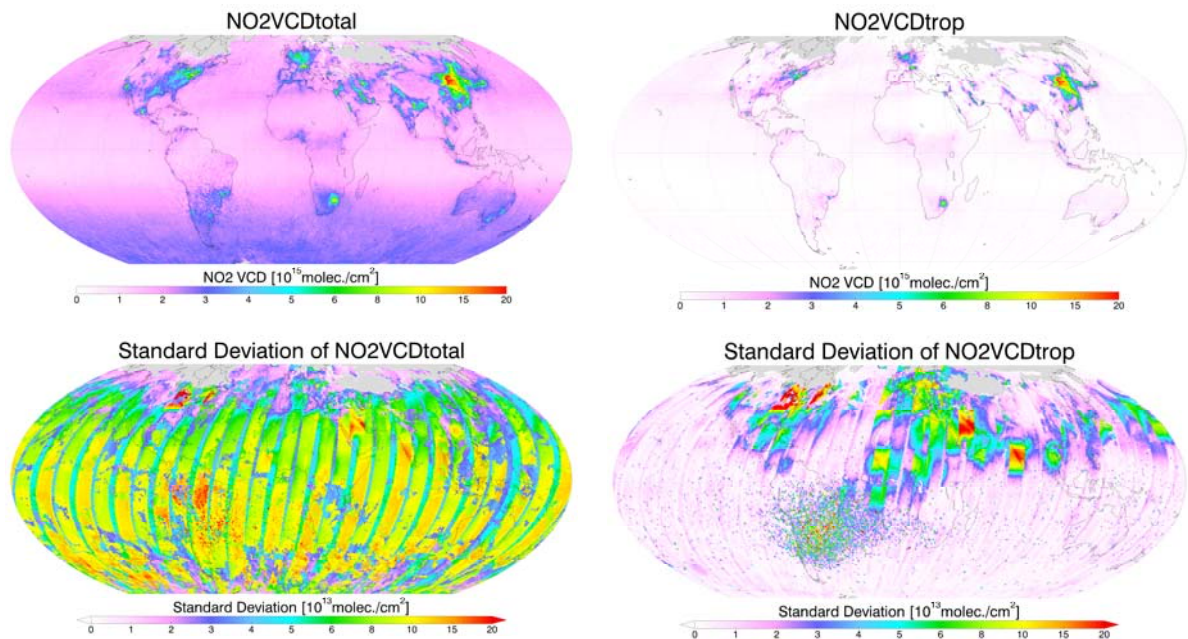


Figure 71 Top: Map of averaged NO_2 VCD_{total} (left) and VCD_{trop} (right) $VCDs$ using the measurement SMR. Bottom: Standard deviation of NO_2 VCD_{total} (left) and VCD_{trop} (right) between use of model and measurement SMR over the whole reference period. Only pixels with cloud radiance fraction less than 50% and SZA less than 80° have used for the figure.

7.4 Conclusion

In order to investigate the effect of SMR on the GOME-2A NO_2 product, NO_2 retrievals have been performed for all orbits within a 3-month period (1st Jan – 31st March 2015) using both the measured SMR and the model SMR. The investigation was performed step by step, based on single orbit measurements, time series analysis and global impact. Using the modeled SMR will introduce a systematic bias of $\sim 10^{14}$ molec/cm² in SCD , and will lead to $\sim 10^{14}$ molec/cm² difference in NO_2 VCD_{total} . However, the bias is mostly removed by the stratospheric correction, and the residual tropospheric slant columns are therefore equivalent, except over polluted areas, where differences in the VCD_{trop} remain of up to 2×10^{14} molec/cm², corresponding to a few percent of VCD_{trop} .

8 Results: Sensitivity of global height-resolved ozone

The impact of using the model SMR rather than observations is assessed through its impact in the RAL ozone profile scheme (Munro et al., 1996 & Miles et al., 2015), which was selected for production of multi-year data sets in ESA's CCI-Ozone project. The scheme employs the ratio of backscattered to direct-sun spectra in a 3-step process: firstly, wavelength dependence of ozone absorption in the Hartley band (260-307nm) is fitted to retrieve height-resolved information principally in the stratosphere; secondly, an effective surface albedo is retrieved in the 335-340nm interval and, thirdly, temperature dependent ozone absorption in the Huggins bands (323-334nm) is fitted to high precision (<0.1% RMS) to extend the profile retrieval into the troposphere. To achieve the required fit precision and accuracy, key spectro-radiometric parameters are retrieved from direct-sun irradiance spectra and a number of geophysical and instrumental parameters are co-retrieved with the ozone profile.

The results presented here demonstrate the impact of replacing the measured SMR with the modeled SMR for both band 1 (260-307nm) and band 2 (323-340nm), with a particular emphasis on the troposphere product due to its sensitivity to small changes in spectra structure.

8.1 Single orbit analysis

Retrievals have been performed for all orbits within the period 1st Jan – 31st March 2015 using both the measured SMR and the model SMR. Figure 72 shows an example the difference of a number of retrieval parameters produced using the different SMR sources, in particular the ozone total column and sub-column differences. This picture is consistent throughout the tested time period. As expected, by the very small spectral differences of the two SMR, there is relatively little impact from using the model, with differences within the normal uncertainty ranges. Total column differences are typically <2DU. Due to the sensitivity to fine spectra structure, the largest differences are seen in the lowest sub-columns, but still typically <3DU. In Northern Polar Regions, an area of known sensitivity due to low light levels and high total column ozone, sub-column errors of ~5DU are seen, but this is still within expected uncertainty at these locations and considered acceptable.

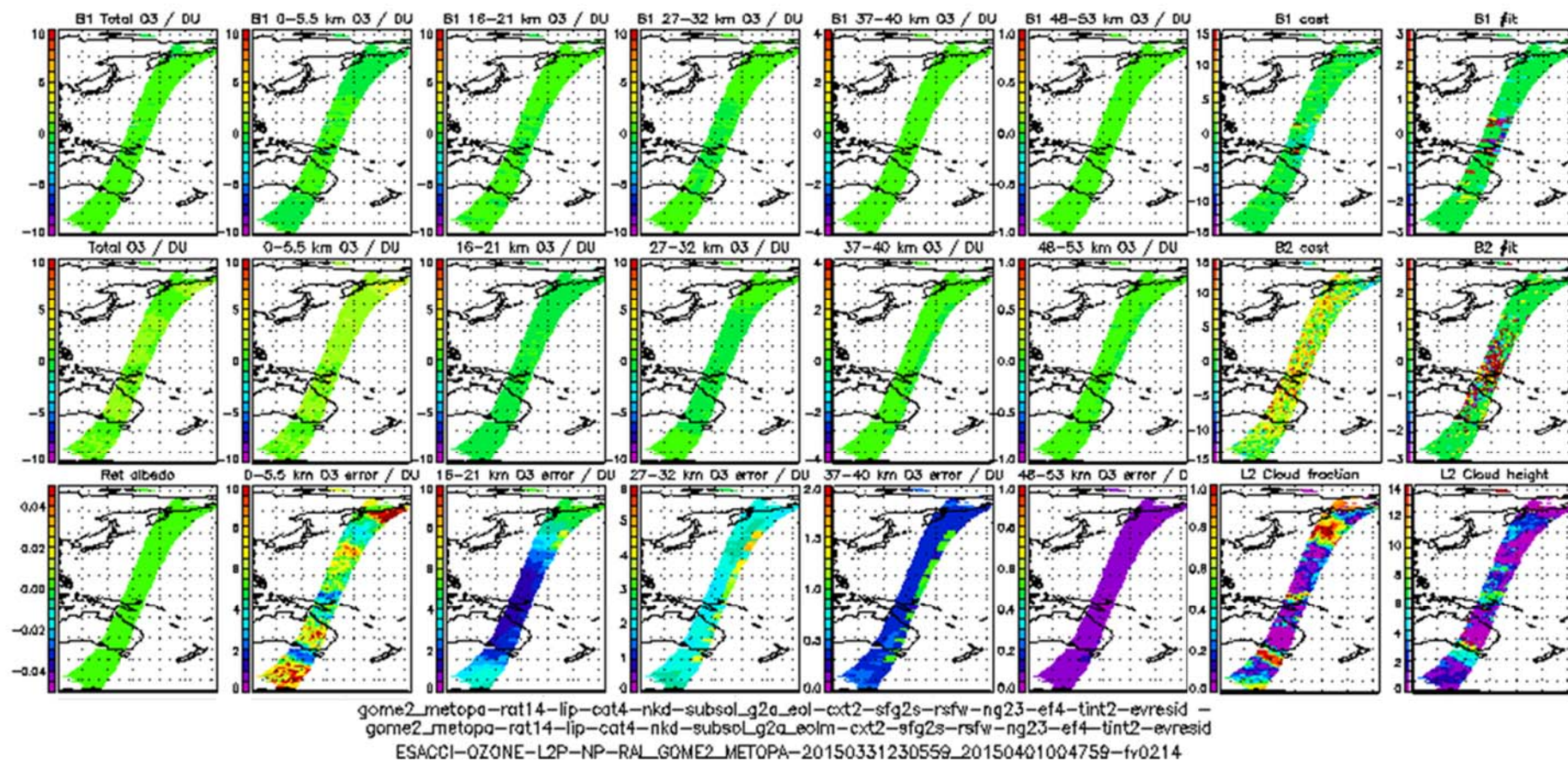


Figure 72 Model vs Measurement retrievals for a single orbit (31.03.2015). Figures show the retrieved total and sub-columns ozone after band 1 (top) and final step (middle) with associated difference to cost, no. of iterations ('#it') and surface albedo. Reference retrieval sub-column estimates, L2 cloud fraction and height also shown.

8.2 Global comparisons

To provide a global picture, gridded daily and monthly means of the retrieved total column and sub-columns have been calculated for the full period. Only 'cloud free' (cloud fraction <0.2) have been used and gridded to 2.5x2.5 degree spatial resolution. Figure 73 shows the monthly mean difference for the first month, which shows the excellent agreement of results using the modeled SMR. As in the previous section, the mean difference is typically <2DU, this is consistent throughout the 3 month test period, although by the 3rd month there is a mean bias of around +1DU, which appears consistent with change in the model – measurement indicated in Figure 74, presented earlier, showing a change in sign, albeit small. The magnitude of sub-column differences, including where step changes of ~1DU are seen, are considered to be at an acceptable level, i.e. within expected uncertainty. Note the high cost values in the South Atlantic Anomaly region are expected due to noise on the Earthshine data and unaffected by the choice of SMR.

It is noted, as shown in Figure 75, some days show a step change in the ~0-6km sub-column introduced in the band 2b retrieval step (primarily related to tropospheric ozone retrieval). This step change is believed to be due to the change in measured SMR, which is updated around midday, and likely due to temporal changes in SMR spectral structure which are not represented by the model.

Time series of the daily zonal means of the retrieved ozone and their differences for the measured and modeled SMR are shown in **Error! Reference source not found.** These figures again indicate a small mean bias of typically <2DU is introduced (in both total and sub-columns), although a gradual trend in time is seen, as mentioned above. The larger differences towards the end of the period in total ozone may become significant. The small changes are considered acceptable over the expected time period for loss of solar visibility.

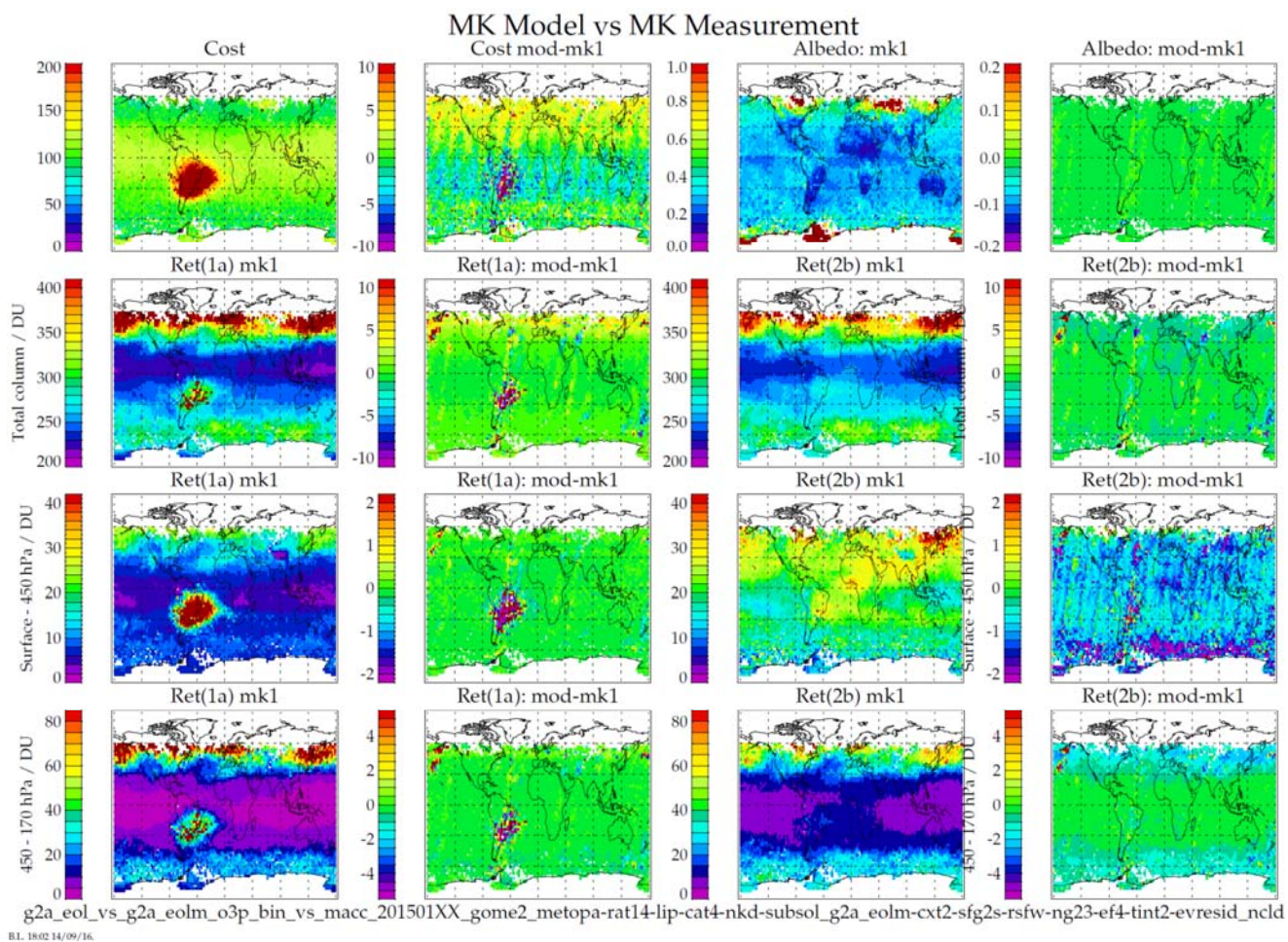


Figure 73 Gridded 'cloud free' monthly of model vs measured SMR retrievals (02/01/2015). Row 1: Retrieval fit cost & surface albedo. Row 2: Total column ozone. Row 3 & 4: ~0-6km & ~6-12km sub-column ozone. Column 1/3: Model SMR values. Column 2/4: Difference with measurement

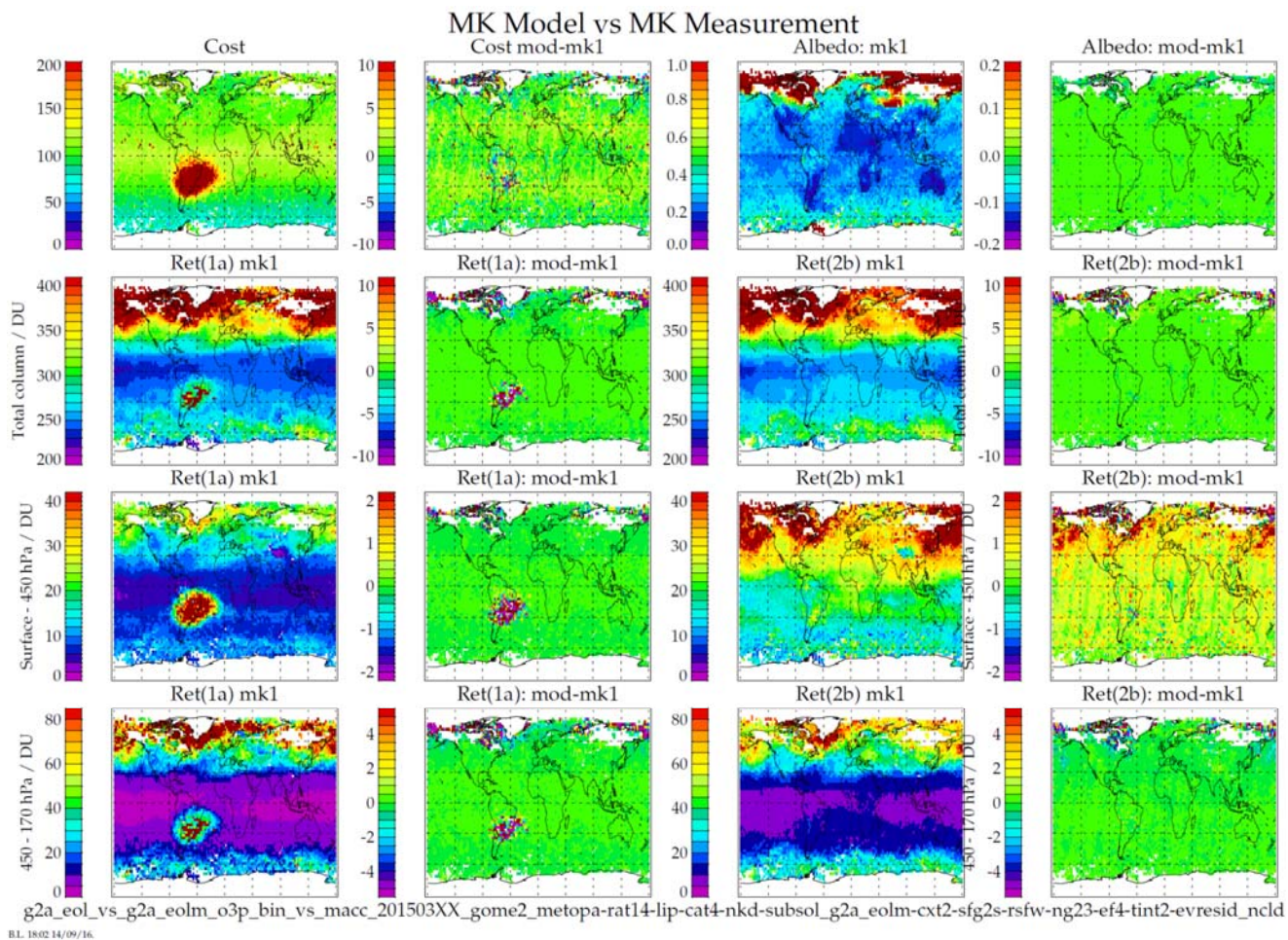


Figure 74 Gridded 'cloud free' monthly means of model vs measured SMR retrievals (03/2015). Row 1: Retrieval fit cost & surface albedo. Row 2: Total column ozone. Row 3 & 4: ~0-6km & ~6-12km sub-column ozone. Column 1/3: Model SMR values. Column 2/4: Difference with measurement.

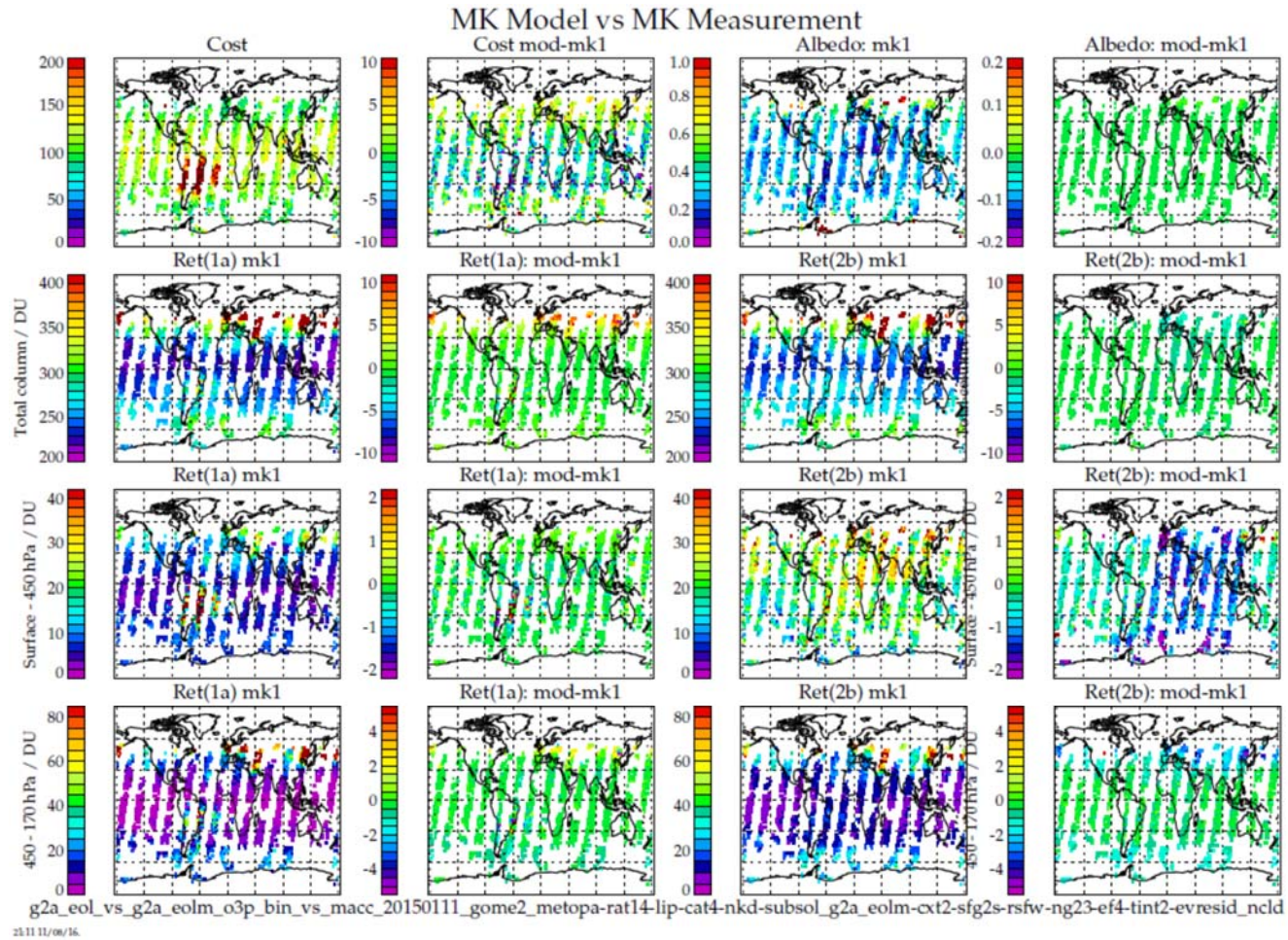


Figure 75 Gridded daily means of model vs measured SMR retrievals (11/01/2015). Row 1: Retrieval fit cost & surface albedo. Row 2: Total column ozone. Row 3 & 4: ~0-6km & ~6-12km sub-column ozone. Column 1/3: Model SMR values. Column 2/4: Difference with measurement.

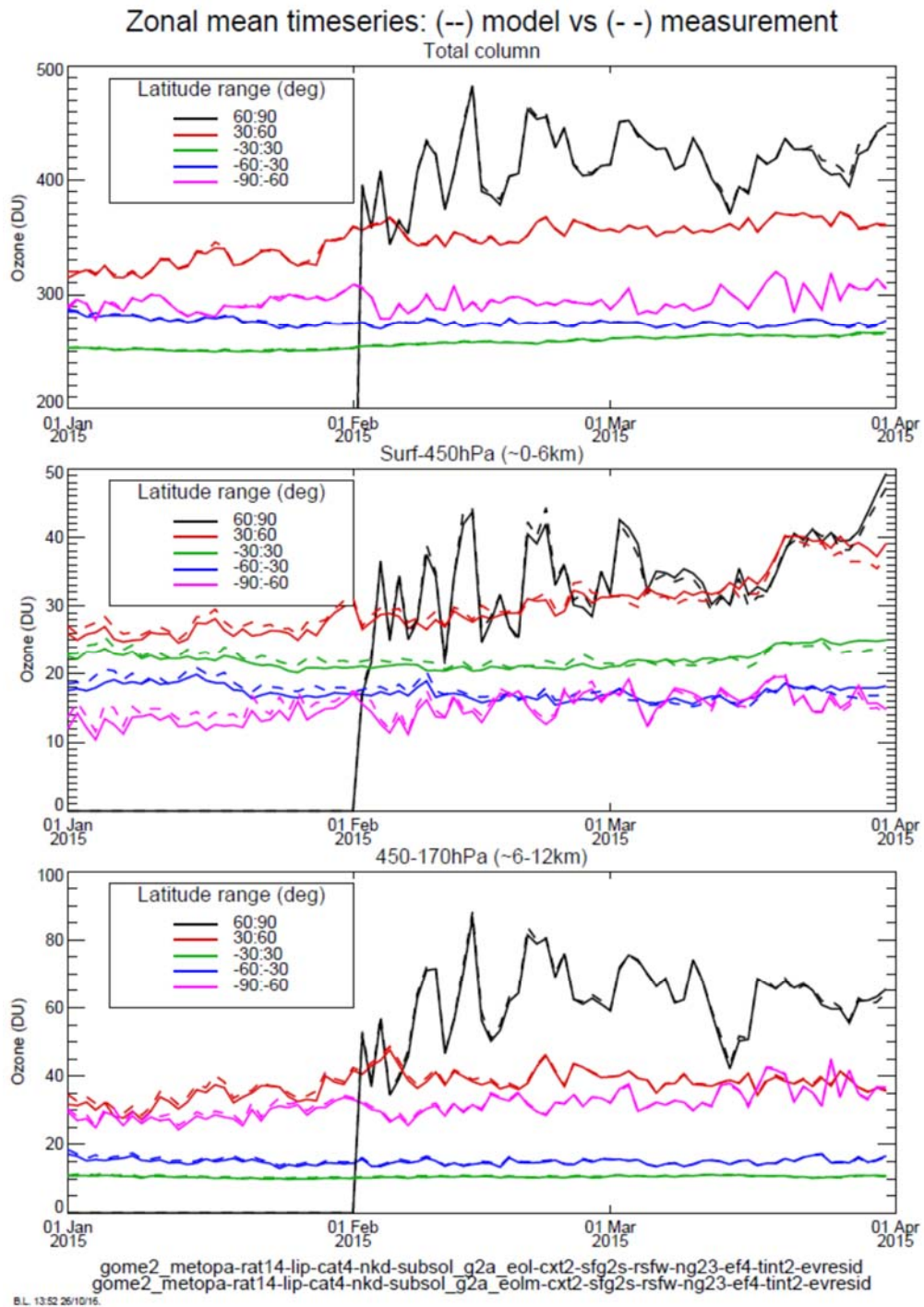


Figure 76 Time series of daily zonal means for ozone total and sub-columns for measured (solid line) and modelled (dashed) SMR

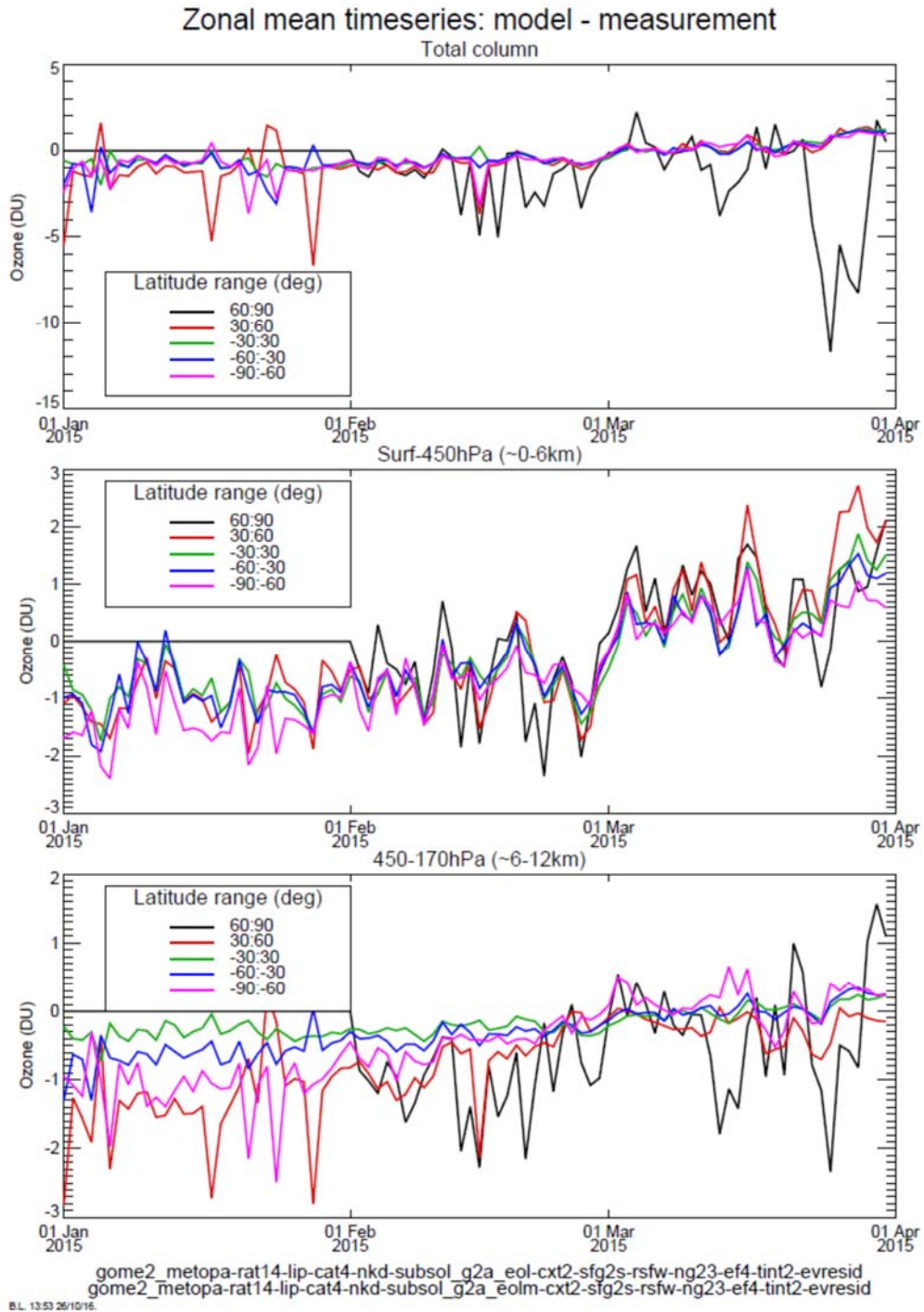


Figure 77 Time series of differences for ozone total and sub-columns for measured (solid line) and modelled (dashed) SMR.

9 Summary and recommendation

Due to the end of life of the Metop-A satellite its orbit configuration will change slowly, putting the satellite in relative positions where it loses direct line of sight to the sun. Direct sun visibility is necessary for the GOME-2 instrument in order to maintain its main reflectivity product for which depends sun spectra are used as reference (SMR, solar mean reference spectra). To mitigate the impact that this loss of solar visibility has on resulting Level 2 products, this study was conducted.

Based on input parameters such as azimuthal solar angle, solar distance, temperature and parameters describing the solar variation (either taken from external databases or derived from GOME2-B measurements) a model has been created, which produces artificial SMRs. By comparing model data to measurements, it can be shown that it represents the real data with high accuracy.

To assess the impact on the quality of the synthetic SMR spectra, results derived from real measurements were compared to results derived from the synthetic SMR for the same period of time. As reference period the first three months of 2015 were chosen as this is the time of the year where loss of solar visibility is expected.

The standard deviation of reflectance for Sahara and the pristine equatorial Pacific is of the order of 10^{-5} . The same conclusions as for the Sahara and Pacific regions can be made to the global observations for a subset of the reference period.

Besides the quality impact on radiance, the impact on level 2 products was assessed as well. For NO_2 , NO_2 retrievals have been performed for all orbits within a 3-month period (1st Jan – 31st March 2015) using both the measured SMR and the model SMR. The investigation was performed step by step, based on single orbit measurements, time series analysis and global impact. Generally, the impact of the loss of SMR measurement on NO_2 retrieval is very small. Using the modeled SMR will introduce a systematic bias of $\sim 10^{14}$ molec/cm² in SCD , and will lead to $\sim 10^{14}$ molec/cm² difference in NO_2 VCD_{total} . However, the bias is mostly removed by the stratospheric correction, and the residual tropospheric slant columns are therefore equivalent, except over polluted areas, where differences in the VCD_{trop} remain of up to 2×10^{14} molec/cm², corresponding to a few percent of VCD_{trop} .

The other level 2 product that was used was height resolved ozone. As expected, by the very small spectral differences of the two SMR, there is relatively little impact from using the model, with differences within the normal uncertainty ranges. Total column differences are typically $< 2\text{DU}$. Due to the sensitivity to fine spectra structure, the largest differences are seen in the lowest sub-columns, but still typically $< 3\text{DU}$. In Northern Polar Regions, an area of known sensitivity due to low light levels and high total column ozone, sub-column errors of $\sim 5\text{DU}$ are seen, but this is still within expected uncertainty at these locations and considered acceptable. When this comparison is extended to a global view then the results are comparable.

Overall it can be concluded that that derived model produces synthetic SMR spectra that match true measurements with high accuracy and thus the effect on resulting products is little. It is however **strongly** recommended to rerun the model shortly before the loss of solar visibility to obtain updated fitting parameters, in order to account for possible instrument changes between this study and the loss of solar visibility.

10 Work packages

The following table shows all work packages of the study:

WP	Description	State
WP1100	Collect Information related to satellite movement	completed
WP1200	Evaluate potential in-flight sources for solar spectra (SMR)	completed
WP1300	Choose model for signal level evolvement during non-vis period	
WP1310	Based on WP1200 and WP1300 discuss and document use of different sources	completed
WP1320	Develop and implement degradation model	completed
WP1330	Apply FM3 degradation to FM2 in order to produce virtual FM3	completed
WP1340	Produce ATBD-like document.	completed
WP1400	Choose reference periods for impact study	completed
WP 1500	Produce Task Report 1	completed

WP	Description	State
WP2100	Evaluate impact on reflectance	completed
WP2110	Get global L1 and L2 data from EUMETSAT for ref periods (Ref data)	completed
WP2120	Produce SMR for use in subsequent reflectance and L2 study	completed
WP2130	Define "impact".	completed
WP2200	Quality impact in time based on regions	completed
WP2210	Pristine equatorial Pacific	completed
WP2220	Sahara	completed
WP2240	Deliver data (document with quality result)	completed
WP2300	Global quality impact based on shorter periods	completed
WP2310	Define short periods and carry out impact study on global data set	completed
WP2320	Deliver document with quality impact analysis	completed
WP2400	Impact on L2 with respect to nominal conditions	completed
WP2410	Synchronizing L2 and reflectance study	completed
WP2420	Analyse sensitivity of global height-resolved ozone	completed

WP	Description	State
WP2430	Analyse sensitivity of L2 NO2 products	completed
WP2500	Produce Task Report 2	completed

WP	Description	State
WP3100	Preparation of report	completed
WP3120	Summarize results on reflectance impact	completed
WP3130	Summarize results on ozone impact	
WP3140	Summarize results on L2 products	completed
WP3150	Merge summaries	completed
WP3200	Produce recommendation backed up by results of report	completed

Appendix A

LIST OF REFERENCES

- Krijger, J. M., Snel, R., van Harten, G., Rietjens, J. H. H., and Aben, I.: *Mirror contamination in space I: mirror modelling*, Atmos. Meas. Tech., 7, 3387-3398, doi:10.5194/amt-7-3387-2014, 2014.
- Miles, G. M., Siddans, R., Kerridge, B. J., Latter, B. G., and Richards, N. A. D.: Tropospheric ozone and ozone profiles retrieved from GOME-2 and their validation, Atmos. Meas. Tech., 8, 385-398, doi:10.5194/amt-8-385-2015, (2015).
- Munro, R., R. Siddans, W.J. Reburn and B.J. Kerridge, Direct Measurement of Tropospheric Ozone from Space, Nature, 392(6672), 168-171. (1996).
- Pagaran, J., M. Weber, J. P. Burrows, *Solar variability from 240 to 1750 nm in terms of faculae brightening and sunspot darkening from SCIAMACHY*, Astrophys. J., 700,1884-1895 , 2009.
- Pinardi, G., Lambert, J.-C., Yu, H., De Smedt, I., Granville, J., Van Roozendael, M. and Valks, P.: O3M SAF ORR VALIDATION REPORT, Reference: SAF/O3M/IASB/VR/NO2/095, 2013.
- Snow, M., Weber, M., Machol, J., Viereck, R., and Richard, E.: *Comparison of Magnesium II core-to-wing ratio observations during solar minimum 23/24*, J. Space Weather Space Clim., 4, A04, doi:10.1051/swsc/2014001, 2014.
- Valks, P., Pinardi, G., Richter, A., Lambert, J.-C., Hao, N., Loyola, D., Van Roozendael, M. and Emmadi, S.: Operational total and tropospheric NO₂ column retrieval for GOME-2, Atmos. Meas. Tech., 4, 1491–1514, doi:10.5194/amt-4-1491-2011, 2011.
- Weber, M.; Pagaran, J.; Dikty, S.; von Savigny, C.; Burrows, J. P.; DeLand, M.; Floyd, L. E.; Harder, J. W.; Mlynczak, M. G.; Schmidt H.: 2011, *INVESTIGATION OF SOLAR IRRADIANCE VARIATIONS AND ITS IMPACT ON MIDDLE ATMOSPHERIC OZONE*, in: *Climate And Weather of the Sun-Earth System (CAWSES)*, Springer, F.-J. Lübken, Dordrecht, The Netherlands.

--End of Document--



cgi.com